LABORATORY STUDY OF THE EFFECT OF AXIAL COMPLIANCE ON ROCK PENETRATION OF PDC BITS

by

© Masoud Khademi

A Thesis submitted to the

School of Graduate Studies

in partial fulfillment of the requirements for the degree of

Master of Engineering

Faculty of Engineering and Applied Science

Memorial University

October 2014

St. John’s Newfoundland

ABSTRACT

Drilling field tests and numerical simulations show that there are relationships between Bottom-hole Assembly (BHA) configuration (compliance and mass), BHA vibrations, and the Rate of Penetration (ROP). In recent years sophisticated down-hole tools (e.g. shock sub, Thruster, and Flex Stabilizer) have been designed and fabricated to mitigate unwanted BHA vibrations and increase the ROP. However, utilization of these tools in field tests shows both positive and negative effects on the drilling process. In order to conceptualize the mechanism behind these effects and further investigate the effect of the compliance element on the ROP, a laboratory test rig with a variable compliance feature is developed. Different levels of compliance are achieved by changing the number and pattern of sandwich rubber mounts in the compliance mounting system. Experimental results verify that changing the compliance value can improve the ROP. An optimum compliance value is also investigated in this laboratory study. Additionally, it is investigated that different compliance values alter the relative bit-rock displacement and positively affect bottom hole cleaning, and negatively affect the cutting surface area.

ACKNOWLEDGEMENTS

First of all, I would like to thank my supervising professor, Dr. Stephen Butt, for his guidance, endless support, and encouragement throughout the course of this research work. Dr. Butt is a highly perceptive supervisor who always helped me a lot to shape my ideas. His scientific insight has been the greatest guide for me to find the solution to many problems. I appreciate his patience and time devoted towards administering my work throughout this research; and I wish to acknowledge him for providing me with the opportunity to learn from and work with him.

I would also like to thank my co-supervisor, Dr. James Yang, for his time and helpful comments. Moreover, I would like to express my sincere appreciation to the members of the ADG, past and present, for their contributions to this research.

I would especially like to express my gratitude to Mr. Farid Arvani, project manager, and Mr. Brock Gillis, project engineer, for their assistance with my research. I am also truly indebted to Mr. Hossein Khorshidian and Mr. Ahmad Ghasemloonia for their time and consultations. Without their encouragement and ideas, this work would have never been completed.

I gratefully acknowledge the financial support of the Atlantic Canada Opportunity Agency (AIF Contract no.781-2636-1920044), Research and Development Corporation

of Newfoundland and Labrador, Husky Energy, Suncor Energy, and the Faculty of Engineering and Applied Science of Memorial University of Newfoundland over the past two years for my M.Eng. education.

I would also thank the personnel of Technical Services at Memorial University of Newfoundland for their support in the fabrication of the experimental setup, and all ADG members who helped me while the experiments were conducted, especially Ahmed Elnahas, Pushpinder Rana, and Zhen Zhang.

Finally, I would like to express deep gratitude to my family, for their understanding, support, and love, without which all this would have not been accomplished.

Table of Contents

List of Tables

List of Figures

List of Symbols, Nomenclature and Abbreviations

A_{ch}	Chamfer area
ADG	Advanced Drilling Group
AGT	Axial oscillation Generator Tool
ASTM	American Society for Testing and Materials
BHA	Bottom-hole Assembly
BHC	Bottom-hole Cleaning
BHP	Borehole Pressure
CCS	Confined Compressive Strength
DAQ	Data Acquisition
DDS	Drill string Dynamic Sensor
DEM	Distinct Element Method
DOC	Depth of Cut
F^b	Back cutter force
F^c	Cutting face force
F^{ch}	Chamfer force
F^c_n	Vertical force on cutter

F^c_s	Horizontal force on cutter
GPM	Gallons per Minute
HSI	Hydraulic Horsepower per Square Inch
ID	Inner Diameter
LPT	Linear Potentiometer Transducer
LVDT	Linear Variable Displacement Transducer
MRR	Material Removal Rate
MSE	Mechanical Specific Energy
MSP	Mechanical Specific Power
MWD	Measurement While Drilling
OD	Outer Diameter
P	Pressure
PDC	Polycrystalline Diamond Compact
Q	Flow rate
ROP	Rate of Penetration
RPM	Revolutions per Minute
RSS	Rotary Steerable System

SDS	Small scale Drilling System
TFA	Total Flow Area
TOB	Torque on Bit
UCS	Unconfined Compressive Strength
VFD	Variable Frequency Drive
WOB	Weight on Bit
Θ	Back rake angle
ζ	Intrinsic specific energy
ψ	Interfacial friction angle
d	Depth of cut
E	Drilling specific energy
S	Drilling strength
μ	Coefficient of friction
γ	Bit constant
σ_1	Principal Stress
σ_3	Confining Stress
Φ	Rock Internal Friction Angle

l	Contact length
σ	Contact strength
σ_0	Hydrostatic stress in the crushed materials
β	Cutter back-rake angle
ω_d	Relief angle

List of Appendices

CHAPTER 1

1. Introduction

1-1. Introduction

In contrast to today's drilling industry, in early ages the primary objective of rock penetration and digging wells was not reaching hydrocarbon reservoirs. The first wells were widemouthed and shallow, and they were drilled as part of the salt production process [1]. However, after decades, and understanding the importance and usefulness of oil and gas, the drilling industry moved to deeper and slimmer wells which were particularly assigned to reach hydrocarbon reservoirs [1, 2]. The invention of the internal combustion engine in the late 19^{th} century had a huge effect on oil demand all around the world, especially in Europe and North America [3]. This increasing demand brought

about a rapid development of the drilling industry, especially in deep well drilling [3]. High cost and operational problems are two main challenges which always accompany drilling. Therefore, from the early years drilling engineers and researchers all over the world have tried to find methods for reducing these costs and decreasing the chance of any accident. One of the main approaches to decrease the cost of drilling is using advanced drilling technologies in order to increase the Rate of Penetration (ROP).

Drilling advancement can be classified into two main categories i) Equipment and material development , and ii) Techniques progression. The former covers all drilling tools and rigs evolutions; moreover, all new technologies which are exerted for faster and more efficient drilling. The latter concerns the methodology of using the available equipment and technologies. Furthermore, it encompasses handling difficulties or emergency situations which usually happen during the drilling process. It should be noted that these techniques are mainly based on drillers' experience.

1-2. Problem Statement

In industry, the design, development, or modification of any tools relies on a valid theory. This theory should first be approved in laboratory tests, as well as in a simulated environment by software. Then the next steps for industrial design of the tool can be followed. During the last decade the role of vibration in drilling has been considered seriously. Many tools such as the vibration dampener or shock sub were designed to

decrease the level of axial vibration, since harsh vibrations can cause many issues such as twist-off, Bottom-hole Assembly (BHA) components and bit failure, low ROP, tool wear, uneven Weight on bit (WOB), and financial loss [4]. On the other hand, some other tools such as DHVOS (Down-hole Harmonic Vibration Oil-displacement System) were designed and implemented to increase the level of vibration in the hole in order to increase the ROP [5]. In recent years the effects of stiffness and flexibility have been considered by many researchers. As a case in point, it was argued by Dunayevsky et al. [10] and Dubinsky et al. [11] that there are relationships between mass of BHA, stiffness of pipe and drill string, and bit vibration. It is also stated that the dynamic components of the forces acting on the cutter are results of the bit and drill string interaction with the rock. In recent years some sophisticated down-hole tools have been designed and fabricated to damp unwanted BHA vibrations and increase the ROP. Utilization of these tools shows both positive and negative effects on the drilling process. Accordingly, a study is needed to conceptualize the mechanism behind these effects; and to elaborate the probable phenomena which happen during this process.

1-3. Focus of the Thesis

This thesis experimentally investigates a simulation based hypothesis which states that the existence of compliance in the drilling system could have a direct effect on drilling response [6]. Moreover, the effect of changing the level of compliance on the ROP is examined in this research. Also, the effect of compliance on bit-rock displacement and bottom-hole cleaning (BHC) are conceptualized through this laboratory study. Simulation

of a single PDC cutter–rock interaction with the distinct element method showed that there is an optimum condition for bit vertical displacement; it also showed that the existence of a damping layer underneath the rock can change the displacement of the rock during the cutting process [7, 40]. Therefore, series of experiments were conducted in order to investigate the aforementioned theories. Bottom-hole Cleaning (BHC), bit-rock displacement, the ROP, and the Mechanical Specific Energy (MSE) of drilling are the factors which are considered during this study.

1-4. Thesis Organization

Chapter 2 provides an extensive literature review about the PDC bit and its penetration mechanisms. It also covers all simulation based studies about rock-cutter interaction by focusing on the effects of a damping layer, axial compliance, and natural vibration on the drilling response. Furthermore, the effects of stiffness and vibration damping on down-hole vibrations and drilling performance are presented in this chapter. Finally the role of BHC in the rock cutting process and its interaction with bit-rock displacement are explained.

Chapter 3 explains the design and fabrication of test equipment. It also describes all the systems which are used during the tests in detail. The described systems are the rotary system, the circulation system, the loading system, the compliance mounting system, and the sensor and data acquisition system.

Chapter 4 describes the procedure of casting rock specimens. Moreover, it describes the curing, preparation, and characterization process of the rock samples before they are used in drilling tests.

Chapter 5 clarifies the design of the experiment. It provides a detailed description of the tests' matrix, and explains the procedure of conducting the drill test. It also presents the method of data analysis on the achieved results. Finally a table of full experimental results is given with analysis in the next chapter.

Chapter 6 presents the result of experiments, and covers a thorough discussion of the analysed results. All the influential test factors are investigated in this chapter as well.

Chapter 7 highlights the accomplished conclusions of this research. It also discusses future open areas for research in this field.

CHAPTER 2

2. Literature Review

2-1. PDC Bit and Its Penetration Mechanisms

2-1-1. PDC Bit

Since 1900, drag bits have been used in rotary drilling [36]. In the drilling industry “Drag Bit” refers to a bit with fixed blades of cutters mounted on the surface of the bit body. In the early years, drag bits were only used for drilling soft formations because of their limited resistance to wear. However, after using harder materials such as tungsten carbide and diamond on the cutter and improving its wear properties, they have been used in hard formations as well. However, just after introducing PDC bits (polycrystalline diamond compact layer for the cutter mounted on the tungsten carbide substratum) in the 1970s,

drag bits became widespread in the oil and gas industry [36]. The figure below shows a typical PDC bit which is made by the Baker Hughes company [39].

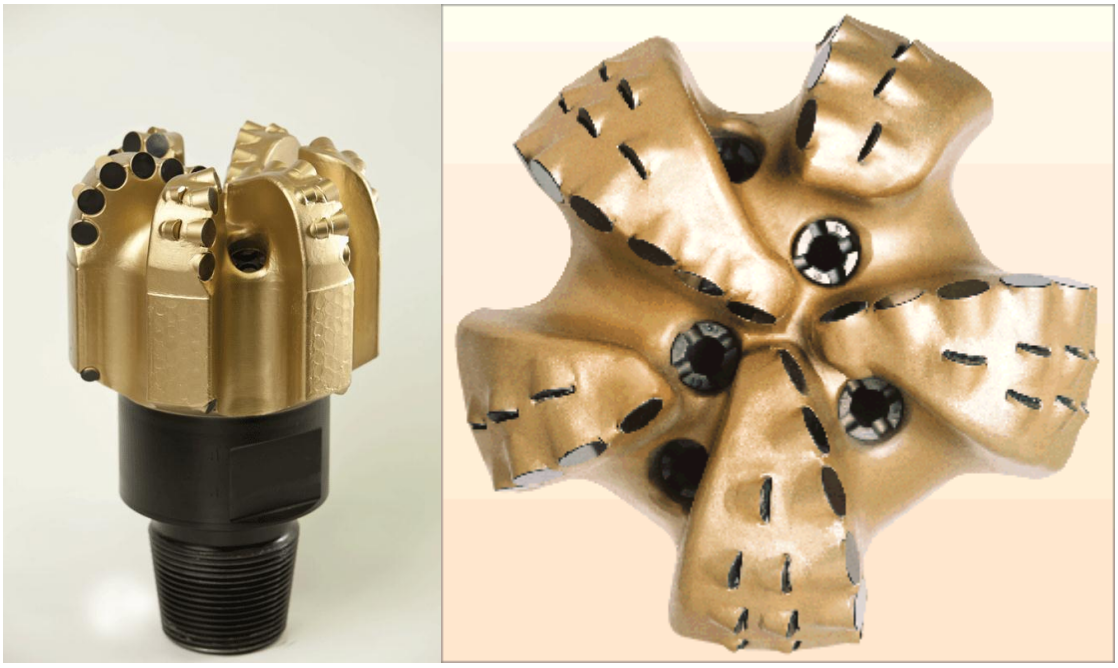

Figure 2-1: PDC bit [39]

2-1-2. PDC Bit Penetration Mechanisms

Nowadays down-hole drilling parameters measurement enables us to analyse real-time bit performance and optimize the ROP. However, a key factor in these kinds of analyses is a good understanding of drill bit response which is a direct function of rock-cutter interaction. Although there are many research papers about PDC bit designs, only a few papers are published regarding rock-cutter interaction models for this type of bit. This section of Chapter 2 succinctly explains the most recent available models for PDC bit-rock interaction.

Glowka [37] analysed the PDC bit design and declared that for a given depth of cut the cutter forces acting on the face of the cutter are proportional to the wear flat area in contact with the rock. He also deduced that the cross-sectional area in rock-cutter interaction plays the main role in determining the cutter forces.

Sellami et al. [34] stated that in some cases in-situ stresses help the development of tensile cracks in the cutting process of a drag bit; however, this phenomenon does not help to increase the ROP in PDC bits. This is due to the high negative rake angle of these bits. Based on experimental and theoretical works which were done by Sellami's research group, they concluded that in-situ stresses do not have any significant effect on the penetration rate. On the other hand, increasing the mud pressure can cause a noticeable decrease in penetration rate. The same phenomenon occurred in this study after increasing the BHP (thorough explanation of results provided in Chapter 6). They also declared that the force applied by the PDC bit comprises two components i) force required to produce rock failure (cutting force) and ii) frictional force which is developed as a result of normal force on wear flat.

Without doubt Detournay was one of the researchers whose work had a big influence in conceptualizing the penetration mechanism of PDC bits. His study was based on the previous researchers' hypothesis about characterizing bit-rock interaction by considering the coexistence of rock cutting and frictional contacts.

To study the drilling response of drag bits, Detournay and Defourny [33] investigated the relation between WOB (W), torque (T), angular velocity (ω), and the ROP (v), and tried to set a series of equations which relate these parameters. In order to achieve this goal they first analysed the mechanical response of a single cutter. Then, by developing a single cutter model and contributing the role of cutters on the bit they reached a solid model for the drag bit.

For such an analysis on a single cutter they considered two types of single cutter; sharp cutter and blunt cutter (cutter with a wear flat). In their model for the sharp cutter the cutter force F^c is separated into two components F^c_s and F^c_n which are respectively parallel and perpendicular to the rock surface (Figure 2-2).

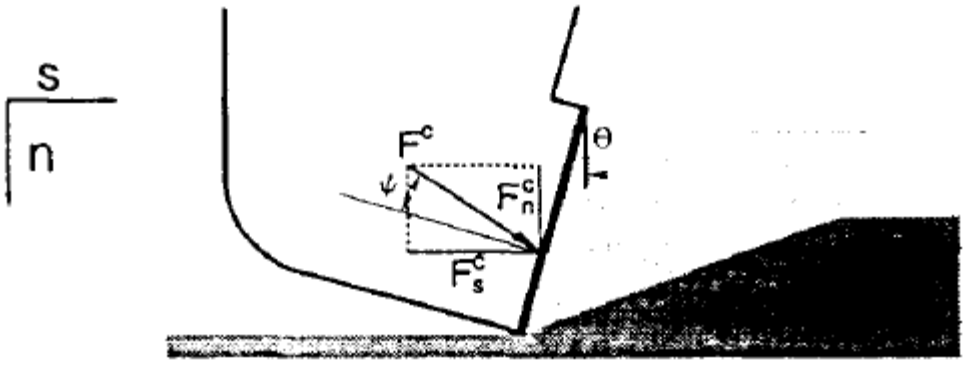

Figure 2-2: Sharp cutter [33]

In this model two components of F^c are calculated as follows:

$$F^c_s = \varepsilon A \qquad (2\text{-}1)$$

$$F^c_n = \zeta \varepsilon A \qquad (2\text{-}2)$$

where A is the cross section area of the cut, ε is the intrinsic specific energy (the amount of energy spent to cut a unit volume of rock), and ζ is the ratio of vertical to horizontal force on the cutting face.

In a blunt cutter, the cutter has a wear flat (Figure 2-3). In this case the cutter force F is divided into two components: F^c (transmitted by cutting face) and F^f (acting across the wear flat). F^c has two components, exactly like the sharp cutter ($F^c_s = \varepsilon A$ & $F^c_n = \zeta \varepsilon A$). As can be understood from the figure the following relations can be derived for the blunt cutter.

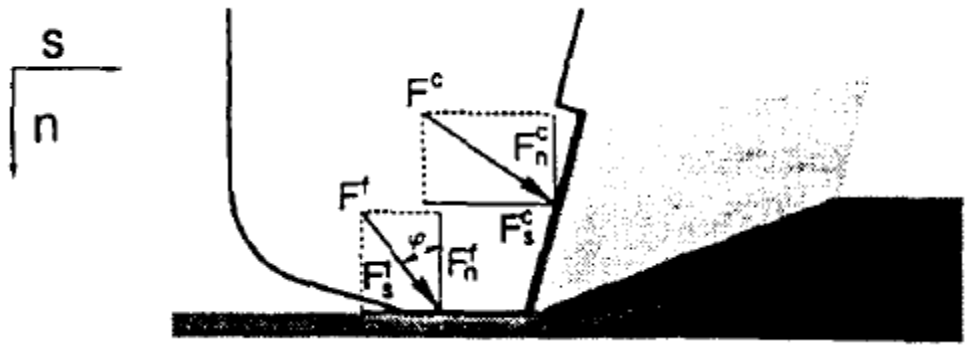

Figure 2-3: Blunt cutter [33]

$$F^f_s = \mu F^f_n \quad (2\text{-}3)$$

$$F_s = F^c_s + F^f_s \quad (2\text{-}4)$$

$$F_n = F^c_n + F^f_n \quad (2\text{-}5)$$

$$F_s = (1-\mu\zeta)\varepsilon A + \mu F_n \quad (2\text{-}6)$$

where μ is the coefficient of friction.

As mentioned before, the model for the drag bit is a generalization of the single cutter model. In the real drilling application, weight on bit (WOB) and torque on bit (TOB) are substitutions for the normal and shear forces respectively.

Detournay and Defourny [33] introduced two new terms, i) drilling specific energy (E=T/d) and ii) drilling strength (S=W/d). Then they suggested a linear relationship between these two terms to describe the drilling process. After that, Detournay et al. [36] modified their previous model by introducing two new quantities that can influence the bit response model, especially the frictional forces: i) characteristic contact length (l) and ii) contact strength (σ). Characteristic contact length shows the wear rate of the bit which is less than 1 mm for the ideal sharp cutter; in other words, it is "an objective measure of bit bluntness". Contact strength also shows "the maximum normal stress that can be transmitted by the cutter wear flat –rock interface".

All aforementioned models just consider three forces based on rock-cutter contact i) drag force ii) normal force iii) side force. Moreover, in all of them only one force acts on the cutter face which is decomposed to the vertical and horizontal components. These models are valid for the bits which do not have any chamfer. This kind of bit is not common in the drilling industry anymore; indeed, the new generation of bits is all chamfered to reach better drillability, especially in hard formations. In addition, none of these models consider the forces acting on the back and front face of the cutter as a result of accumulated crushed materials squeezed from the bottom of the cutter.

Gerbaud et al. [35] was the first to introduce a new model for rock-cutter interaction which takes into account the effects of i) chamfer size and shape, ii) crushed material edge on the cutter face, and iii) back cutter force due to rock deformation. All previous analytical and empirical models assume that the magnitude of the cutting force on the cutter is proportional to the cut surface area. This assumption is only true for sharp bits with a low back rake angle. However, when the back rake angle increases or the cutter is chamfered, the theoretical results show higher force value than the real experimental results. The effects of back and side rake angles are considered in the Gerbaud model by introducing the concept of the build up edge of crushed materials on the cutting face (Figure 2-4).

As illustrated in Figure 2-4, the cutter inclination is defined by back rake angle (ω_c) and side rake angle. These two angles play an important role in the cutting force which was not considered in the previous models. In Gerbaud's model, forces acting on the PDC bit are divided ino three categories: 1-Force acting on the cutting face surface (F^c) 2- Force acting on the chamfer surface (F^{ch}) 3- Force acting on the back cutter surface (F^b).

$$F= F^c + F^{ch} + F^b \tag{2-7}$$

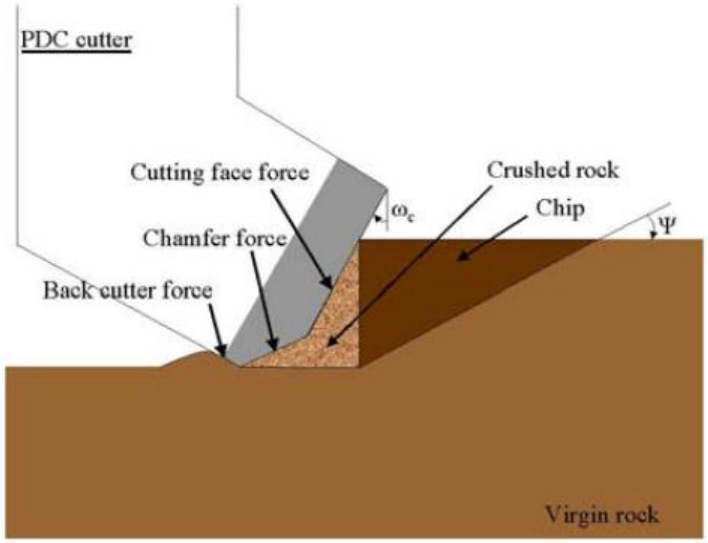

Figure 2-4: Forces acting on PDC cutter [35]

Cutting force is normally considered a pure force which is used for penetrating the rock. As depicted in Figure 2-4, the force applied on the cutting face is transferred to the rock by the edge of crushed materials. This force causes the creation of chips with the specific failure angle (ψ) which is independent of PDC orientation. The effects of back and side angles show themeselves in the frictional contact between the crushed material and rock surface.

As stated before, these days almost all PDC bits have cutter chamfers. The main reason for introducing the chamfer was to avoid the diamond chipping during the cutting process of hard rocks. With respect to the DOC, two diverse mechanisms happen in the chamfer. The first situation occurs when the DOC is higher than the chamfer height. In this case the crushed materials are trapped between the cutting face and the rock; hence, additional friction forces are created at the bottom of the groove. The second situation

occurs when the DOC is lower than chamfer height. In this case the chamfer face acts as a cutting face with a higher rake angle; in other words, the chamfer forces are cutting forces.

Another force which is applied on the cutter is the back cutter force. The new elasto-plastic rock behaviour model shows rock deformation occurs on the back of the cutter during the cutting action. In addition, many laboratory observations show that some parts of crushed materials are driven to the back of the cutter. The last force which is considered by Gerbaud et al. is the wear force. This force is generated when the PDC bit drills a hard and abrasive formation. In this situation the PDC cutter is wearing, and the wear face is generated parallel to the rock surface. It should be noted that when the wear flat emerges, the back cutter force and the chamfer force disappear.

The effect of crushed particles under the cutter was also analysed by Ledgerwood [38]. The result of his experiments showed that the crushed particles under hydrostatic pressure have very high strength; in fact, he deduced that the lowest strength of particles in such a condition is as high as the strength of virgin rock.

2-2. DEM Modeling of PDC Bit Cutter-Rock Interaction

One of the acceptable approaches to study the bit-rock interaction phenomena is numerical simulation. Numerical simulations enable us to apply various drilling conditions and investigate their effects on penetration mechanisms, such as vibration, load on cutter, axial compliance etc. Early studies illustrated that numerical simulations using the discrete element method (DEM) are in a satisfactory agreement with experimental data. Indeed, they can demonstrate phenomena affecting penetration [46].

For this reason DEM simulation of three influential factors is explained in this chapter and their effects on the drilling response of a single PDC cutter are further discussed. These factors are bit's natural vibration, damper layer, and axial compliance respectively. It should be noted that all these simulations were done by ADG members at Memorial University of Newfoundland [6, 8, 40].

2-2-1. Role of Natural Vibration in Penetration of Single PDC Cutter

Vertical oscillation always happens during drilling with PDC bits. This phenomenon has both positive and negative effects on penetration efficiency. Still it is unclear whether the PDC bit vibration can assist the drilling operation [40, 41]. To investigate the effects of this phenomenon, a single PDC cutter-rock interaction was simulated by DEM.

The main reason for the cutter and drill string vertical vibration is the force acting on the bit cutter face and wear flat. Investigation of a single cutter-rock interaction can show the effects of drilling parameters such as load on cutter or cutter mass on drilling responses such as DOC, MSE, vertical vibration, or cutter force components [7].

The cutting action is the result of applying a sufficient load on the cutter and moving it in the direction of cut. During the discontinuous process of chip generation, the force components acting on the cutter oscillates, and causes vibration in the cutter [9]. It was argued by Daniyevsky et al. [10] and Dubinsky et al. [11] that dynamic components of the mentioned force are the result of bit and drill string interaction with rock. Furthermore, they stated that there are relationships between mass of BHA, stiffness of pipe and drill string, and bit vibration. Based on the research of Richard et al. [12], torsional and vertical vibration of PDC bit are coupled and these vibrations can be controlled by changing WOB and RPM.

Payne et al. [42] declared that force fluctuation in the direction of cut can result in bit stick-slip which yields an increase in the risk of BHA failure.

McCray and Cole [43] reported the advantage of magnetostriction vibratory drilling. They declared that by adding this tool which produces vibration on roller cone bits the ROP can be doubled up to a depth of 100 m. They did not state anything about the result of this

tool for deeper wells. However, it is often assumed that at greater depths the increase in the ROP was reduced due to the chip hold down and imperfect cleaning effects. In addition, the hydraulic actuator tool is applying vibratory force in front of the bit by generating pressure pulsation. This tool increased the ROP (33%) in laboratory scale and at a BHP of 20 MPa, but it did not show any effects in real field trials [44].

Akbari et al. [9] contended that applying vibratory forces on the cutter of the PDC bit can create larger fractures in the rock. They also added the generation of these fractures was restricted at high pressures. Pessier et al. [45] showed that using a hybrid bit (a combination of the PDC bit and the roller cone bit) can improve the ROP in hard rocks because of the vertical movement which happens during drilling with this bit.

Khorshidian et al. [8] simulated single cutter penetration using Distinct Element Method (DEM) modelling, as shown in Figure 2-5.

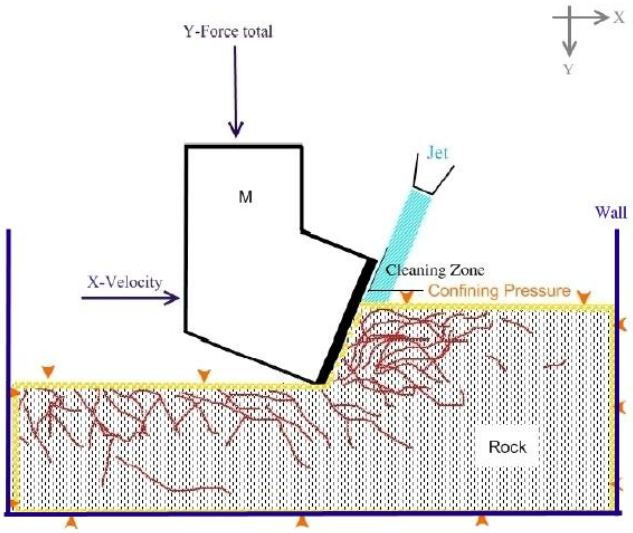

Figure 2-5: Conditions and components of the simulation [8]

Based on their simulation, the DOC declines by decreasing the vertical load on the cutter; however, it was not affected by changing the mass of the cutter. In this simulation, the cutter mass change means changing cutter's inertia without any effect of that on the vertical load on it. Furthermore, an increase in the load on the cutter causes an increase in the value of the Mechanical Specific Energy (MSE). MSE, (J/m^3), is defined as the amount of energy (J) spent removing a unit volume of rock, V_{rock}, (m^3) [57]. The unit of MSE is N/m^2 (Pa) like the strength of a rock. The MSE also can be defined as the apparent strength of a rock that is penetrated by the bit. They stated the increase in MSE could be for several reasons, such as insufficient cleaning, containment of plastic flow of generated chips and friction between the cutter and the rock particles [8].

We know that the horizontal movement of the cutter during the cutting process is in conjuction with the vertical oscillation in the forms of vibration in the vertical position,

vertical velocity, and vertical force components of the cutter. It is asssumed by Khorshidian et al. [8] that the main reason for the cutter vertical vibration is the accumulation of crushed particles between the cutter and the resultant ramp on the rock. It should be noted that these particles which are held down by confinig pressure at the bottom-hole can move the cutter upward till the next chip is generated or untill the vertical load on the cutter is higher than the upward force of the acculumated particles.

Figure 2-6 shows the spectrum of the vertical velocity for different values of the cutter mass in the simulation of Khorshidian et al. [8]. As can be seen, the vertical velocity peak amplitude is higher for the lower cutter mass, since when the cutter is lighter (has lower mass), the vertical load on the cutter and vertical force from the cutting action can excite the cutter with greater acceleration. Moreover, the spectrum of the vertical force and the vertical position of the cutter for different values of the cutter mass in their simulation are presented in Figure 2-7 and 2-8. As can be seen, both vertical force and vertical position amplitudes of the cutter with lower mass show higher peaks than the other cases. Although simulation by Khorshidian et al. provide us good understanding about many influential factors in bit vibration, it should be noted that during this study just one small PDC bit with a constant light mass is used. Therefore, the effect of bit mass, bit type, and bit geometry are not considered which can be a worthy next step for investigation in this field.

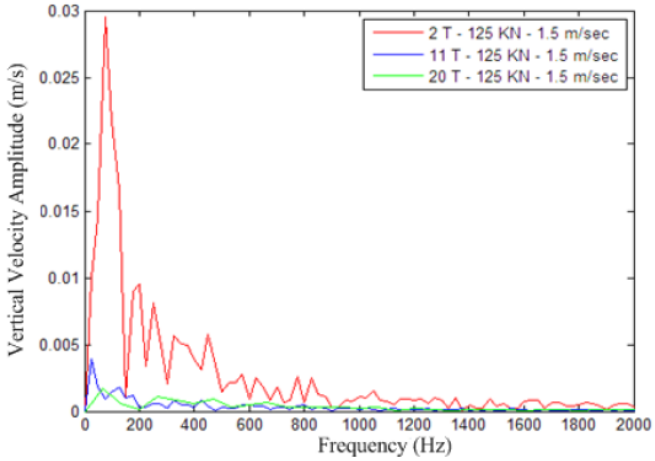

Figure 2-6: Spectrum of cutter vertical velocity at vertical load of 125 kN [8]

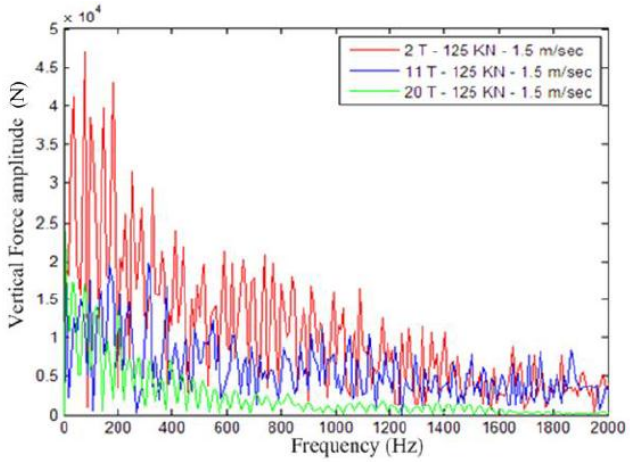

Figure 2-7: Spectrum of cutter vertical force at vertical load of 125 kN [8]

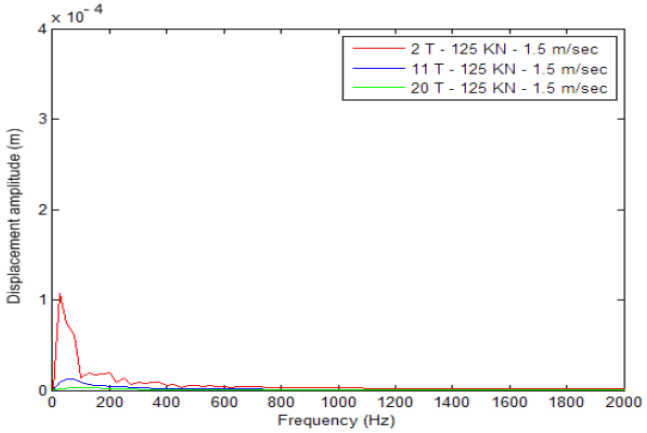

Figure 2-8: Spectrum of cutter vertical position at vertical load of 125 kN [8]

The positive effect of the vertical vibration is more obvious when the cutter imposes enough impact on the rock for cratering, even though going beyond the optimal level of the vertical vibration causes a rise in the MSE. It is also known that the extreme fluctuation in the cutter's vertical position decreases the ROP since in this situation the cutter is likely to slide on the rock instead of crushing or chipping. Two main positive effects of vertical oscillation on the penetration mechanism are to decrease the needed horizontal force for cutter advancement and to generate larger chips and craters.

The process of cutting generation is shown in two following figures. In Figure 2-9 there is not any significant vertical force oscillation, but in Figure 2-10 the rock is under high vertical force vibration [8]. As can be seen in Figure 2-10 the shape of the chips is converted to a crater. Also, some cracks are generated underneath the rock surface due to the high energy impact of these oscillations. In addition, it is hypothesized that when the cutter has a lower inertia it applies less pressure on the rock [8]. This pressure is due to accumulation of crushed particles between the rock and cutter. Furthermore, it should be noted that the effects of the cutter vertical oscillation are in a direct relation with many other drilling factors such as BHP, drill string stiffness, bit wear etc. Therefore, to get the optimum result from the cutter vertical vibration all of these conditions should be considered. Although results of the previous studies showed substantial effects of the bit motion on the penetration mechanism, there is still not any clear insight about the effects of vibration on the penetration mechanism.

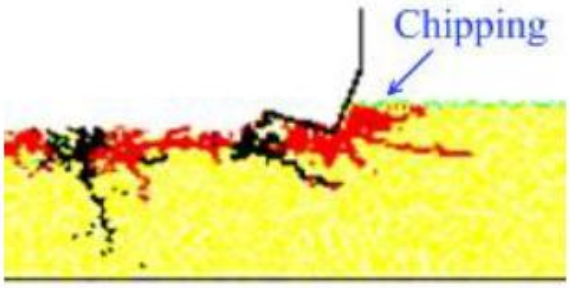

Figure 2-9: Chip generation with no impact [8]

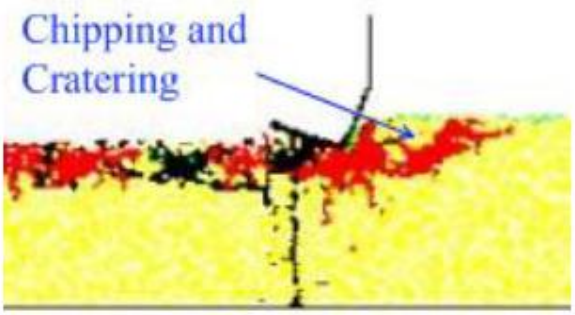

Figure 2-10: Chip generation after impact [8]

In addition, Khorshidian [7] conducted a series of drilling tests and showed that the performance of a bit in the penetration of rock is significantly reduced under the borehole pressure. He also added that the accumulation of cuttings, and consequently the intensity of cutting flow, is more problematic in the presence of high borehole pressure. He also declared that an appropriate BHC condition can improve the drill bit performance through cleaning the generated cutting materials. However, when the generated cuttings are cleaned efficiently, a further increase in hydraulic horsepower may constitute a negative impact on the bit performance by producing nozzle jet impact forces that counteract the WOB [15].

2-2-2. Effects of Damping Layer

In Mozaffari's rock-cutter simulation by DEM, the interaction between the rock and bit can be vibratory. Depending on the type of the vibration which is used in the simulation (force or displacement), the vibration can be applied to the bit either by vibrating the vertical force or by vibrating the whole rock by shaking the confining wall [40]. One of the important features in Mozaffari's simulation is that "the position of cutter with respect to the rock is not pre-specified but is a response of contact force between cutter and rock" [40].

One of the challenges that Mozaffari faced during the simulation of a single cutter was the small scale of the system compared to the applied vertical force on the cutter [40]. In his model there is not any bond between the walls and the rock; consequently, applying the vertical force on the rock can easily lead to rock specimen vibration in its place inside the walls.

To overcome this problem he designed a layer of 10mm thick of particles around the system which increased the density of this layer 100 times. As a result, the rock specimen becomes too heavy to vibrate in its place with the applied vertical force. Despite the beneficial effect of this high density layer in stabilizing the rock in its place, it causes more severe wave reflection inside the system, especially from the boundary of the system or the walls. Therefore, the damping coefficient of this layer increased to absorb all the waves and reduce their reflection.

To investigate the effect of this damping layer on the displacement and vibration of particles in the rock, the displacement of a particle in the middle of rock is plotted versus time in the presence and absence of the damping layer (Figure 2-11 and Figure 2-12). As can be seen, the vibrations of the particle have been significantly lessened after exerting the damping layer [40].

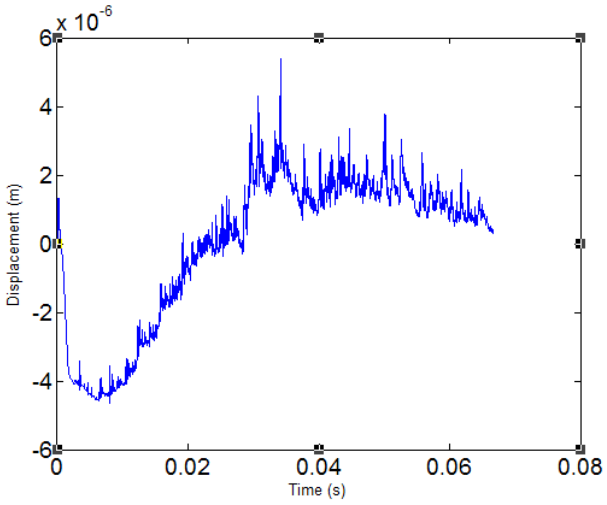

Figure 2-11: Displacement vs. time for a specific ball in the presence of the dampening layer [40]

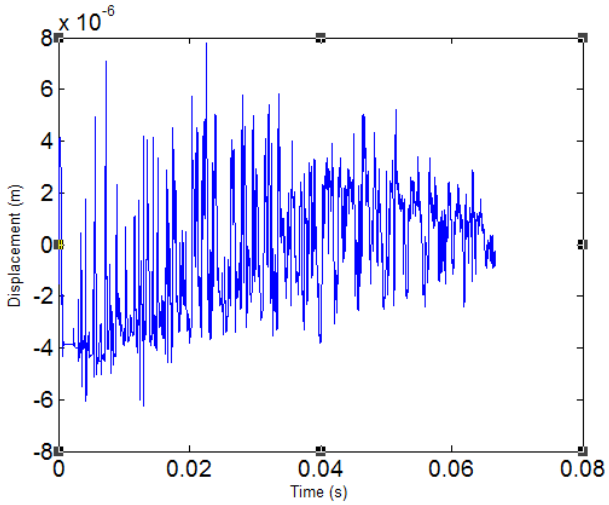

Figure 2-12: Displacement vs. time for a specific ball in the absence of the dampening layer [40]

In another part of this simulation the position of cutter with respect to the rock and its effect on the volume of removed cuttings are analysed. The results showed that decrease in the vertical position of the cutter above the rock causes reduction in the volume of cleaned cuttings and leads to less penetration in the rock [40]. This phenomenon can be due to the effect of the crushed zone under the cutter.

Another interesting point about Mozaffari's simulation is that in the presence of confining pressure during the cutting process, most of the energy is dissipated through particle friction rather than from breaking the rock and overcoming the bond forces. It means that the crushed zone under the cutter plays a substantial role in the penetration process. Indeed, when this part is perfectly cleaned, an increase in ROP and Material Removal Rate (MRR) is expected [40].

2-2-3. Effects of Axial Compliance in Drill String

To investigate the effect of axial compliance in the penetration mechanism, especially its effect on the ROP, a series of simulations was done by Gharibiyamchi [6]. This section describes the methodology of applying axial compliance in his simulations and explains the obtained results.

The source of axial compliance in Gharibiyamchi's simulation was a shock tool. In order to explore how this shock tool could affect the penetration rate, he simulated the drilling process of two hydraulic pulsing drilling tools (1- AGT 2- Hydropulse tool) with and

without using the shock tool. The main difference between AGT and Hydropulse is their methods to create pressure pulses. In the former the pressure pulses are created by restricting the flow area of fluid, but in the latter pressure pulses are created by periodic complete stoppage of the fluid flow. Also in AGT output pressure profile is sinusoidal rather than impact profile. After comparing the results, Gharibiyamchi [6] concluded that the installation of the shock tool above the hydraulic pulse tools can greatly improve the penetration mechanism. Moreover, he asserted that the effect of the shock tool is greater when it is used in combination with AGT than with the Hydropulse tool.

The following table shows the MSE and the MRR values for both hydraulic pulsing tools with and without using a shock tool. It should be noted that in all of these simulations the BHP was equal to 1000 psi.

Table 2-1: Simulation results of the AGT and Hydropulse tool without and with the shock tool [6]

AGT without Shock Tool		**AGT with Shock Tool**	
MSE (KJ/m^3)	MRR (10^{-3} m^3/s)	MSE (KJ/m^3)	MRR (10^{-3} m^3/s)
338000	0.08	6880	4.01
Hydropulse Tool without Shock Tool		**Hydropulse Tool with Shock Tool**	
MSE (KJ/m^3)	MRR (10^{-3} m^3/s)	MSE (KJ/m^3)	MRR (10^{-3} m^3/s)
5870	2.99	5680	4.88

As shown in the table, after using the shock tool in the assembly the MSE values decreased in both cases; however, the MRR values increased. Gharibiyamchi stated that

this phenomenon is due to axial compliance that the shock tool provides for the system [6]. The shock tool which was used in these simulations comprises an axially spring loaded mandrel that is sealed between the drill pipe pressure and annulus pressure. This shock tool works as an oscillatory system for the setup. In other words, it creates an open pump area that pressure pulses of hydraulic pulse tools act on. This process makes the mandrels oscillate up and down. The mandrel itself contains Bellville springs which are schematically shown in the figure below. Therefore, the shock tool converts the pressure pulses generated by the tools to mechanical force and motions [6].

Figure 2-13: Oscillating system of AGT [6]

Figures 2-14 and 2-15 show the cutting process of the AGT and Hydropulse tool with and without the shock tool respectively. As can be seen, when the AGT is operated without the shock tool, its performance is poor (i.e. very low ROP). The reason is that in the absence of the shock tool, the sinusoidal force which is created by the AGT does not damp in the upward direction, and causes the whole assembly to bounce. Accordingly, sometimes the bit does not even touch the rock surface [6]. Moreover, as illustrated in the figures below, after exerting the shock tool the DOC increases and the cutter penetrates more smoothly with a higher rate.

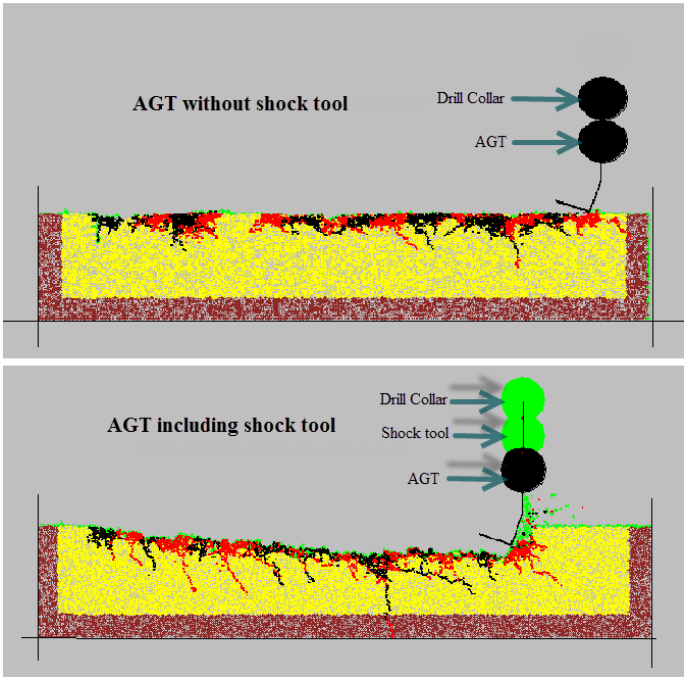

Figure 2-14: Effect of shock tool in drilling performance of the AGT (BHP = 1000 psi, WOB = 60 kN and sinusoidal force amplitude of 19.25 kN) [6]

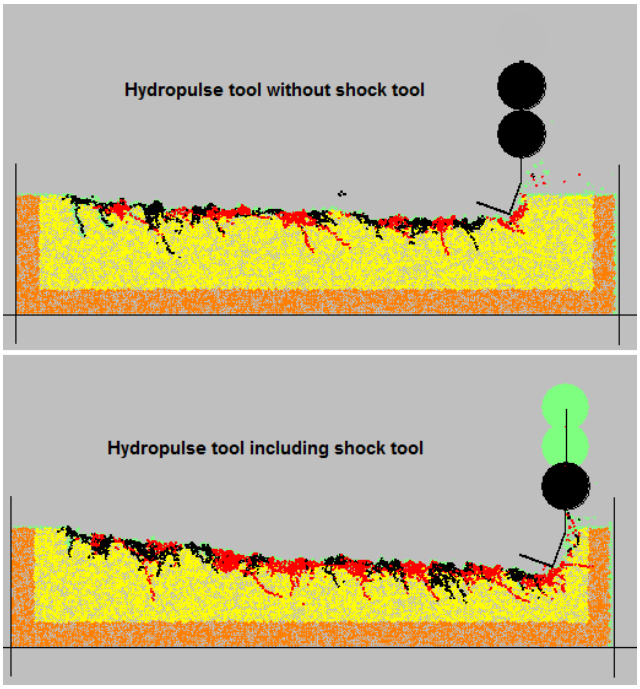

Figure 2-15: Effect of shock tool in drilling performance of the Hydropulse tool (BHP = 1000 psi, WOB = 60 kN and pulse amplitude of 198.5 kN) [6]

Note that, based on Gharibiyamchi's simulations, the required power to drill a unit volume of medium strength rock is less in vibration drilling in comparison with conventional drilling [6]. Furthermore, by analysing the MSE and the MRR curves for different runs Gharibiyamchi concluded that the higher vibration amplitude results in better drilling performance for both MRR and MSE. In other words, higher vibration amplitude brings about a higher MRR value and lower MSE value when all the other conditions are the same [6].

2-3. Effects of Stiffness, Damping, and Compliance on Down-hole Vibration and Drilling Performance

As stated in the previous section, it was argued by Dunayevsky et al. [10] and Dubinsky et al. [11] that there are relationships between the BHA configuration (mass and compliance), stiffness of pipe and drill string, and the bit vibration. Furthermore, it is proved that the dynamic components of the forces acting on the cutter are results of the bit and drill string interaction with the rock.

In recent years, many sophisticated down-hole tools have been designed and fabricated to mitigate unwanted BHA vibrations and increase the ROP. This section of Chapter 2 is allocated to describe the main features of these tools and explain how they affect down-hole vibrations and drilling performance.

2-3-1. Effects of Flex Stabilizer (Flex sub)

Bailey et al. [18] developed a method to describe and quantify the vibration tendency of alternative BHAs. They have used this method as an approach to design the new generation of tools which innately have a lower tendency for vibration. Changing the stiffness and flexibility of the BHA was one of the modifications that they studied for their effects on vibration and drilling response. Therefore, they used a flex stabilizer in the BHA above the Rotary Steerable System (RSS) (BHA-1A) and compared it with a normal configuration which does not have the flex stabilizer (BHA-1B) (Figure 2-16) [18].

The flex stabilizer includes a stabilizer with flex sub attached, sometime as an integral unit. The flex sub is an interconnecting link that has a full size tool joint and comprises a smaller outer diameter (OD) section in the middle to facilitate flexure. It typically has a wire passing through for communication [18].

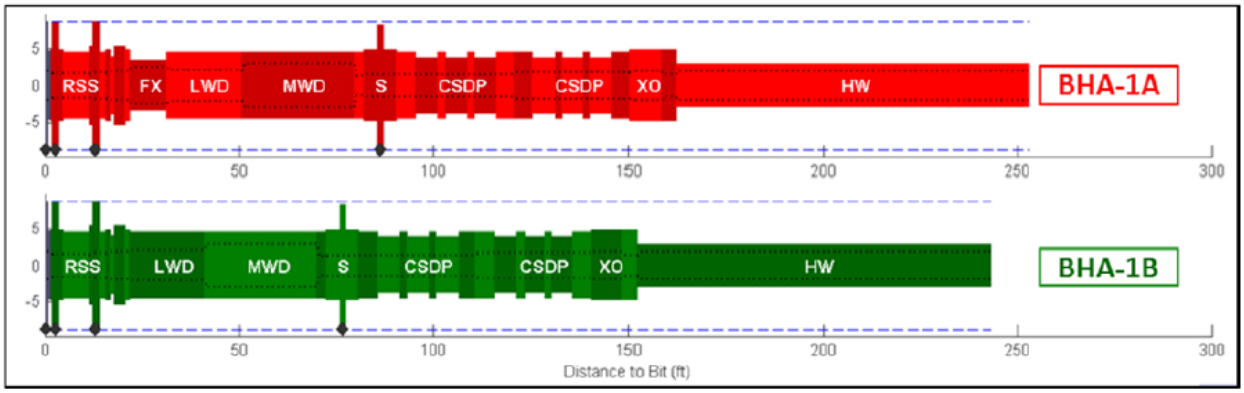

Figure 2-16: BHA configurations with and without flex sub above the RSS [18]

Utilization of this flex stabilizer was examined by conducting drilling field tests and analysing the simulation results. The results include the vibration in flex and twirl modes. Based on the Bailey et al. vibration model, vibration in the flex mode is defined as bending in a plane in response to the lateral force applied at the bit (lateral in-plane bending excitation). Vibration in the twirl mode is rotational motion excited by centrifugal forces (rotary centrifugal excitation) [18]. These vibration modes are displayed in Figure 2-17.

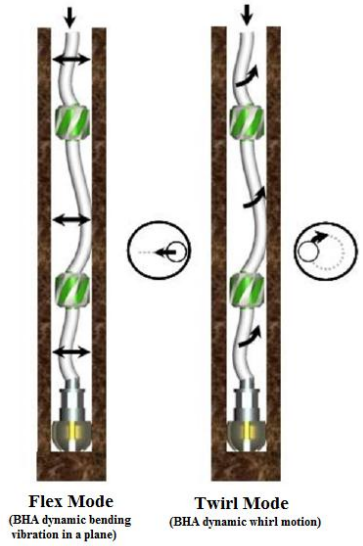

Figure 2-17: Flex and twirl vibration modes [18]

As shown in Figure 2-16, both assemblies are the same except for the presence of the flex stabilizer above the RSS in the BHA-1A. The figure below shows the simulation model results for these two BHA designs. As can be seen, the level of lateral vibration (flex and twirl) for BHA-1A is much higher than for BHA-1B.

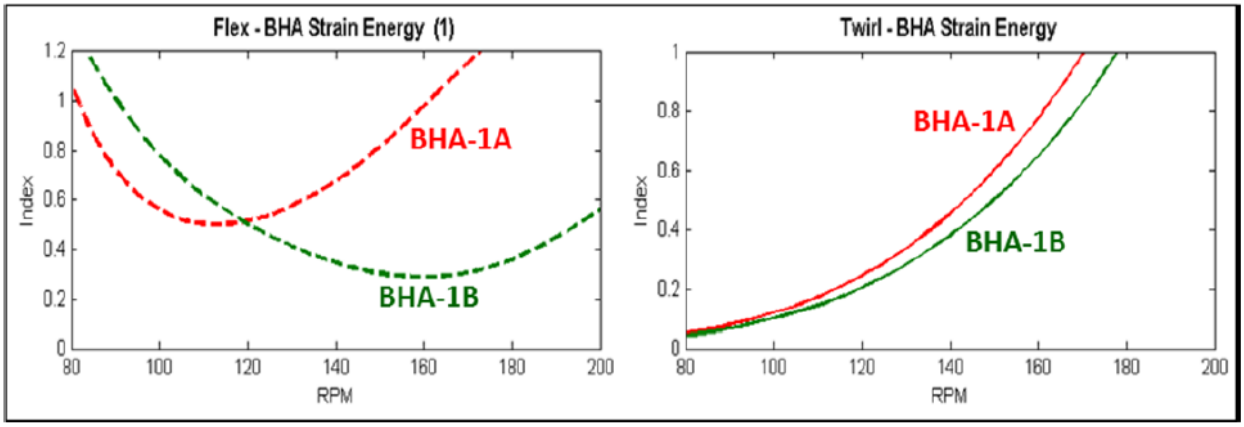

Figure 2-18: Flex and twirl model results for the two BHA designs [18]

Moreover, the following figures display the vibration results of the drilling tests with both BHA configurations. As illustrated in Figure 2-20, sweet spots for the BHA-1B are lower in value, broader, and at higher RPMs in comparison with the BHA-1A [19].

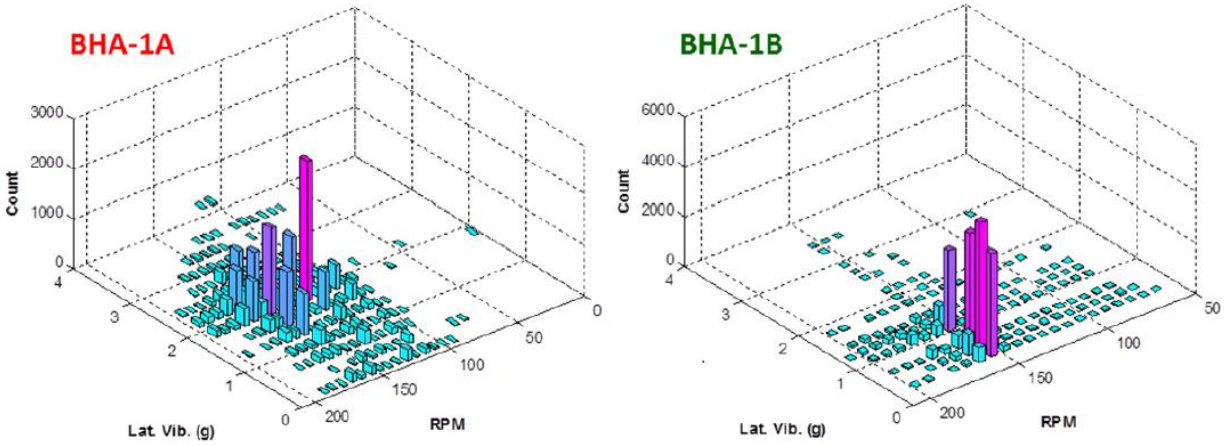

Figure 2-19: Lateral vibration distribution for two BHA designs [18]

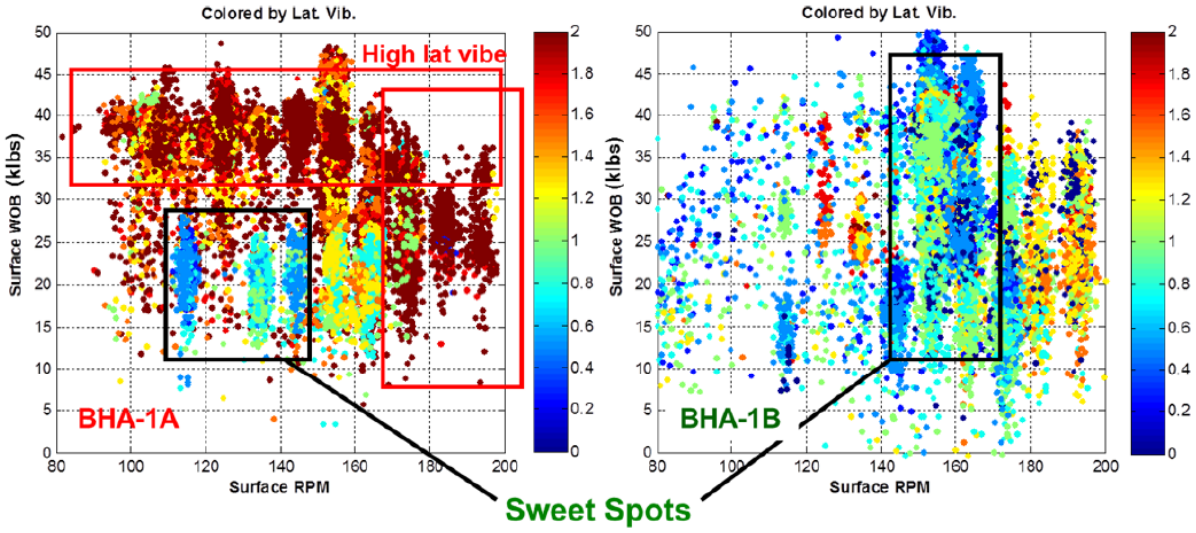

Figure 2-20: Lateral vibration data for the two BHA configurations [19]

Two main reasons that cause increase in the lateral vibrations (loss of lateral stability) are i) increasing the span flexibility by reducing the OD because of the presence of the flex sub and ii) increasing the span length between the RSS stabilizer and the string stabilizer above the MWD by flex sub [18].

The spans between contact points of the bit and BHA and their natural frequencies are a function of basic properties of assemblies such as their outer diameter and length. Usually the spans' properties and their operating conditions place them (spans) close to their natural frequencies [19]. Moreover, all these spans are under tension or compression which makes the whole story more complicated. It is known that each natural frequency has its own wavelength. Therefore, if the distance between two adjacent contact points is much less than the wavelength of the main vibrating mode, the lateral bending wave will not be disturbed and the wave acts as if both contact points are one. In other words, two

contacts points are not detected by the wave because of short distance between them. This problem can be solved by increasing the distance between contact points, but excessive increase in the span length leads to a decline in natural frequency and interference between the nodes [18].

In conclusion, based on the study of Bailey et al. [18], decreasing the stiffness of BHA by using a flex sub, increases the vibration tendency of the system.

2-3-2. Effects of Shock sub

It is known that axial vibration occurs during the drilling of hard rocks. This vibration causes a dynamic load on the bit which is several times stronger that the static load [23, 24]. This heavy load results in bit and drill string damage. Traditional approaches to prevent this damage are i) altering the operational condition ii) changing the BHA design, and iii) using more robust bits [25]. However, after the 1960s another method was applied to protect the drilling equipment, using a shock sub [26].

Considering the reviewed literature the utilization of a shock sub is beneficial for many reasons such as 1) allowing axial bit displacement without corresponding collar displacement that reduces bit load, 2) decreasing the probability of exciting the drill string’s natural frequency by bit displacement, 3) changing the phase angle between bit

force and bit displacement that could prevent the formation of 3 lobe pattern for tricone bits, and 4) increasing the bit bearing and bit cutter life [27, 28].

As stated before, the use of a shock sub is common for decreasing the harmful effects of axial vibrations, but its effects on lateral vibrations are not clear [30]. Therefore, a series of tests was conducted by Warren et al. [21] to assess the performance of conventional shock sub designs. To investigate the effects of a shock sub on lateral and axial vibration, they used three basically different shock subs in the tests. Each shock sub has a specific type of spring element and internal damping mechanism. The former decreases the acceleration force, and the latter eliminates the kinetic energy of axial drill string vibration [21]. In order to record and monitor the axial and lateral vibration Warren et al. utilized two DDSs (drill string dynamic sensor- 3axial accelerometers) [31]. Moreover, they ran the tests on two different BHA designs (Figure 2-21). As can be seen, in one of them, the shock sub is located above a near bit stabilizer. In the other one the shock sub is located above the three stabilizer packed hole assembly. In both cases one DDS is located between the bit and the first stabilizer and another one is located above the shock sub. In general, investigation of all cases showed that the first design of BHA (BHA1) has a better performance than the second one (BHA2).

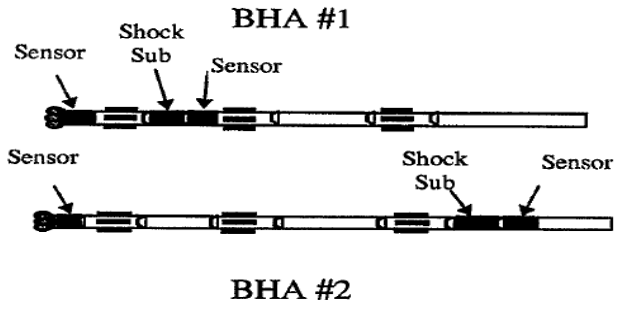

Figure 2-21: Schematic of shock sub assemblies [21]

It is generally thought that the axial vibration generated in the bit is the main source of axial drill string vibration. Therefore, after running the tests it was expected that the sensor above the shock sub would show a reduced amount of axial vibration, in comparison with the near bit sensor. Additionally, it was expected that the near bit sensor would show less vibration after a using shock sub in the drill string. Both of these phenomena happened as presumed [21]. However, the lateral vibration of the drill string has different sources such as the bit, stabilizer, and other drill string components above the shock sub. Hence, it was not expected that the upper sensor would show a reduced amount of the lateral vibration.

The following figure plots the axial (Z axis) and one of the lateral (Y axis) vibrations for both top and bottom sensors before and after using the mechanical shock sub in BHA1. As expected, without the shock sub (base case) the axial acceleration for both upper and lower sensors was the same because of BHA stiffness. Moreover, the lateral vibration for the upper sensor was smaller because the sensor is located between two stabilizers which

protect it from large lateral displacement [21]. After using the shock sub, although the near bit sensor shows the same amount of vibration as the base case, the upper sensor shows a 77% and 49 % reduction in axial and lateral vibration respectively.

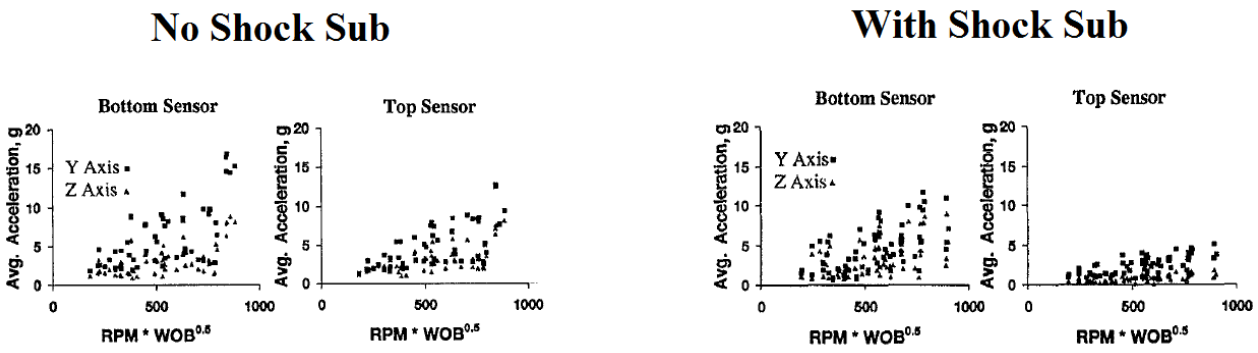

Figure 2-22: Acceleration from the runs without and with shock sub [21]

It can be concluded from the tests of Warren et al. [21] that the main reason for utilizing a shock sub is to relieve the harmful effects of axial vibration. It also can mitigate the lateral vibrations which are initiated by axial vibrations.

Warren et al. also observed the drill string whirl during their tests. They stated that one of the main reasons for whirl is the lateral vibration at the bit. They also proposed that this kind of vibration can be mitigated by using a shock sub near the bit stabilizer. In fact, if a shock sub is used above the packed assembly it increases the lateral acceleration, whirl probability, and fatigue damage although it can still reduce the axial vibration.

Based on the reviewed literature, it can be concluded that the shock sub can noticeably reduce the amount of axial vibration for the drill string. However, it has little effect on the bit vibration. But it is postulated, without any measurements, that the shock sub reduces the dynamic force on the bit by altering the vibrating mass. Furthermore, the lateral vibration decreases after using shock sub; however, in some cases using a shock sub causes an increase in lateral acceleration.

2-3-3. Effects of Down-hole Thruster

Vibrations (axial, torsional, and lateral) are unavoidable during drilling. Harsh vibrations cause twist-off, BHA components and bit failure, low ROP, tool wear, fishing, uneven WOB, variation in reactive torque, and financial loss [4]. Therefore, to optimize the drilling process a method for controlling these vibrations should be found.

As explained in the previous section, one conventional approach to control these vibrations is using the shock absorber. This tool decouples the bit from the drill string, eliminates the main source of excitation, and improves the axial vibration. It cannot maximize drilling efficiency, and exacerbates the lateral vibration [32].

Another control method is using a thruster. A thruster can decouple the lower part of BHA from its upper part. It also can control the WOB hydraulically and keep it closely constant. In addition, it looks like a hydraulic shock absorber that damps axial vibration,

balances uncontrolled sliding, and improves the drilling condition, especially in wells with vibration, shock, or sliding problems [4].

In the first trials of the thruster, it was used in a deep well in Germany and reduced the well cost as much as 24% without the loss of drilling efficiency. Then it was used in many other wells all around the word which have shock and vibration problems such as wells in the British North Sea, the Netherlands, and Canada [32]. In all cases the thruster proved its capability in increasing the ROP, bit life, and bit steerability, also decreasing the down-hole failure and torque vibration. For instance, in an exploration well in offshore Brunei the thruster ran with a mud motor and decreased the variance of WOB (50%), increased the ROP (100%), and reduced the TOB vibration (75%) [4]. This enhancement is due to applying even and constant WOB with the thruster; moreover, there is less axial vibration, and better bit bore-hole contact during penetration [4, 32].

The thruster uses the differential pressure between the annulus and inside of the BHA to create the WOB. A thruster has two main parts i) a cylinder and ii) a piston. The cylinder comprises the drill string and the thruster housing. The piston comprises the bit, mud motor, and all the other tools located below the thruster that can contribute to pressure drop [4, 32]. As shown in Equations 2-8 and 2-9 , the thrust force (F_{thr}) which acts on the piston is a function of the piston's cross section area (A) and differential pressure between the piston pressure and annulus pressure (i.e. total pressure drop-P). Some other parameters which have indirect impacts on the thrust force are mud flow rate, bit total flow area (TFA), bit aggressiveness, mud motor characteristics, thruster's operation stage,

mud density and mud viscosity. These factors show their effects by changing the total pressure drop.

The schematic diagram of a thruster, its main components, and other BHA tools that usually come with it are shown in the following figure [4].

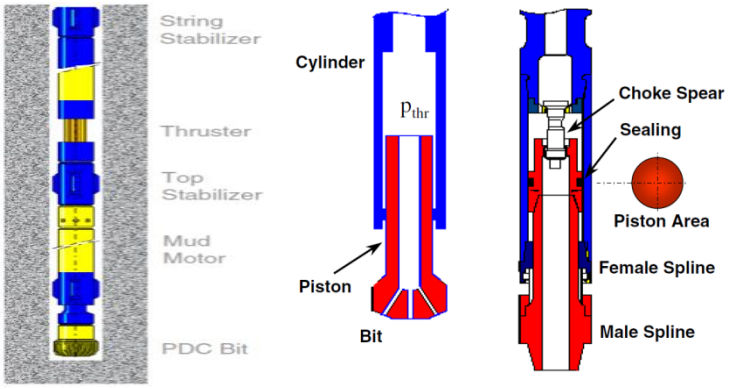

Figure 2-23: Schematic diagram of thruster [4]

$$F_{thr} = P * A \quad (2\text{-}8)$$

$$P = P_{thruster} + \ldots + P_{mud\ motor} + P_{bit} \quad (2\text{-}9)$$

Finally, it should be noted that actual WOB is not just a function of the thrust force. The WOB also includes the weight of the drill string which is located under the thruster, and the friction force which is applied on the part of the drill string which is under the thruster [32].

To sum up, based on reviewed literature optimal use of the thruster in the drilling system can improve the ROP and drill string dynamics; indeed, it damps unwanted vibrations and increases the BHA lifetime.

2-4. Effects of Bottom-Hole Cleaning on Rock Penetration

Bottom-Hole Cleaning (BHC) means the removal of the generated cuttings which are produced during rock penetration. The role of fluid circulation in the bottom of the hole is vital for many reasons. The first and the most important reason is that the fluid flow in the bottom-hole flushes the cuttings from the rock face and carries the generated fragments to the surface from the bottom of the well. It also can cool the bit, reduce the bit wear, and be used as a lubricant for the drill string and the drill bit [47, 48]. Another application of drilling fluid is creating bottom-hole pressure which is needed for well control and bore-hole stability, especially in deep wells. Above all, in this section, the focus is on the effect of BHC on the ROP.

Maurer was one the first researchers who investigated the effect of BHC on the ROP in rotary drilling. Based on his theory, the ROP is a function of WOB, rotary speed, rock strength, and the bit diameter [49]. However, as can be seen in Figure 2-24, when the drilling is conducted at a high WOB and high rotary speed the increasing trend of the ROP versus WOB and RPM will be stopped. Maurer stated that this phenomenon happens because of the shortage of bottom-hole cleaning. He added that in the absence of

sufficient BHC, the bit is floundering on the previously crushed rock, and it tries to re-drill the cuttings [49]. Based on this conceptualization, it can be concluded that the BHC can directly affect the ROP; in other words, in the presence of a good BHC condition a higher ROP is expected.

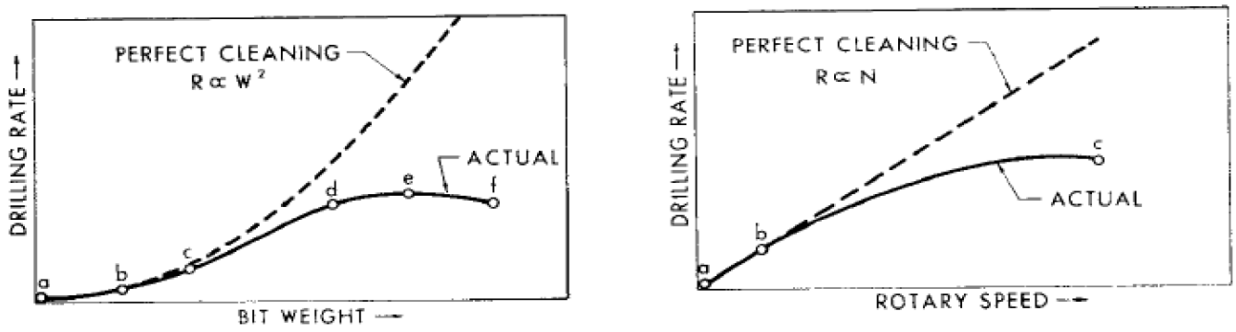

Figure 2-24: ROP curves vs. WOB and rotary speed for ideal and actual drilling conditions (Maurer model) [49]

Another effect of the BHC is to prevent balling in the bottom-hole due to bit plastering. As argued by Garner [50], in the absence of good BHC the crushed particles could stick between the bit cutters and cause a problem which is called bit balling. Based on their experiments which were done on shale and with a roller cone bit, bit balling can dramatically decrease bit efficiency and the ROP. This reduction in the ROP can be mitigated by good BHC, since in that situation drilling fluid can flush and clean all produced fine particles in the crushed zone and carry the generated cuttings to the surface more efficiently.

The bit balling phenomenon happens in PDC bits too, and it is usually more severe when PDC bits are used to drill soft to medium rocks such as shale. Ledgerwood and Salisbury [51] stated that in poor BHC condition, when there is not sufficient flow to remove the cuttings, the generated fragments are compacted between the rock and the bit. Due to this compactness, they lose their water content and create a stuck mass in the penetration zone. In other research for application of the PDC bit on shale which was performed by Wells et al. [52], it was observed that with a high WOB and low bit hydraulic horsepower, bit balling is a very probable phenomenon.

Figure 2-25: Balled up PDC bit [53]

Feenstra and Leeuwen [54] also worked on BHC. Based on their experiments on soft and medium rocks, they contended that the ROP is decreased when bit balling occurs, and this

reduction can be up to 50% for a high WOB. They also added that in order to diminish this problem a high jet velocity and good BHC condition are needed.

Rabia [55] stated that appropriate hydraulics not only can prevent bit balling and remove the generated cuttings, but also can positively affect bit performance and increase the ROP. It should be mentioned that his study was performed on Gulf Coast shale, and he did not consider the relationship between BHC and BHP.

In the research of Wells et al. [52] on bit balling mitigation in PDC bits, they argued that the effect of HSI on the ROP is only limited to soft rocks such as shale. In other words, they contended that the effects of flow rate and HSI on the ROP enhancement in hard rocks are negligible.

In research to find the optimum drilling technique, Speer [56] claimed that the positive effect of bit hydraulic in increasing the ROP is limited to cleaning all the generated crushed materials and cuttings (i.e. perfect BHC). He also added hydraulic does not have any significant effect on the rock failure.

As can be concluded from the reviewed literature the effect of bit hydraulics, especially jet impact force, is more considerable with a roller cone bit than with a PDC bit. The reason behind this phenomenon can be the position of nozzles with respect to the zone of penetration. In fact, PDC bit nozzles are usually located in a place that the outcoming fluid can easily cover all surfaces of the PDC cutters and prevent bit balling. Instead, in

the roller cone bits, the jet nozzles are pointed to the cones' teeth and the formation; therefore, both of them are subjected to the jet force [7].

A series of tests was conducted by Tutlouglu [57] to investigate the mechanics of rock cutting by a single cutter under atmospheric conditions and fixed DOC. Based on achieved results he stated that the major issue which limits the performance of the cutter is accumulation of crushed materials in front of the cutter. He also contended that crushed zone cleaning leads to considerable improvement in the specific energy of the penetration.

Mozaffari [40], as stated previously, in his rock-cutter simulation showed that in the presence of the confining pressure during the cutting process, most of the energy is dissipated through the particles' friction rather than from breaking the rock and overcoming the bond forces. He also added that the crushed zone under the cutter plays a substantial role in the penetration process and when this zone is perfectly cleaned an increase in the ROP and MRR are expected.

Accordingly, it can be concluded that any approaches for cleaning the crushed zone can lead to an increase in the ROP.

CHAPTER 3

3. Design and Fabrication of Test Equipment

3-1. Drilling Rig (Small scale Drilling System)

The figure below shows the drill rig setup which is used in the drilling tests. This Small scale Drilling System (SDS) comprises several systems, such as the rotary system, the circulation system, the loading system, the compliance mounting system, and the data acquisition system which are all explained in detail in the following sections of this chapter. Moreover, this chapter describes the characteristics of the main components of the drill setup such as the drilling cell, PDC drill bit, and sandwich rubber mount.

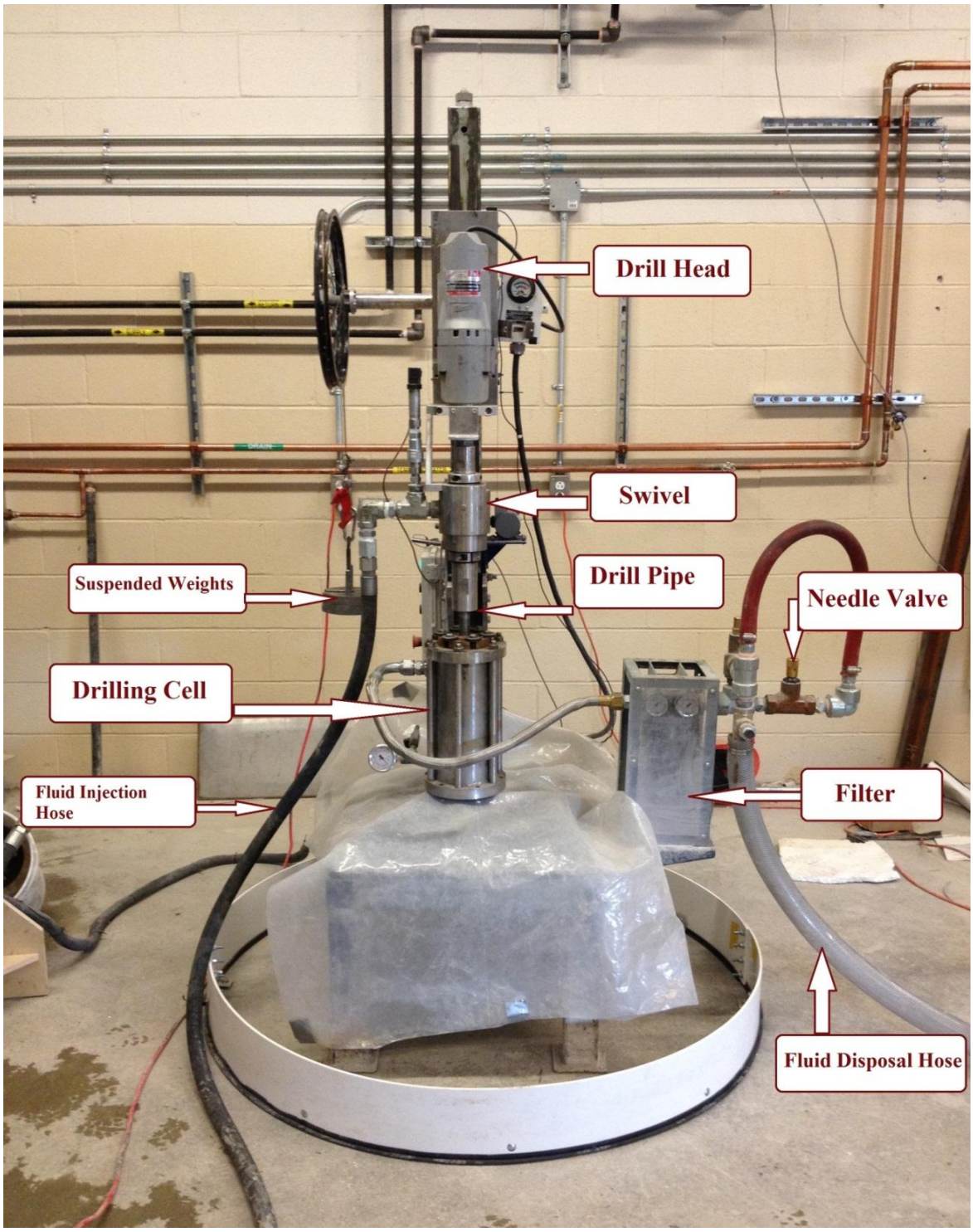

Figure 3-1: Drill rig setup (SDS)

The laboratory drill rig setup is designed to penetrate the rock in atmospheric and down-hole drilling conditions. In order to get more consistent and clear results, and investigate the effect of compliance on rock penetration, some modifications are applied to the existing rig. These modifications include adding the compliance mounting system, improving the data acquisition system, fixing the rig frame to the ground, and fabrication of a new hooking system and suspended weights.

As illustrated in Figure 3-1, the general procedure for drilling the rock starts when the pump directs the water into the drill pipe via the swivel. This water flows into the drilling cell where the rock specimen is installed. The pressure of the drill cell and other parts of the system is controlled by the different values which are installed at different spots (detailed explanation can be found in Sections 3.1.2 and 3.1.6). The penetrating is done by a PDC bit which is attached to the end of the drill pipe. The bit begins to penetrate after applying adequate load and rotary power to the drill pipe. During the whole procedure the DAQ system is recording the data, such as pressure, load, bit position, rock position, motor current of the drill head, and acceleration of the drill pipe.

3-1-1. Rotary System

As displayed in Figure 3-2, the rotary system of the setup comprises a motor as a rotary head. This motor can deliver the maximum bit power of 4kW. Furthermore, the maximum torque and thrust of this motor are 80 Nm and 3500 N respectively [7]. This rotary head can provide two different levels of RPM which are nominally 300 and 600. These RPMs change slightly during rock penetration because of the alteration in the drilling condition.

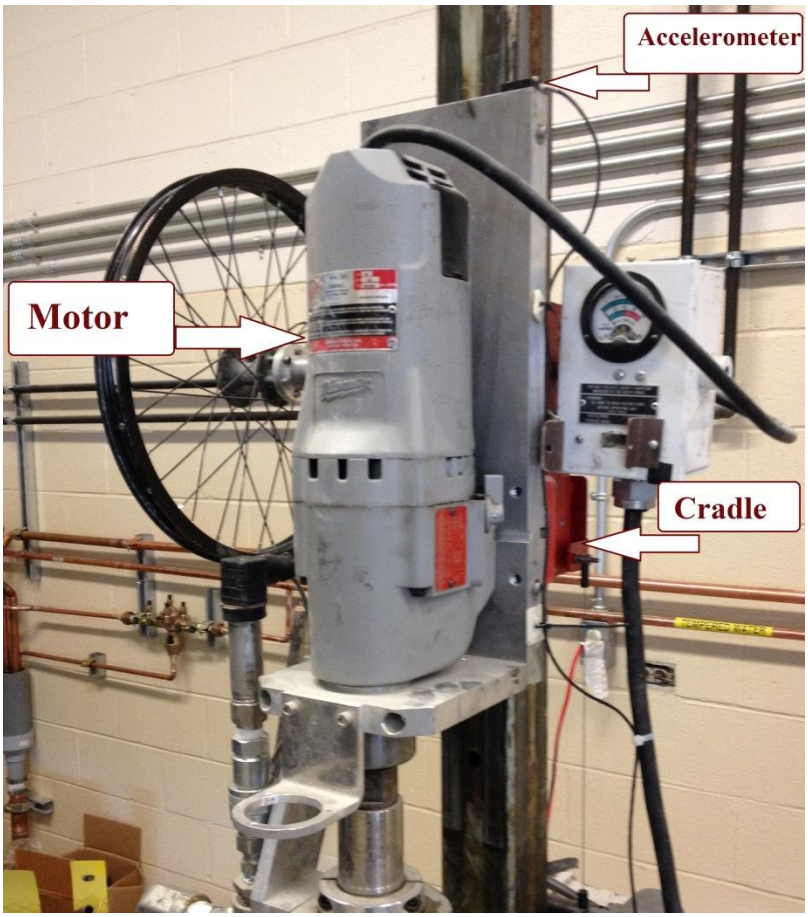

Figure 3-2: Rotary drill head attached to the cradle

3-1-2. Circulation System

The circulation system of the SDS contains many segments. The main parts of this system are the triplex pump and fluid tank. The triplex pump works with a 20kW motor which enables the pump to drain the water with a maximum flow rate of 150 L/min and a maximum pressure of 6900 kPa [7]. In order to control the flow rate of the pump it is equipped with a variable frequency drive (VFD) that can adjust the rotary speed of the motor. Another feature of the circulation system is a fluid tank which is placed above the pump. It should be noted that the capacity of this tank is 1000 L and it is filled with water, since water is the drilling fluid used for the whole experiment. The other component of this system is the flow meter to measure the outlet flow of the pump. This system also has pressure transducers and pressure gauges to measure the pressure at the outlet line of the pump and in the disposal hose. Moreover, a level meter is installed in the tank to monitor the circulation condition. The water flow starts from the tank; then it respectively goes through the injection hose, swivel, drill pipe, drilling cell, filter, and finally it ends at the disposal hose. The swivel, drilling cell, filter, injection and disposal hose are other parts of the circulation system which are installed on the rig and are further explained in section 3.1.6. Figures 3-3 and 3-4 display all parts of this system.

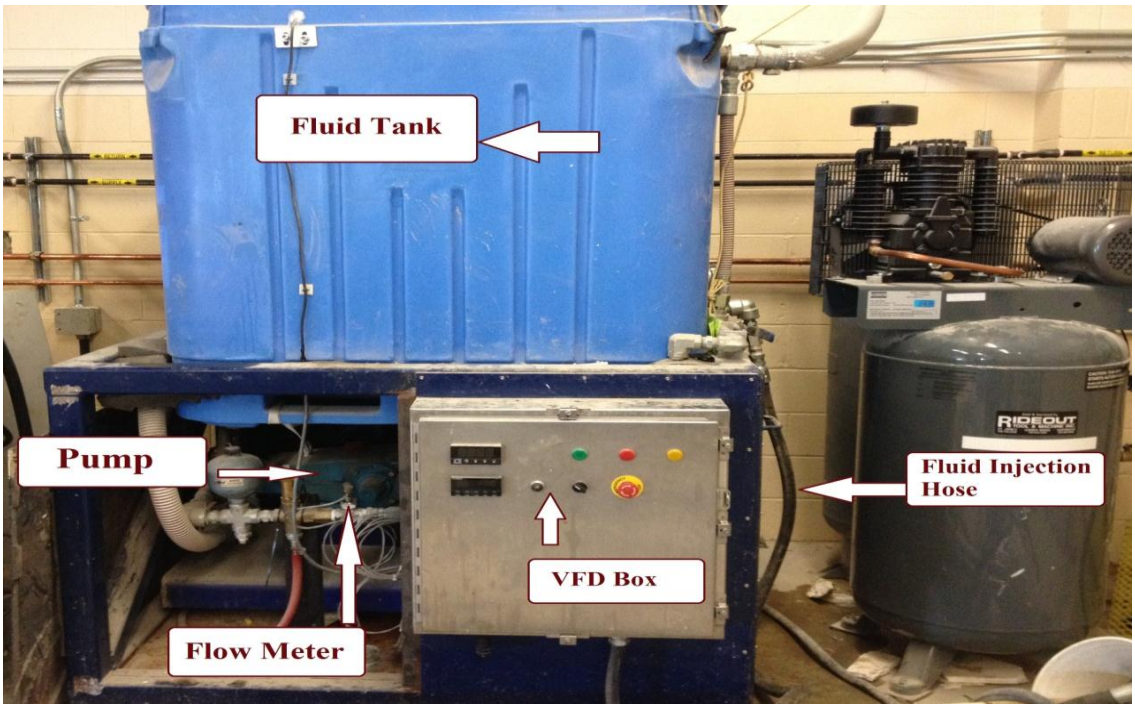

Figure 3-3: Circulation system

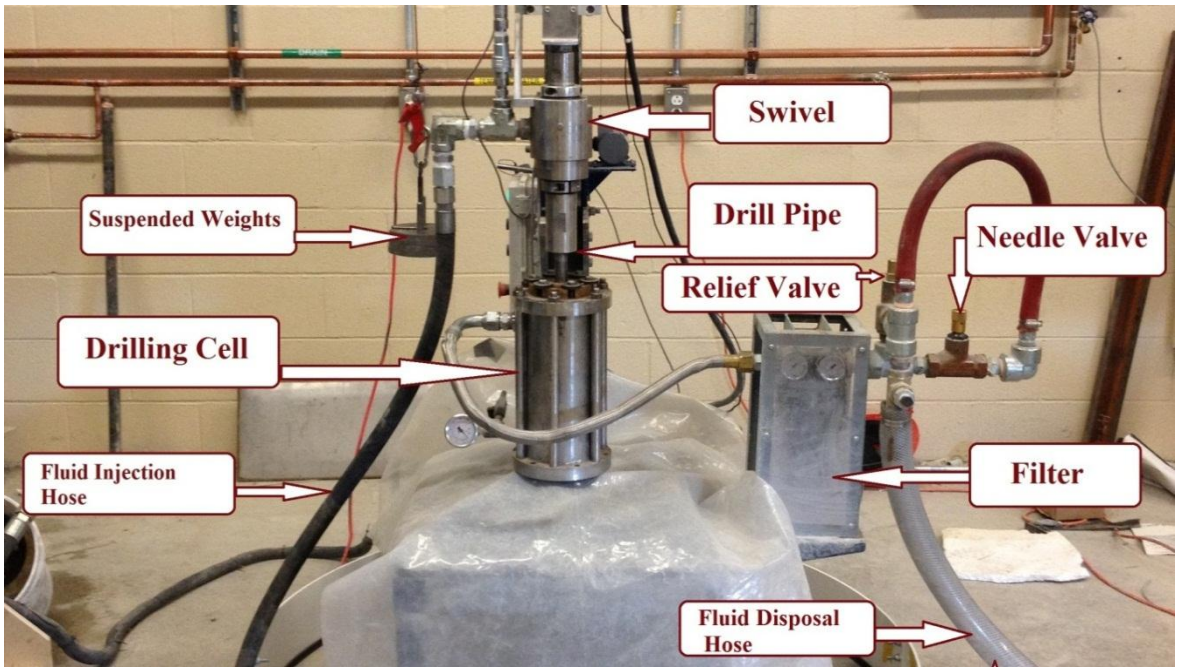

Figure 3-4: Circulation system components

3-1-3. Loading System

The main objective of the loading system is to provide WOB. The applied load on the bit contains two parts. The first part is constant, and it equals the weight of the rotary head components (50 kg). As cited before, the rotary head includes a motor, cradle, swivel, and drill pipe. The second part of the load is applied by suspended weights (mass disks) with a rack and pinion system. As illustrated in Figure 3-5, the rack and pinion system converts the suspended weight to a greater static load on the bit. Between different runs of the experiment, whenever a change in WOB is needed the number of mass disks changes. This weight is monitored by the load cell which is located underneath the rock specimen. Figure 3-6 shows the masses which are used as suspended weights. The weight of each mass is 1.5 kg, and they are connected to the wheel by a simple hooking system.

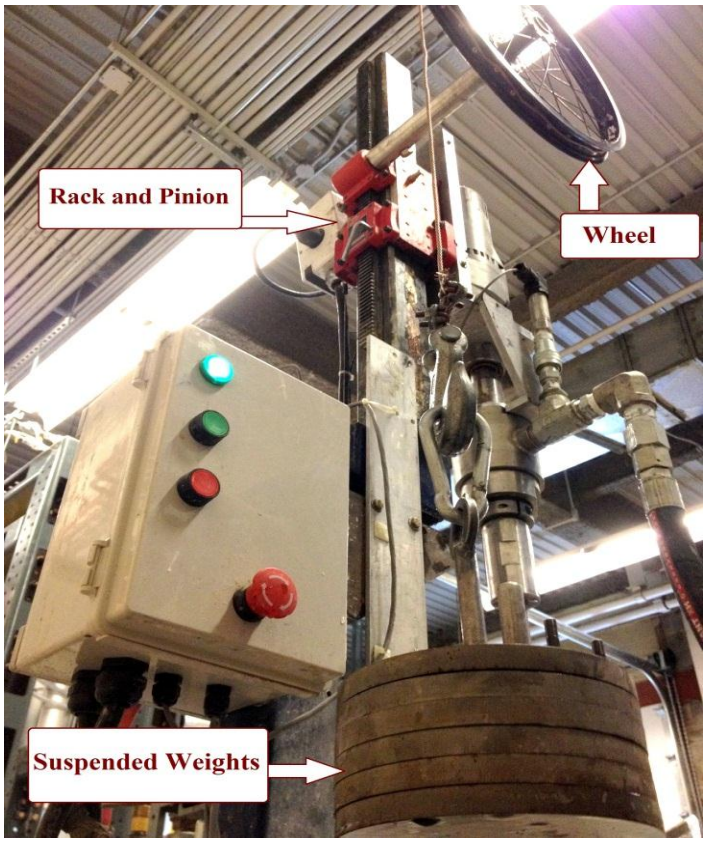

Figure 3-5: Loading system

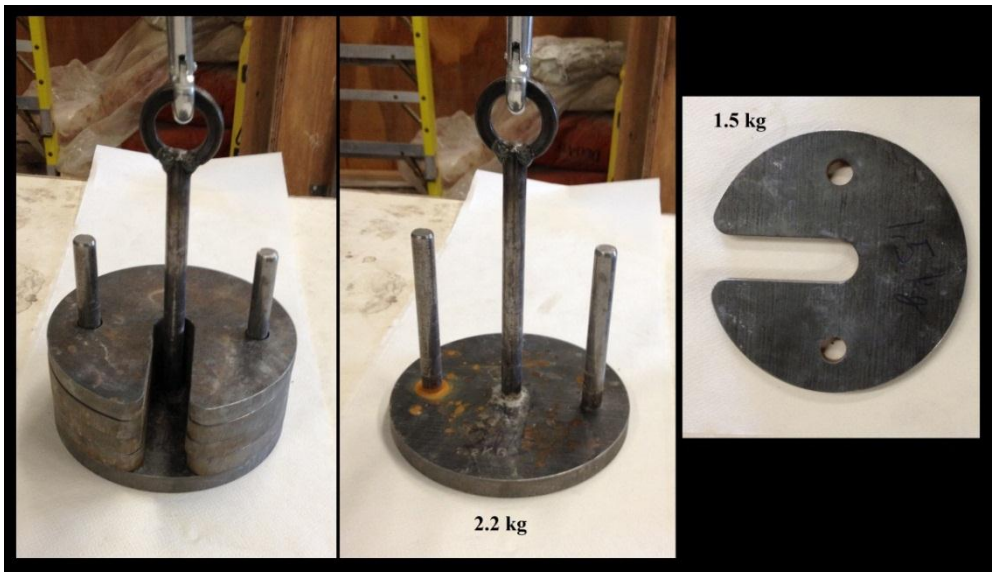

Figure 3-6: Suspended weights

3-1-4. Compliance Mounting System

In order to investigate the effect of compliance on rock penetration, especially ROP, a system with a variable compliance feature is needed. Having this aim in mind, a compliance mounting system was designed and fabricated. This section of Chapter 3 describes components of this system, and its design procedure. Furthermore, it explains the levels of compliance that can be achieved by this system.

Investigation of the effects of axial compliance by compliance mounting system is the preliminary step for designing and fabricating a new series of down-hole tools that have the capability of changing the compliance in the drill string. But before moving forward to this stage, the effectiveness of the axial compliance in ROP enhancement should be examined which is the main scope of this research.

3-1-4-1. Vibration-Damping Sandwich Mounts

The pivotal part of the compliance mounting system is the compliance element which is used in this system. After reviewing all the possible options that can be used as a compliance element, a vibration-damping sandwich mount was selected (Figure 3-7). This sandwich mount is made from natural rubber which has superior resistance to tear and abrasion. It also has good flexibility at a wide range of temperatures (-10^{o} to 150^{o} F) [16]. There is a stainless steel threaded stud on one end of this mount which is used for attaching the mount to the mounting plate (further explanation in Section 3.1.4.2).

Figure 3-7: Vibration-damping sandwich mount

The detailed configuration and specifications of this rubber mount are depicted in Figure 3-8 and Table 3-1.

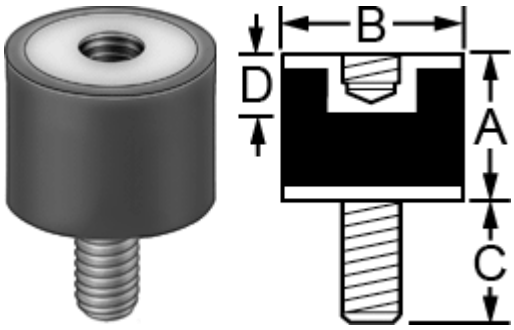

Figure 3-8: Vibration-damping sandwich mount configuration [16]

Table 3-1: Vibration-damping sandwich mount specifications [16]

			Thread	
Thread	Ht. (A)	Wd. (B)	Lg. (C)	Dp. (D)
3/8"-16	1 5/8"	2"	5/8"	3/8"

3-1-4-2. Mounting Plate Design

After selecting the appropriate sandwich mount, a setup is needed to put the mounts together, and to attach them to the drill setup. The mounting setup has several components which are shown in Figures 3-9 and 3-10. The front view of the assembled setup on the drill rig is also depicted in Figure 3-11.

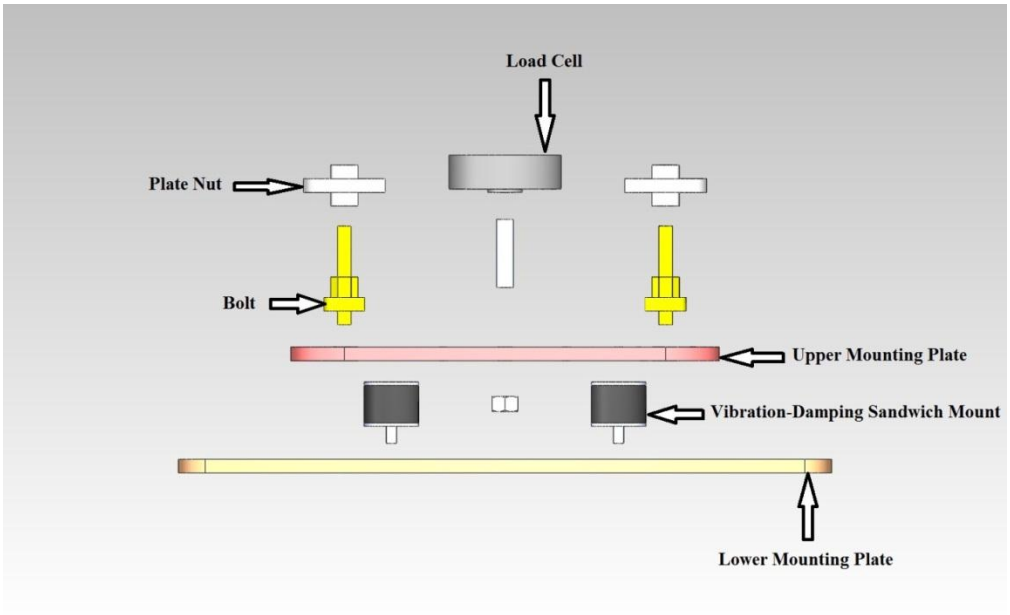

Figure 3-9: Exploded front view of compliance mounting system

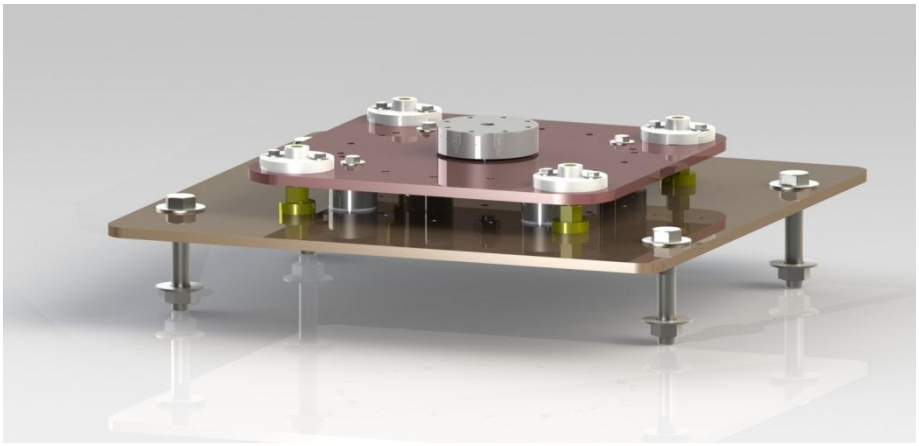

Figure 3-10: Schematic view of compliance mounting setup [20]

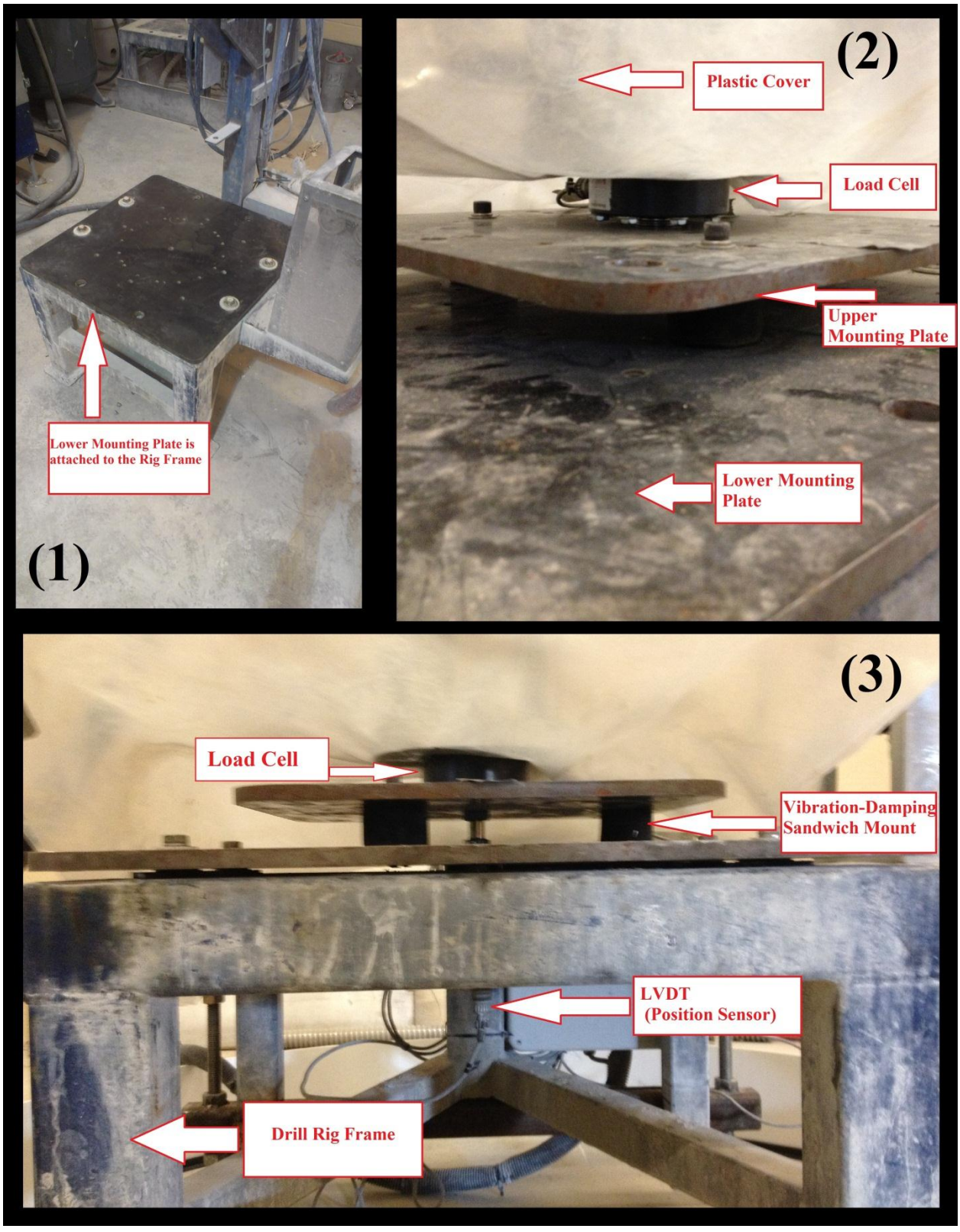

Figure 3-11: Compliance mounting setup on the drill rig

As can be seen in Figure 3-11, there are two plates in this setup (the upper plate and lower plate). In each plate there are several threaded holes for the sandwich mounts to be attached. These holes follow specific patterns that enable us to use different numbers of mounts to get different levels of compliance. Figure 3-12 shows all mounting patterns in one diagram, and Figure 3-13 demonstrates the threaded holes position for some of these patterns in the upper plate.

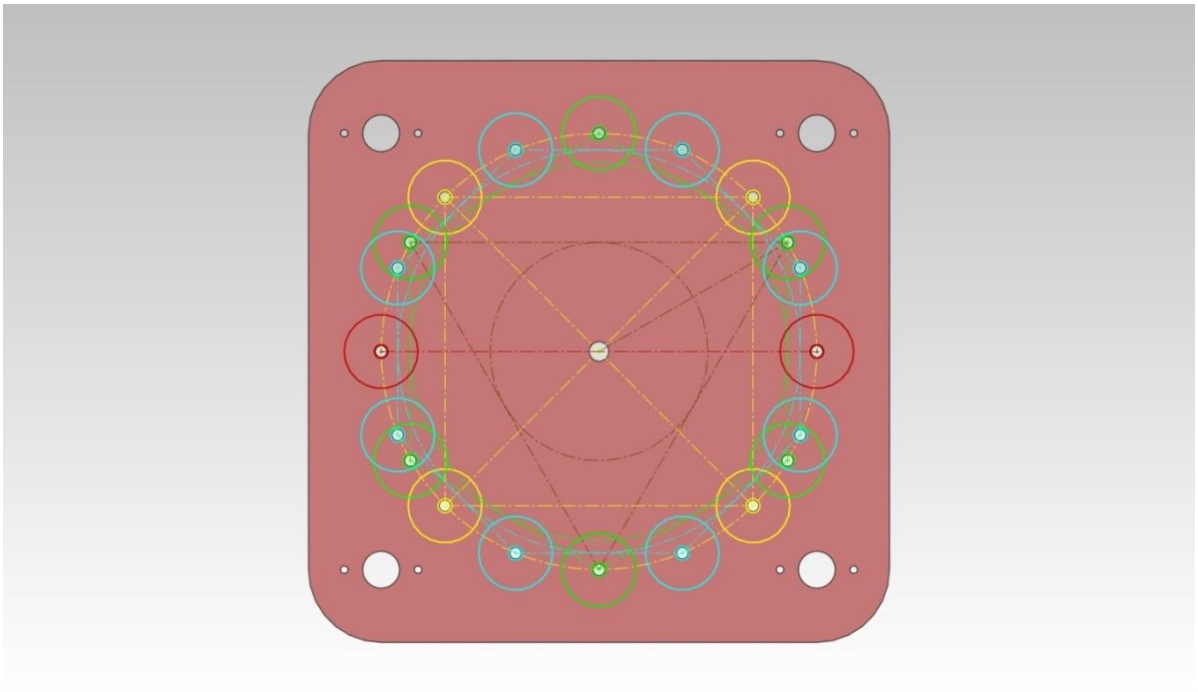

Figure 3-12: Sandwich mounts position patterns

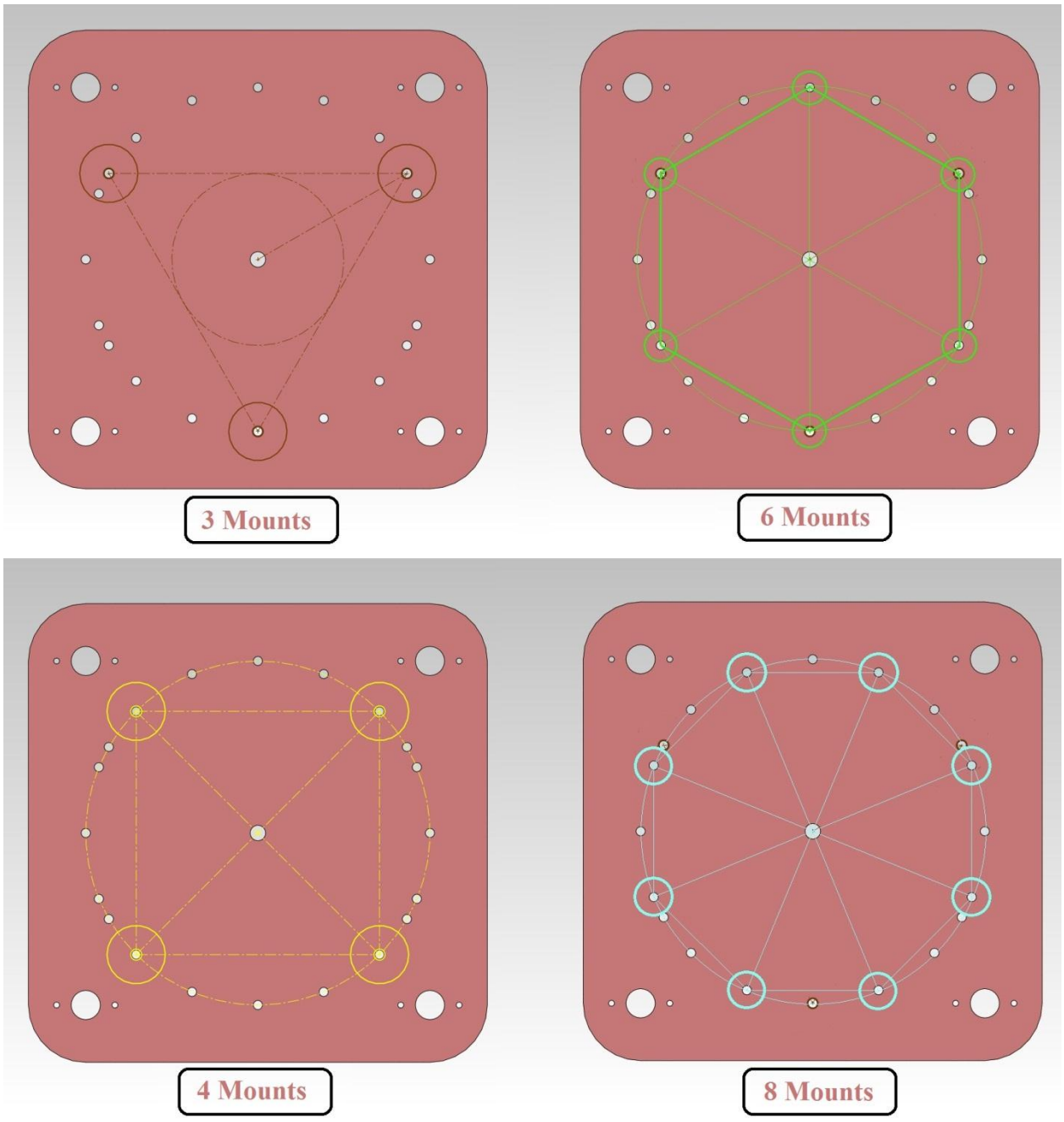

Figure 3-13: Holes position for different patterns in the upper mounting plate

The following figure displays the mounts after they are attached on the lower mounting plate for using 3 and 8 mounts patterns.

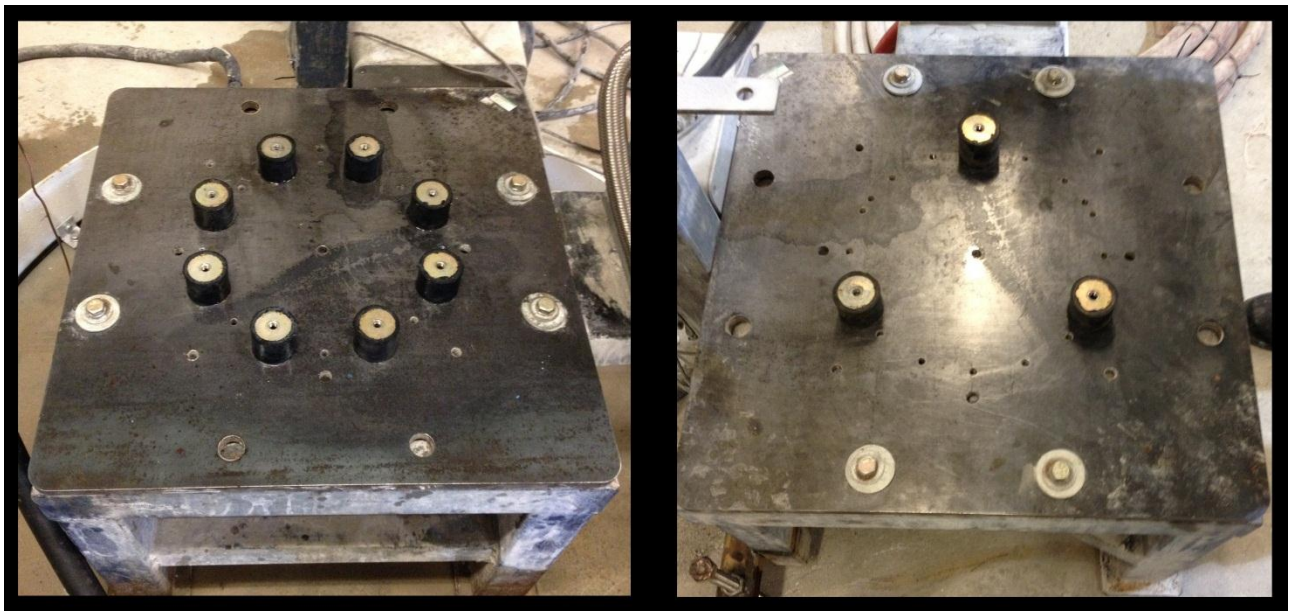

Figure 3-14: Attached mounts on the lower mounting plate

3-1-4-3. Stiffness and Compliance Calculation

Stiffness (k) shows the rigidity of an object; in other words, it indicates the extent to which an object resists deformation in response to an applied force. The inverse of stiffness is compliance which is measured in the unit of meter per newton (m/N) [17]. As discussed in the previous section, to apply axial compliance in the drill setup, sandwich rubber mounts are used in different patterns. This section focuses on the calculation of the stiffness and compliance for these patterns.

Each mount has a specific value for stiffness or compliance which is measured by conducting a test. Moreover, in all used patterns, sandwich mounts are placed side by side each other. Therefore, based on mechanical rules they could be interpreted as parallel

springs. In mechanics, parallel springs can be assumed to be a single spring with higher stiffness [17]. Accordingly, the following formulas are used to calculate the total stiffness and compliance of each pattern.

$$K_{total} = K_1 + K_2 + \ldots + K_n \quad (3\text{-}1)$$

$$1 / C_{total} = 1/C_1 + 1/C_2 + \ldots + 1/C_n \quad (3\text{-}2)$$

where n, K, and C are number of mounts in each pattern, stiffness, and compliance respectively. Since all used mounts in each pattern are identical, the above formula can be rewritten as follows:

$$K_{total} = n \times K \quad (3\text{-}3)$$

$$C_{total} = 1 / K_{total} \quad (3\text{-}4)$$

In order to calculate the stiffness or compliance of each mount, it is placed between two compressing platens of an INSTRON machine and the system is moved gradually downward into the number of positions. At each of these positions, when the system becomes steady, the force and displacement are measured (Figure 3-15). It should be noted that before resting the mount in the INSTRON machine, a bushing is manufactured for the top of the mount to protect its threaded rod from rupture during the loading process (Figure 3-16).

By plotting the measured force versus displacement, and calculating the slope of the resulting curve, the stiffness of the mount can be achieved. The resulting curve is shown in Figure 3-17, as indicated in the graph. The stiffness of the rubber mount is equal to 0.187 kN/mm. Consequently, by having the *k* value for a single mount, and using the equations 3-1 to 3-4, the stiffness and compliance of each pattern is computed (Table 3-2).

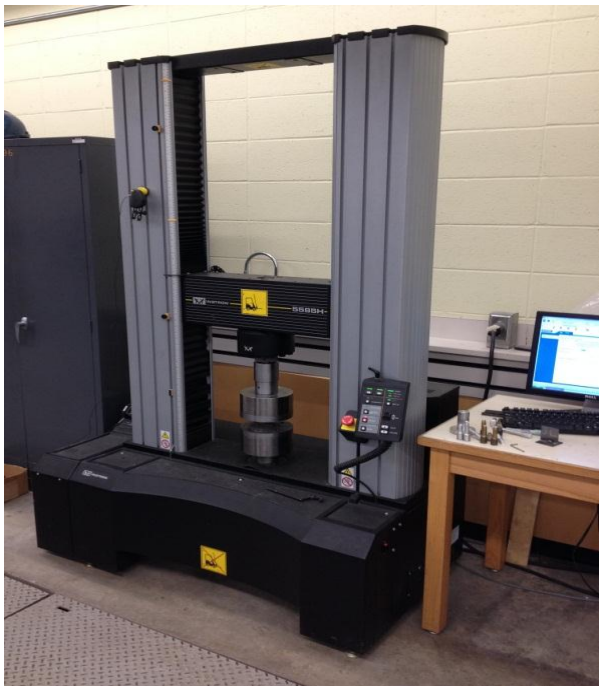

Figure 3-15: INSTRON machine-model 558

Figure 3-16: Rubber mount bushing

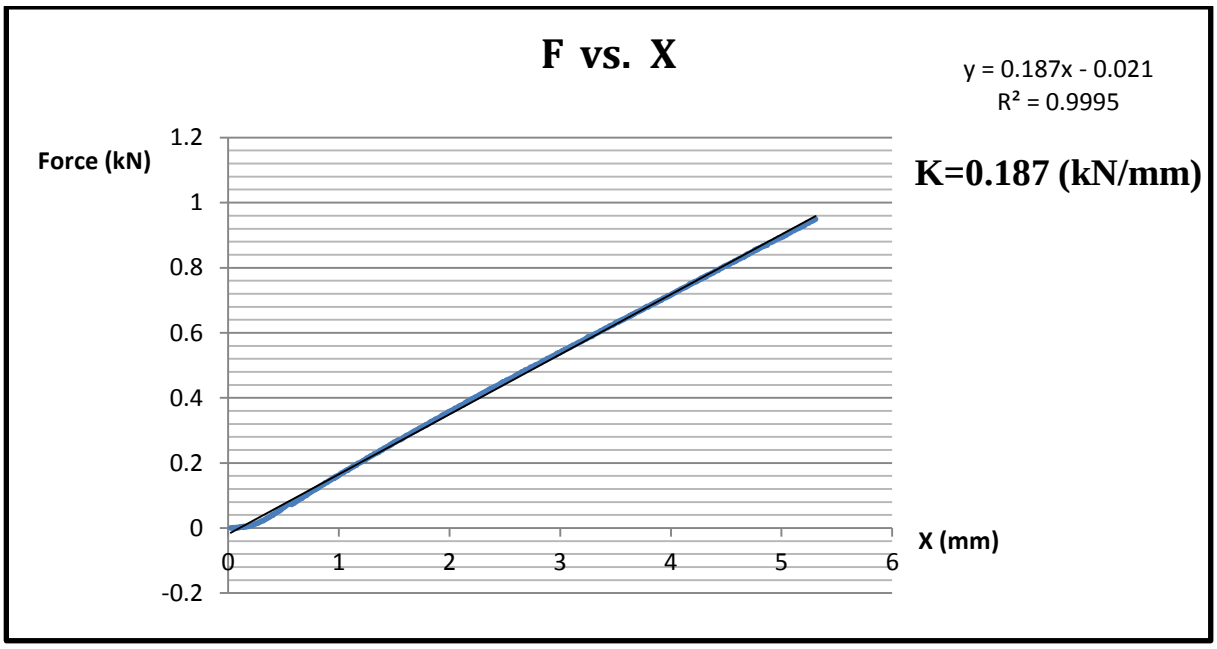

Figure 3-17: Load vs. displacement curve

Table 3-2: Stiffness and compliance values for different mounting patterns

Mounting Pattern	Stiffness (kN/mm)	Compliance (mm/kN)
3 Mounts	0.56	1.78
4 Mounts	0.75	1.33
6 Mounts	1.12	0.89
7 Mounts	1.31	0.76
8 Mounts	1.50	0.67

3-1-5. Sensors and Data Acquisition System

Instrumentation of the SDS includes seven sensors and a data acquisition system which records all the drilling parameters during the whole experiment. Figure 3-18 shows the sensors' position in the drill setup, and Figure 3-19 schematically displays how the sensors are mounted to the frame. As displayed in Figure 3-20 the load cell is installed below the drilling cell to measure the applied load on the rock or the dynamic WOB. The load cell is manufactured by Honeywell company. The maximum capacity of this load cell is 13.34 kN with the accuracy of 9.30 N. Moreover, in order to measure the position of the drilling pipe or the bit a tension string Linear Potentiometer Transducer (LPT) is installed in the drill setup. This LPT is manufactured by celesco company. This sensor can measure the position up to 101.60 cm with the accuracy of 0.15 cm. Figures 3-19 and 3-23 displays how it is attached to the system. Another position sensor which is used in this system is the Linear Variable Displacement Transducer (LVDT) which is placed underneath the upper plate of the mounting system. This is sensor is manufactured by AST Macro sensor company; moreover, it can measure the displacement up to 6.350 mm with the accuracy of 6.3 μm. This sensor shows the movement of the upper mounting plate during the experiment; in other words, it shows the position of the rock at each instant during the penetration. The rock is installed in the drilling cell, and the drilling cell is rigidly attached to the upper plate of the mounting system. Therefore, the position of the upper plate can be interpreted as the position of the rock (Figures 3-19 and 3-25).

In addition, an accelerometer is utilized to record the oscillation of the drill pipe during penetration. Figure 3-24 shows how this sensor is installed above the drill head. Two pressure sensors (pressure transducer) are used to measure the pressure of the fluid in the system. One of them is located right before the inlet of the swivel which shows the inlet fluid pressure. This sensor is manufactured by General Electric company. The maximum capacity of this sensor is 68950 kPa with the accuracy of 28 kPa (Figure 3-22). The other pressure sensor is located at the outlet hose of the load cell which shows the pressure of the drilling cell. This sensor is manufactured by Endress and Hauser company. The maximum capacity of this sensor is 4000 kPa with the accuracy of 20 kPa (Figure 3-21). To calculate the MSE of the drilling process, a calculation of the power consumption of the drill head is needed. Therefore, an amperemeter is used to record the motor current of the drill head. The amperemeter is manufactured by Milwaukee company with maximum capacity of 30 A (Figure 3-24). (Details of the MSE calculation are explained in Section 5-3). Finally a DAQ system with a sampling rate of 1000 Hz is used to record all the delivered data from the system (Figure 3-26).

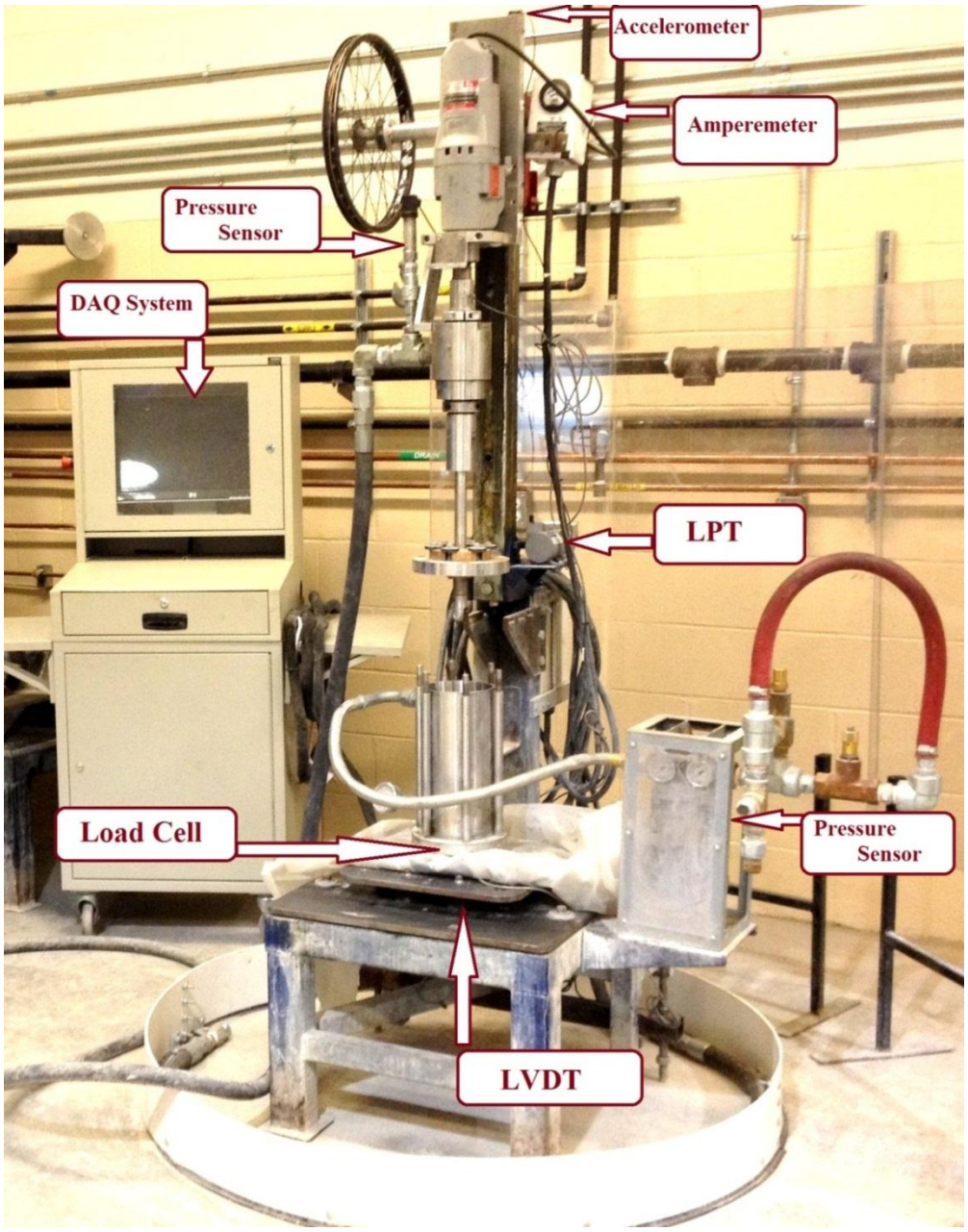

Figure 3-18: Sensor positions in drill setup

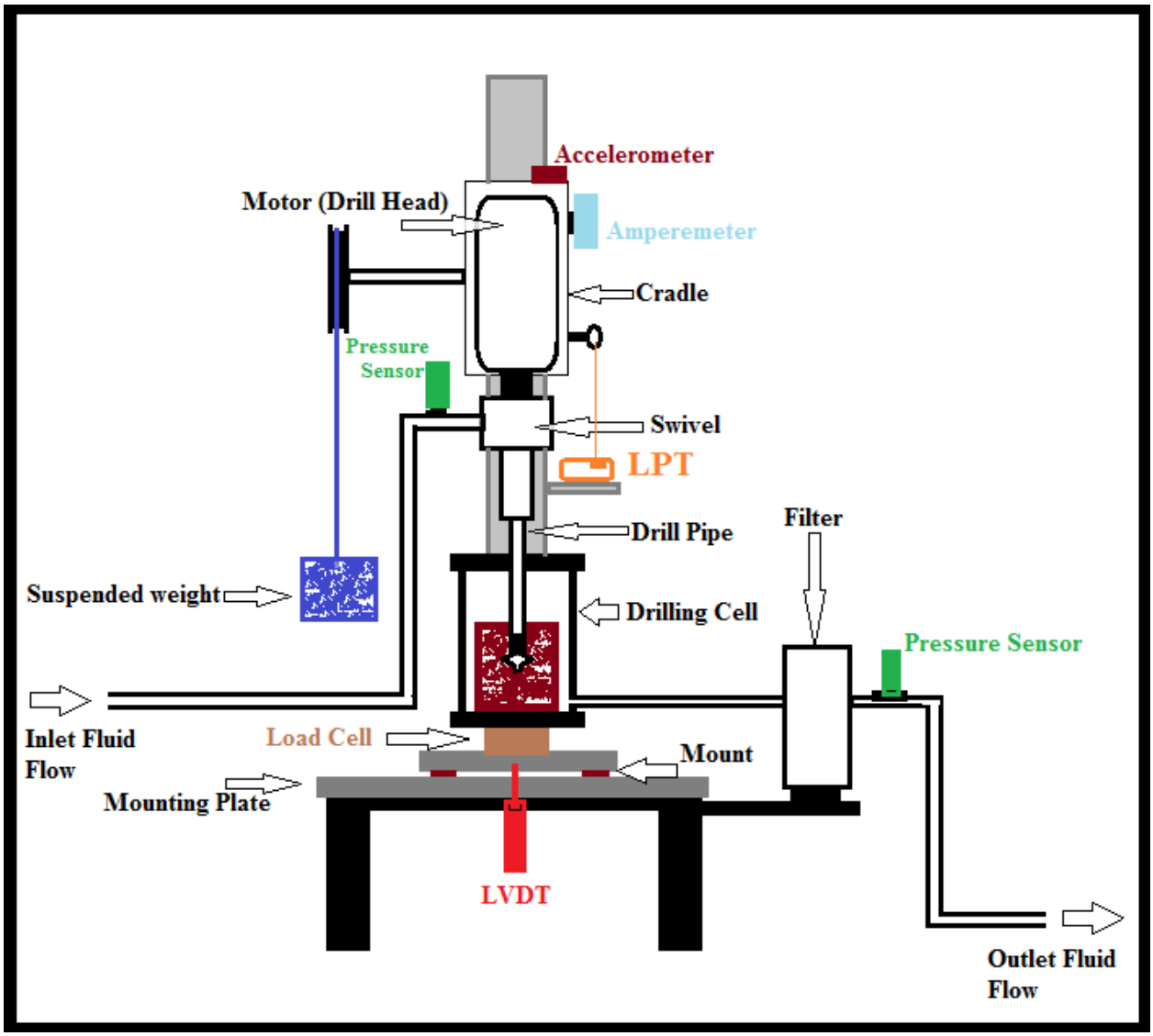

Figure 3-19: Mounting position of the sensors

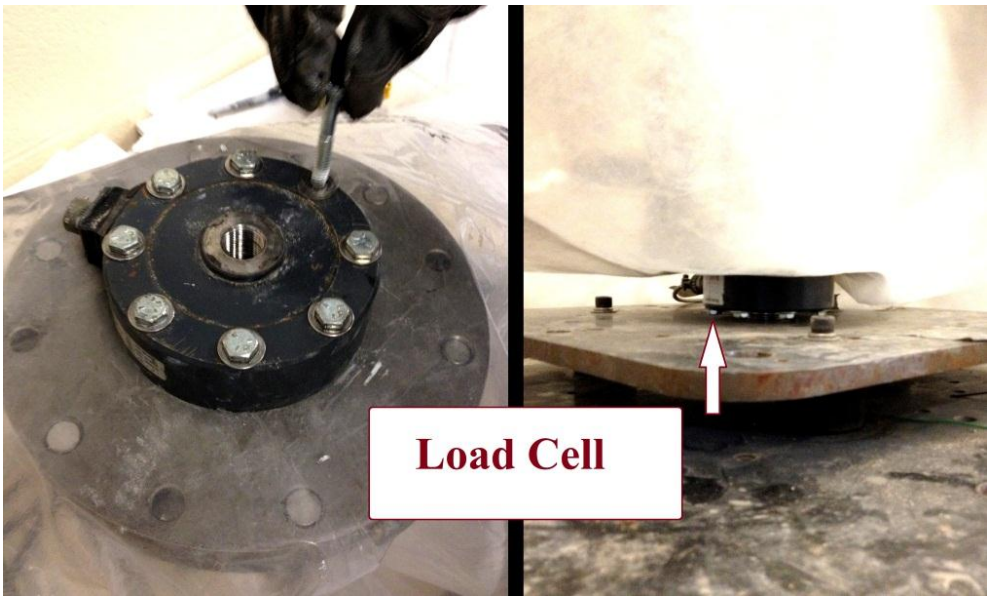

Figure 3-20: Load cell underneath the drilling cell

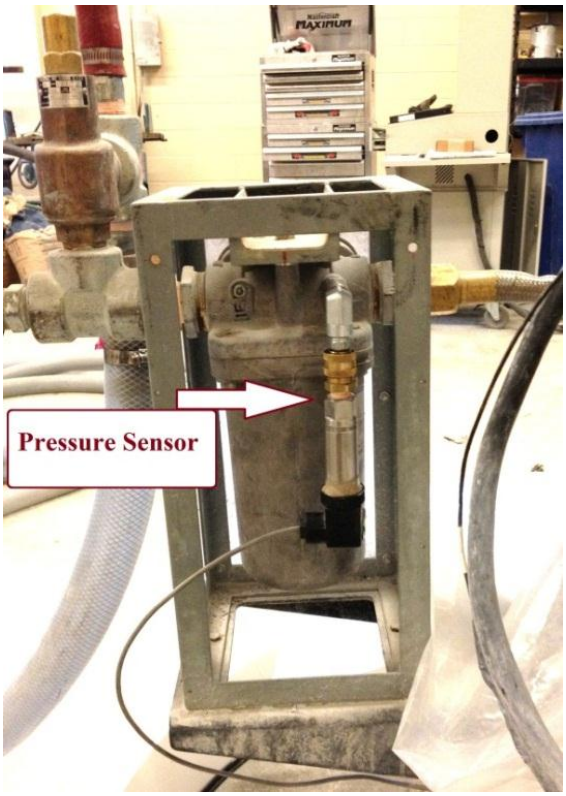

Figure 3-21: Pressure sensor at outlet hose of the drilling cell

Figure 3-22: Pressure sensor before the swivel

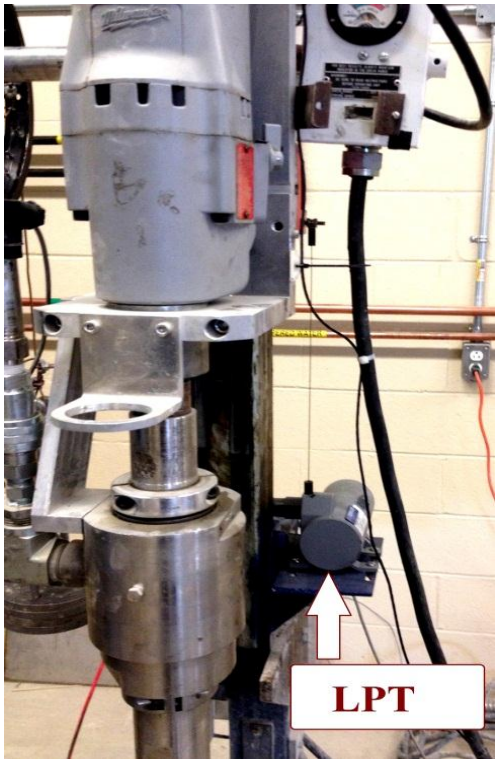

Figure 3-23: Linear potentiometer transducer (LPT)

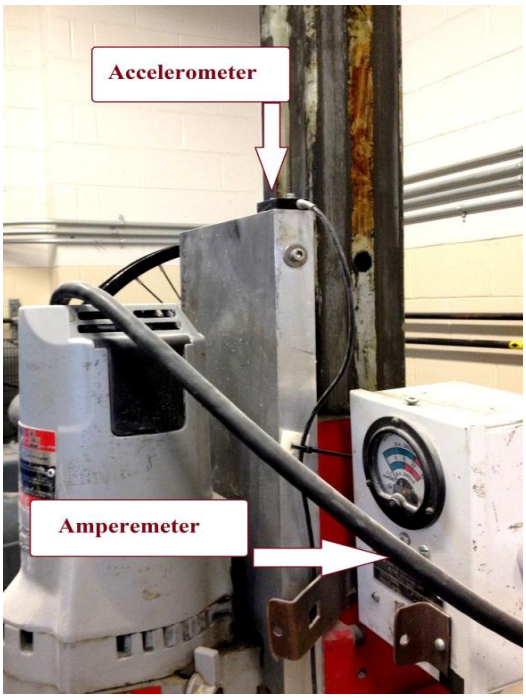

Figure 3-24: Accelerometer and amperemeter

Figure 3-25: LVDT (position sensor) attached to the upper mounting plate

Figure 3-26: DAQ system monitor

3-1-6. Drilling Cell

The drilling cell is used to simulate the down-hole drilling condition. The main features of the down-hole condition are high BHP due to the fluid column and a high nozzle flow rate. This drilling cell is designed to tolerate pressure up to 2500kPa with a safety factor of 1.5. As shown in Figure 3-27, to build the BHP, an adjustable relief valve and needle valve are used in the outlet line of the drilling cell. It should be noted that the outlet fluid line of the drilling cell always contains some rock fragments and contaminants. These fragments which are known as cuttings are trapped in the filter which is installed before the relief valve, although the relief valve is capable of passing these fragments. Figure 3-27 shows the exact location of the filter and valves in this setup.

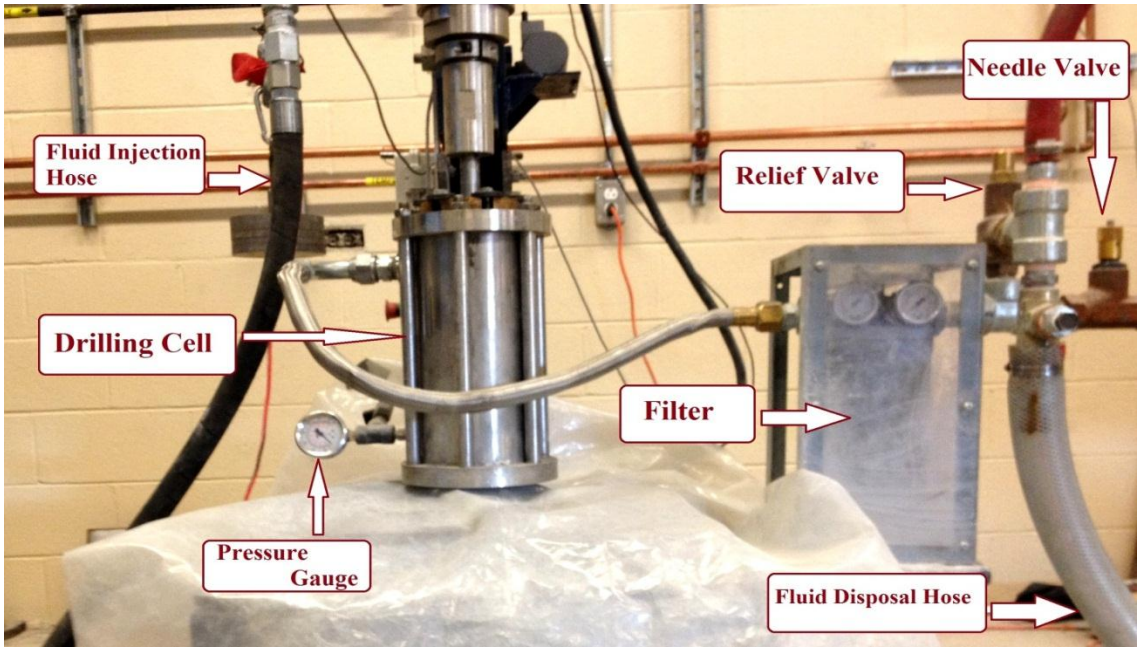

Figure 3-27: Assembled drilling cell

The rock specimen needs to be installed in the drilling cell before building up the pressure in the cell. A plate which is called the specimen holder does this task. This plate clamps the rock sample at the bottom and center of the cell (Figure 3-28). In addition, there is an O-ring at the center and bottom of the rock which protects this part of the rock from exposure to the high pressure of the drilling cell. Through this system the rock filtrates can be exposed to atmospheric pressure. This means that the far field pore pressure of the rock equals zero.

Figure 3-28 shows a transparent view of the drilling cell and all its internal components. As displayed in this figure the rock specimen should be placed in the appropriate chamber to build the pressure inside the cell. Figure 3-29 shows more clearly how the rock sample is installed at the center of the bottom cap. It also depicts how the tie rods are used to assemble the upper cap, lower cap, and the shell of the cell as one unit. The rock to be installed in the cell should not be larger than 100 mm in diameter and 150 mm in length. Therefore, all casted samples are cut into the right size before use in the drilling cell.

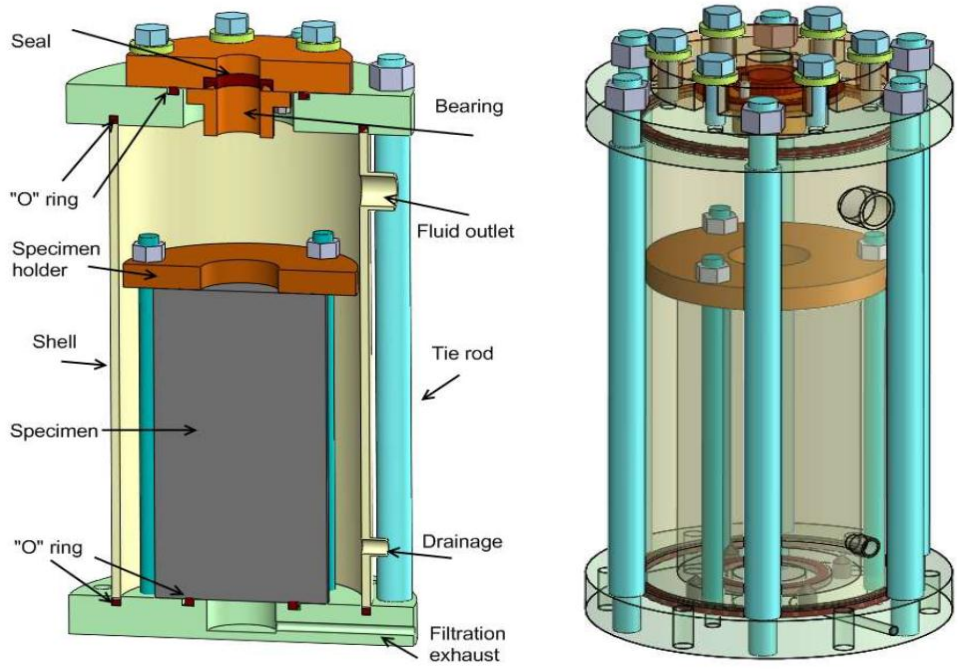

Figure 3-28: Assembled drilling cell [7]

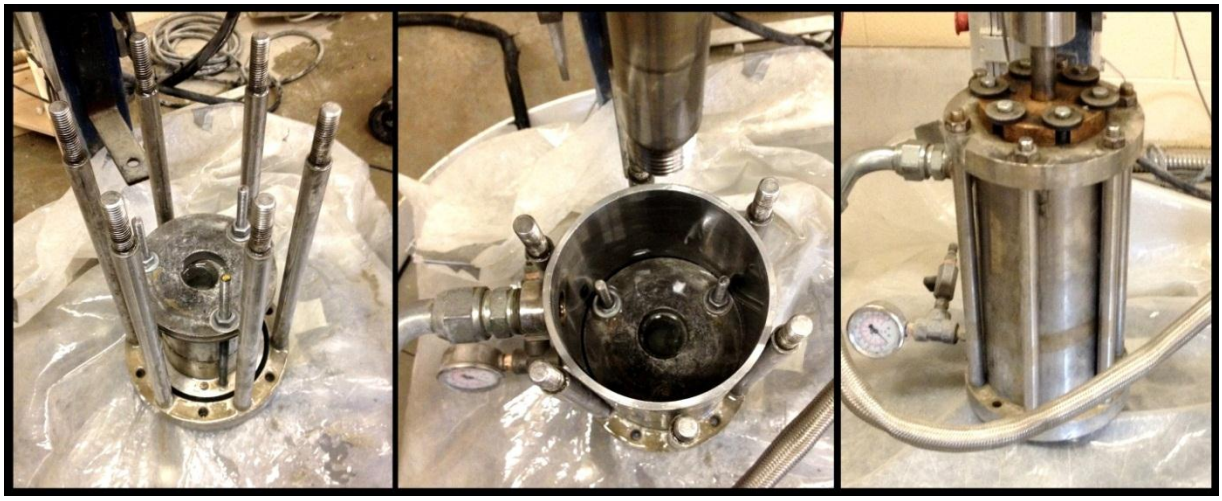

Figure 3-29: Opened drilling cell

To drill the rock specimen a drill pipe is passed right through the center of the upper cap. A PDC drill bit with a diameter of 35 mm is attached to the end of this drill pipe. The

drill pipe itself has the OD of 24 mm and the ID of 10 mm. It is centralized and sealed in the cell using a bearing and V-rip rotary sealing (Figure 3-30) [7]. It should be mentioned that two O-rings are used in the upper and lower cap of the cell to fully seal the drilling cell (Figure 3-28).

Figure 3-30: Drill bit condition in the drilling cell

3-1-7. PDC Drill Bit Configuration

The bit which is used in the experiments has two PDC cutters, and the diameter of the bit is 35 mm. This PDC bit previously used in other experiments; however, it is not a worn bit since it has not been used in hard and abrasive rocks. Therefore the condition of cutters and chamfer is very good. As displayed in Figure 3-31, the cutters are joined to a shank with the face angle of 25^{o} and back rake angle of 25^{o}. Also the cutter has a chamfer

with the back rake angle of 75^{o} [7]. As displayed in the figure below and discussed earlier in Chapter 2, the PDC cutter has two regions of penetration. The first one is penetration under the depth of chamfer, and the other one is penetration above the depth of the chamfer with the cutter face. The depth of chamfer in this bit is 0.15mm. Moreover, in order to clean the cuttings which are produced by the bit cutters, two identical nozzles are located on the body of the bit. These nozzles are designed as a coupling to attach the bit to the drill pipe. The nozzle configuration is also displayed in Figure 3-31.

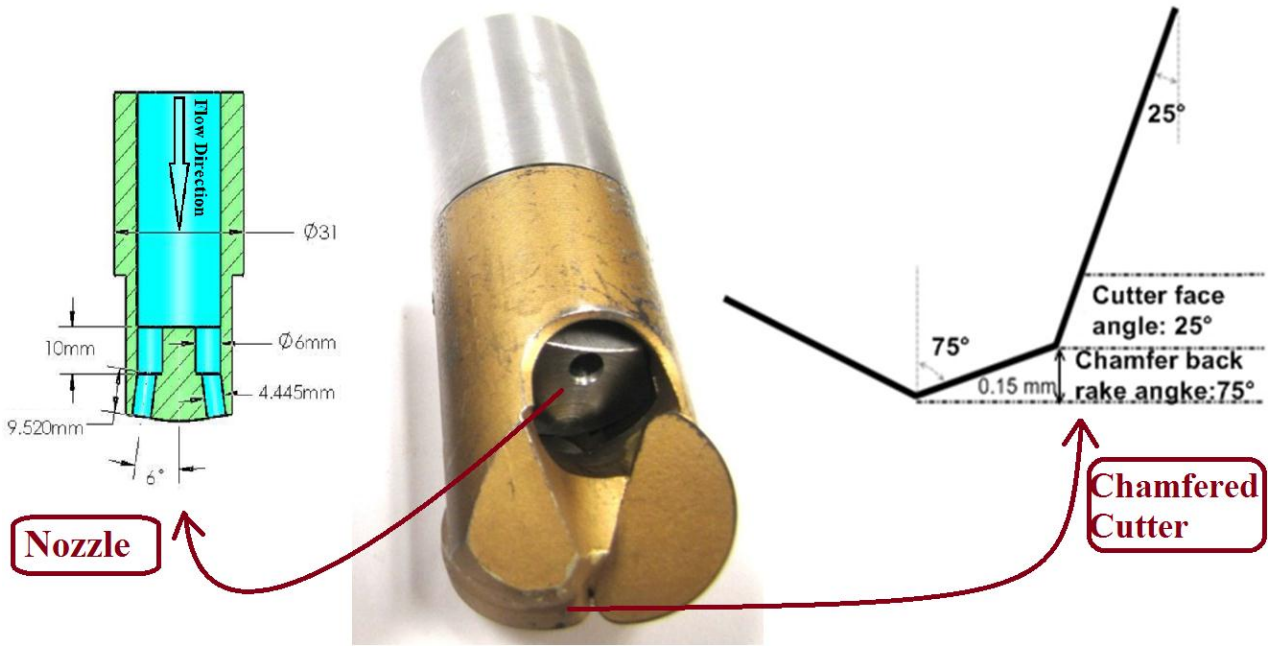

Figure 3-31: PDC bit, its cutter, and its nozzle configuration

CHAPTER 4

4. Preparation and Characterization of Rock Specimen

This chapter explains the procedure for casting rock samples. Moreover, it describes the curing, preparation, and characterization processes of these samples before they were used in the drilling tests. A fine grained concrete is used instead of natural rocks due to the high level of reproducibility of strength and other material properties. A separate study by Zhang [58] developed these rock-like materials and validated their use for drilling experiments.

4-1. Mixing Design of Concrete Slurry

Concrete slurry with a specific design is used to make the rock samples. The slurry includes sand, concrete, water, and super plasticizer. The ratio and percentage of these materials in the concrete slurry is shown in the table below. It should be noted that the sand used contains different types of aggregate. The detailed petrographic information and grain size distribution of these aggregates can be found in appendices A and B.

Table 4-1: Material percentage in concrete slurry [58]

Material	Percentage in Slurry	Ratio (Sand : Cement : Water)
Sand	67.45	3
Cement	22.45	1
Water	10.10	0.45
Super plasticizer	600 ml of Daracem19A* is used per 100 kg of cement	

*[13]

4-2. Casting Procedure

Before mixing the materials we should make sure that all cement materials are kept in a dry place and at a room temperature between 20^{o} to 30^{o}C. Then the moisture content of the aggregates should be calculated and subtracted from the required amount of water base in the design formula. In order to calculate the moisture content of the aggregates, a sample of sand (aggregates) with the specific mass, wet weight, is placed in the oven for a certain amount of time to evaporate all moisture content in it. After the sample becomes completely dry and its weight does not change anymore, it is weighed again. This new weight is called the dry weight. The difference between wet and dry weights gives the

exact amount of water. Also, the percentage of moisture content in the aggregates can be calculated as follows:

$$\text{moisture content percentage} = \frac{\text{mass of wet aggregate} - \text{mass of dry aggregate}}{\text{mass of wet aggregate}} \times 100 \qquad (4\text{-}1)$$

The next step is putting the sand, cement, and water in the mixing machine. First the sand and cement are put in the mixer, and the mixer rotates for one minute. Then water is added and rotation of the mixer continues for the next 3 minutes. After this mixing period, the mixture rests for 2 minutes. After the rest period, the mixing continues for the next 5 minutes and the super plasticizer is added to the mixture. It should be noted that during the resting period the mixture is covered by a plastic cover to avoid any water evaporation. After adding super plasticizer (Daracem 19A) the mixer mixes the cement slurry for 2 more minutes. Finally, the mixture is ready to be molded.

When the concrete mixture is ready, it is molded into the plastic molds which have a 20 cm height and 10 cm diameter (Figure 4-1). Then an internal vibration rod is placed inside each mold for 50 seconds to remove the air from the mixture and minimize the void space in the concrete matrix. Finally, the mold caps cover the head of each mold to prevent water evaporating from the molded slurry.

Figure 4-1: Mixing and molding the concrete slurry

4-3. Curing and Cutting Procedure

The curing procedure starts right after the concrete slurry is molded. For the first 24 hours the casted concrete samples should be kept at the temperature of 23±2℃ without any contact with water. After that, specimens are removed from the mold and kept under saturated lime water at 23±2℃ for the next 10 weeks (Figures 4-2 and 4-3). In order to

make the saturated lime water the hydrate lime is added to the water in the water tank. Then all casted samples are placed in the tank.

Figure 4-2: Resting the rock specimens in the saturated lime

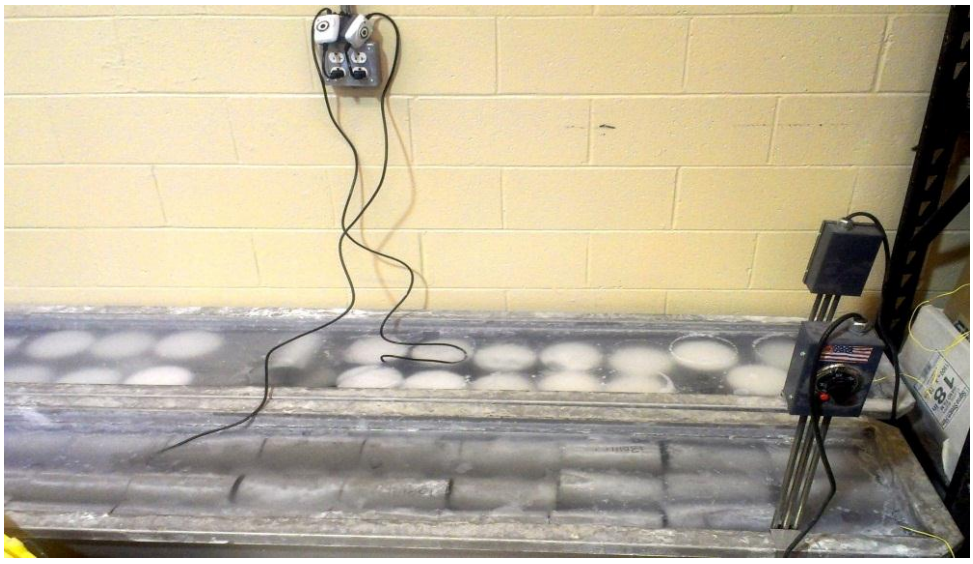

Figure 4-3: Temperature control of the water tank with automatic heaters (temperature: 23±2℃ in the curing period)

Five weeks after placing the samples in the water tank they were brought out from the tank for a short time. They were cut in half and then placed in the tank for the rest of the curing period. The samples were cut to fit the specific design of drilling cell; indeed, only samples with a specific height and diameter can fit in the drilling cell. Therefore, the height of each sample has to be modified before using it in the test. Figure 4-4 shows how the samples were cut in half using a circular saw.

Figure 4-4: Cutting casted rock specimens with circular saw (sample size: diameter=10cm & height=10cm)

4-4. Rock Specimen Characterization

In order to measure the physical properties of the rock specimen, several core plugs were produced from the center of the prepared rock specimens. After preparing the core plugs, the Unconfined Compressive Strength (UCS) and Confined Compressive Strength (CCS) tests were conducted on them based on American Society for Testing and Materials standard (ASTM) [29]. Figure 4-5 displays the Mohr-Coulomb graph for these tests. In addition, Table 4-2 shows the results of these tests and other measured properties of the rock specimen. It should be noted that the uncertainty of the reported results is 2 % [58].

Table 4-2: Physical properties of rock specimen [58]

USC	**55 MPa**
CCS^1 (at σ3 = 3 MPa)	**75 MPa**
CCS^2 (at σ3 = 6 Mpa)	**85 MPa**
Young's Modulus	**7.3 GPa**
Density	**2314 kg/m^3**
Friction Angle	**40 °**
Cohesion	**13 MPa**

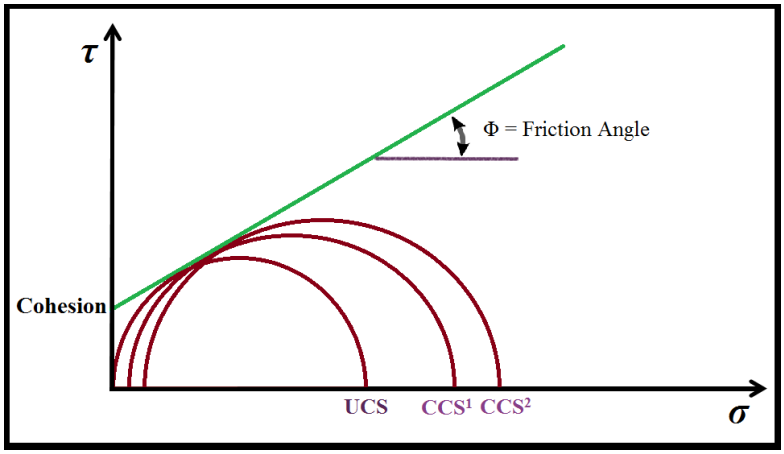

Figure 4-5: Mohr-Coulomb graph [58]

CHAPTER 5

5. Design of Experiment

This chapter describes the test matrix; it also explains the exact procedure of conducting experiments. Furthermore, it illuminates the method of data analysis and clarifies the formulas used. Finally a table of experimental results is given with analysis in the next chapter.

5-1. Design of Test Matrix

The goal of this laboratory study is to investigate the effect of the axial compliance element on rock penetration, especially the ROP. Indeed, the main question which this study attempts to answer is whether changing the level of compliance in the system has

any effect on the ROP. Therefore, the tests matrix is designed in a way firstly to answer this question and secondly make any conclusion reliable.

The main input variables of these tests are the level of compliance (number of mounts) and the WOB. The BHP (pressure of the drilling cell) is also changed as another variable in the tests' matrix to make the results more comprehensive.

As discussed in Chapters 1 and 3, when drilling with the PDC bit there are two distinct modes of penetration based on DOC. The first mode happens when the DOC is completely or almost under the depth of chamfer, and the second mode happens when the DOC is greater than the depth of chamfer. In the former mode, the bit's chamfer plays the main role in rock penetration and in the latter the bit's cutter face does this task.

In this laboratory research, the focus of experiments is on the second mode, because this mode (drilling above the depth of chamfer) is more probable in efficient field drilling and is our zone of interest to study.

In the zone of interest, the compliance of the mounting system is changed using 6 levels. These levels are achieved by using 3, 4, 6, 7, and 8 mounts plus the complete rigid system. As described in Chapter 3, these various mounts lead to different levels of compliance in the system. In addition, the WOB was not constant for all tests; indeed, it was changed with 3 levels, up to 2.3 kN which is the maximum limit that can be applied to the drill setup. The BHP was also changed in the range of 130 to 1400 kPa. Moreover,

the RPM of the rotary head was constant and is estimated to be 500 for all tests. Finally, the ROP, MSE, and rock displacement in each test were evaluated as the major outcomes of the experiment. Further explanation of the test results is provided in Chapter 6.

5-2. Drilling Test Procedure

This section of Chapter 5 describes the exact method of conducting the drill test experiment. As indicated before, in these experiments there are four factors which need to be adjusted before each run. These factors are i) mounting pattern (system compliance), ii) WOB, iii) flow rate, and iv) BHP. Consequently, the first step is connecting the exact number of mounts to the mounting plates (further explanation about the compliance mounting system is covered in Section 3.1.4). After adjustment of the mounting system and installation of the rock specimen in the drilling cell, the water pump is set to the specific level of flow rate in order to direct the flow into the drilling cell. Afterwards, in order to apply WOB a specific number of mass disks are added to the loading system. Finally, an adjustment is performed on the relief valve to apply pressure in the drilling cell. It should be noted that all adjustments in flow rate, pressure, WOB, and compliance are carried out in reference to the test matrix.

The next step is predrilling the rock specimen. The predrill for 15 mm depth causes all surfaces of the bit to meet the rock surface which makes the drilling results more accurate [7]. Ten seconds before starting the penetration, the bit is kept off bottom. Then the circulation system and drill head are turned on. Right after that the data acquisition

system is set to recording mode in order to record all the delivered data with sampling rate of 1000 Hz. Finally the rotary head is slowly released and the bit contacts the rock specimen. After the sample is completely drilled, the pump and rotary head are turned off. Finally, the recording mode of the DAQ system is stopped for subsequent adjustments of the test.

5-3. Experimental Data Analysis

As stated before, the ROP is one the main factors in analysing the test results. In order to find the ROP of a test, the position of the drill pipe is plotted versus time. The slope of the resulting curve gives the ROP. It should be noted that the evaluation of the recorded data starts after 5 seconds of penetration. This lapse is needed for the drill bit to reach the steady state condition in penetration. The position of the drill pipe is measured by an LPT, as described in Section 3.1.5.

Another output of this experiment is the rock displacement which is recorded by the LVDT located underneath the drilling cell. The LVDT gives the position of rock specimen at each instant. Knowing the position of the rock at each moment enables us to calculate the rock displacement during each test.

Mechanical specific energy (MSE) is the other parameter which is considered in the test results analyses. MSE, (J/m^3), is defined as the amount of energy (J) spent removing a unit volume of rock, V_{rock}, (m^3) [57]. The unit of MSE is N/m^2 (Pa) like the strength of a

rock. The MSE also can be defined as the apparent strength of a rock that is penetrated by the bit. One way to calculate the MSE is using the Mechanical Specific Power (MSP) of the bit. The MSP of a bit is the ratio of transmitted power to the bit to bit area. In addition, the ratio of the MSP to MSE gives the ROP. Therefore, by having the ROP and MSP, the MSE can be calculated (Equation 5-2) [57].

Subtracting the power consumption of the drill head during penetration from its power consumption when the bit is off bottom (before penetration) gives the power consumption of the bit itself. In order to compute the power consumption of the drill head, the recorded current of the amperemeter is multiplied by the voltage which is measured as 122.5 V. Furthermore, it is assumed that the drill head motor has an efficiency of 90%. The average efficiency of motors varies with the size of the motor and the size of the load being driven; moreover, the peak efficiency is often reached at or near the full load. The typical motor efficiencies for electrical motors can be assumed base on their maximum mechanical output power [7, 59, 60]. Accordingly, is our case the drill head efficiency is assumed to be 90% which means that only 90% of nominal mechanical power is delivered to the drill pipe. Therefore this 90% mechanical efficiency is applied in all calculations. Note that, since this motor efficiency has been assumed and not measured, the discussion of MSE results is qualitative, and no quantitative analysis of the MSE results is given.

In summary, the MSE of a test can be calculated with the following formulas. As indicated below, the total MSE is the summation of torsional MSE and the MSE which results from the WOB. Torsional MSE is estimated by dividing the bit specific power by the ROP, and the MSE resulting from the WOB is calculated by dividing the WOB by the area of the bit.

$$ROP = (MRR) / (A_{bit}) \quad (5\text{-}1)$$

$$ROP = MSP / MSE \quad (5\text{-}2)$$

$$Total\ MSE = \frac{(Power\ Consumption\ of\ the\ Bit)}{Drill\ Bit\ Area * ROP} + \frac{(WOB)}{Drill\ Bit\ Area} \quad (5\text{-}3)$$

5-4. Table of Experimental Results

As previously stated, the major outcomes of these experiments are the ROP, MSE, and rock displacement. Table 5-1 shows full experimental results. Further explanation of the test results is provided in Chapter 6.

Table 5-1: Results of experiments

Flow Rate *(L/min)*	BHP *(kPa)*	WOB *(kN)*	No. of Mounts	Compliance *(mm/kN)*	ROP *(m/hr)*	MSE *(MPa)*	Rock Displacement *(mm)*
98.5	138	1.97	0	0	7.73	353	N/A
			8	0.67	7.95	324	0.04
			7	0.76	9.04	272	0.05
			6	0.89	8.36	305	0.06
			4	1.33	7.98	371	0.08
			3	1.78	7.76	399	0.09
		2.13	0	0	9.77	341	N/A
			8	0.67	12.95	301	0.04
			7	0.76	16.34	208	0.06
			6	0.89	13.89	232	0.07
			4	1.33	12.10	325	0.08
			3	1.78	10.53	359	0.09
		2.30	0	0	10.56	313	N/A
			8	0.67	14.95	245	0.05
			7	0.76	18.68	190	0.07
			6	0.89	18.17	210	0.08
			4	1.33	13.40	284	0.09
			3	1.78	11.52	344	0.10
	1378	1.97	0	0	3.36	689	N/A
			8	0.67	4.83	468	0.04
			7	0.76	6.40	379	0.05
			6	0.89	5.26	610	0.06
			4	1.33	3.93	660	0.08
			3	1.78	3.55	695	0.09
		2.13	0	0	3.90	640	N/A
			8	0.67	5.33	441	0.04
			7	0.76	7.55	319	0.05
			6	0.89	6.54	505	0.06
			4	1.33	4.56	620	0.08
			3	1.78	4.17	641	0.09
		2.30	0	0	4.33	613	N/A
			8	0.67	6.89	394	0.04
			7	0.76	8.38	303	0.05
			6	0.89	7.22	402	0.07
			4	1.33	5.78	528	0.09
			3	1.78	4.92	606	0.10

CHAPTER 6

6. Analysis and Discussion of the Experiments

This chapter presents analysis of the results of the experiments; it also explains the influential factors in the test results. In addition, the analysed results are further discussed in this chapter to propose the phenomena which occurred in the tests.

6-1. Results of Experiment

The experiment results are in terms of ROP and MSE. For instance, Figure 6-1 shows the ROP curves versus WOB for selected levels of compliance. As can be seen, part of this graph is placed between two vertical lines. As explained in Chapter 5, this section is our

zone of interest in this study because the DOC is almost double the depth of chamfer in this zone, and the cutter face plays the main role in rock penetration, as happens in normal field drilling.

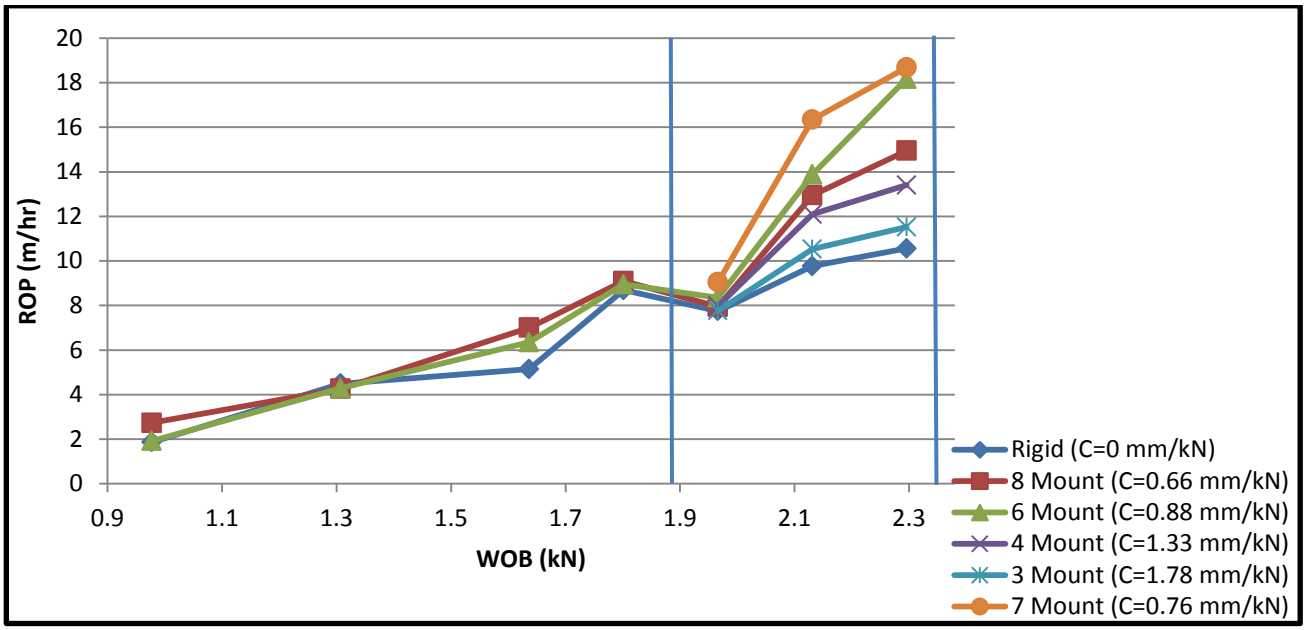

Figure 6-1: ROP vs. WOB and compliance at BHP=138 kPa

There is a direct relationship between the DOC and the ROP. In fact, by having the ROP and dividing it by the RPM, the DOC can be calculated. Figures 6-2 and 6-3 display the ROP and DOC curves in the zone of interest versus WOB for selected levels of compliance, respectively. The blue dash line in Figure 6-3 shows the depth of chamfer which is equal to 0.15 mm.

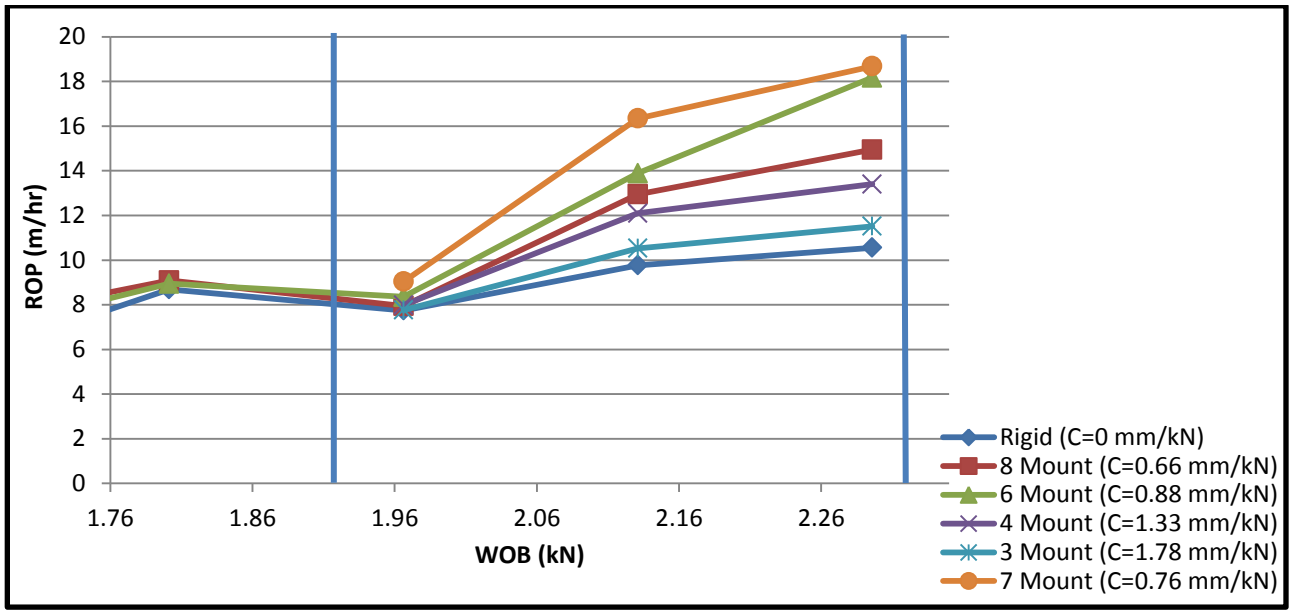

Figure 6-2: ROP vs. WOB and compliance at BHP=138 kPa

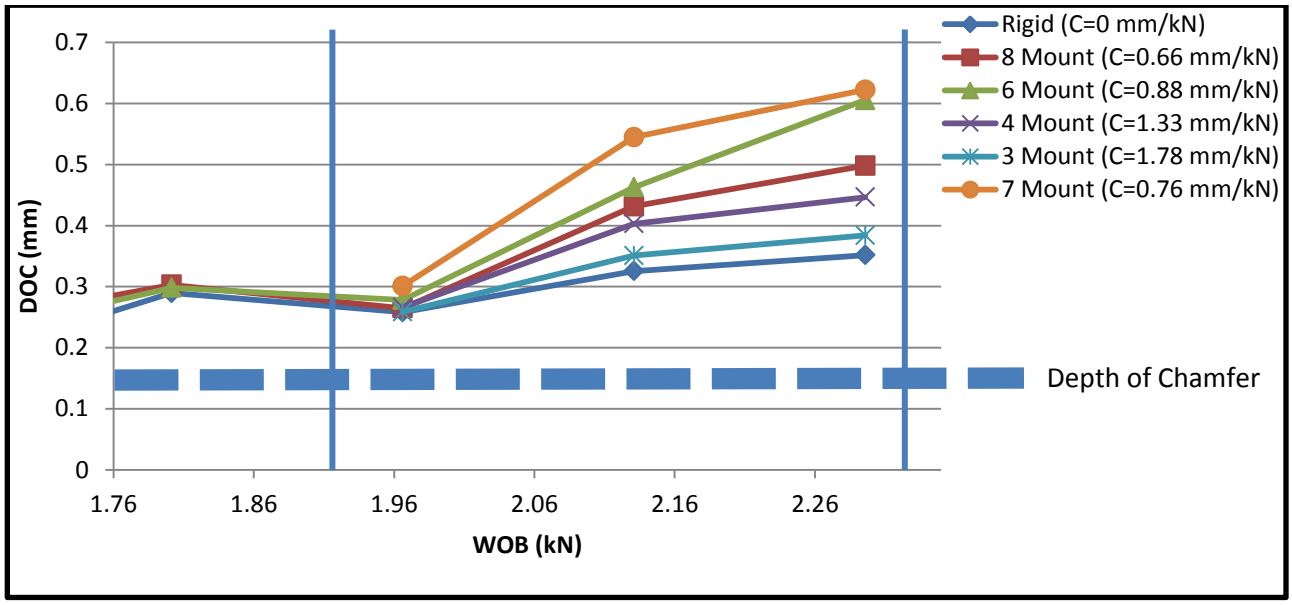

Figure 6-3: DOC vs. WOB and compliance at BHP=138 kPa

As displayed in Figure 6-2, at each specific level of WOB the ROP changes by altering the number of mounts (changing the level of compliance in the system). Figure 6-4

demonstrates the ROP versus compliance for selected levels of WOB. As can be seen, decreasing the compliance of the system down to an optimal level results in an increase in the ROP; however, making the system more rigid than that optimal level causes a drop in the ROP. Moreover, this figure demonstrates that increasing the WOB at a constant level of compliance leads to a rise in the ROP.

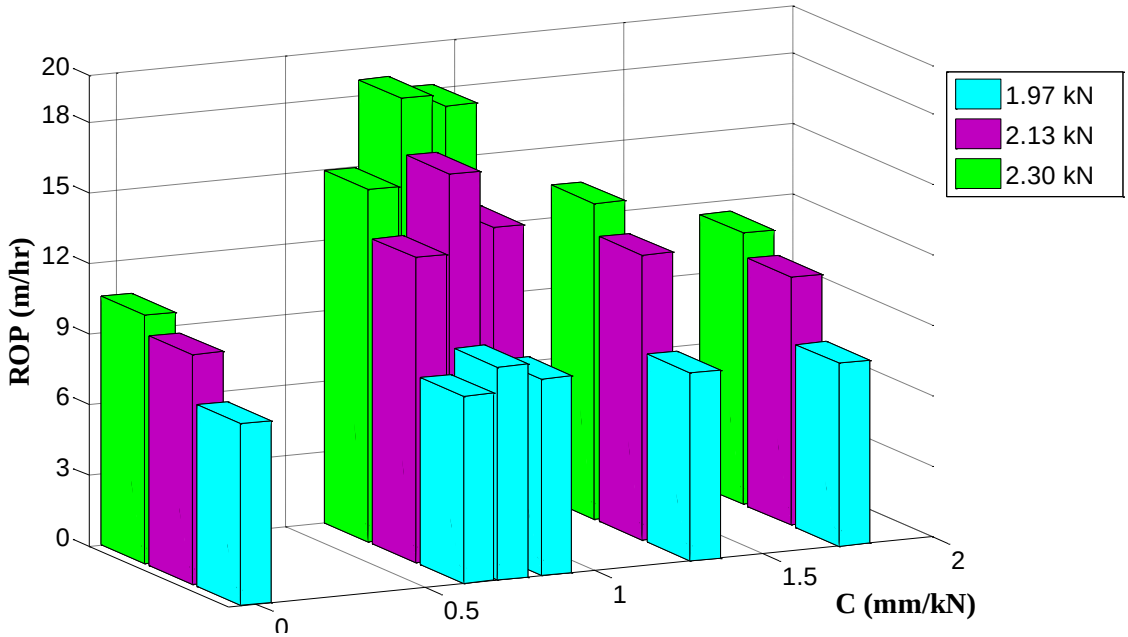

Figure 6-4: ROP vs. compliance at BHP=138 kPa & 3 WOBs (1.97, 2.13, and 2.30 kN)

Figure 6-5 illustrates the MSE versus compliance for selected levels of WOB. As shown in this figure, the MSE varies in an inverse trend of the ROP with respect to the level of compliance. In other words, the highest points of the ROP graphs correspond to the lowest points of the MSE graphs at all levels of WOB, which is the expected outcome.

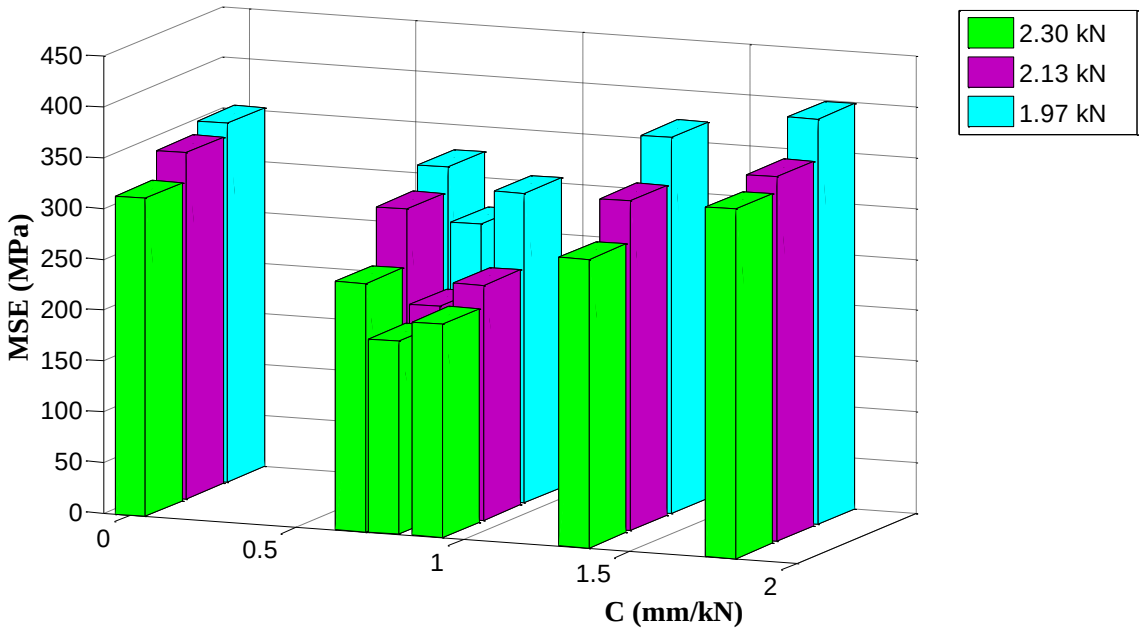

Figure 6-5: MSE vs. compliance at BHP=138 kPa & 3 WOBs (1.97, 2.13, and 2.30 kN)

In order to make any conclusion from the experiments more extended and reliable, the same series of tests was conducted at a high BHP. The pressure of the drilling cell was adjusted to 200 psi for these tests. Figure 6-6 shows the ROP curves versus WOB for selected levels of compliance at high BHP.

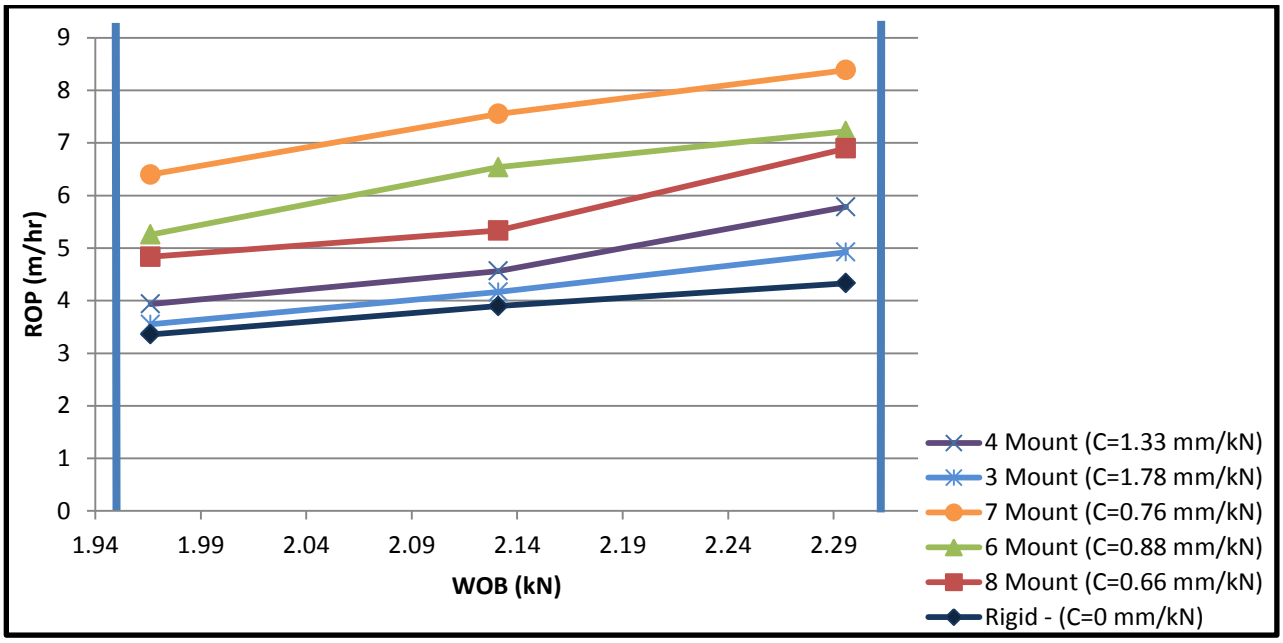

Figure 6-6: ROP vs. WOB and compliance at BHP=1378 kPa

As displayed in Figure 6-6, at each specific level of WOB the ROP changes by altering the level of compliance (changing the number of mounts). Figure 6-7 demonstrates the ROP versus compliance at three levels of WOB. As can be seen, the trends of graphs are similar to the results at BHP=138 kPa and show that decreasing the compliance of the system down to the optimal level results in an increase in the ROP; nevertheless, making the system more rigid than that optimal level causes a reduction in the ROP. Furthermore, similar to what was reported for the low pressure tests, Figure 6-7 illustrates that increasing the WOB at a constant level of compliance leads to a rise in the ROP.

The standard deviation of the ROP results is 0.14 m/hr. This value is calculated based on the variability of the results with the same WOB when WOB is less than 1.9 kN,

condition under which varying the compliance did not seem to have any drastic effect, in the set of tests at low BHP.

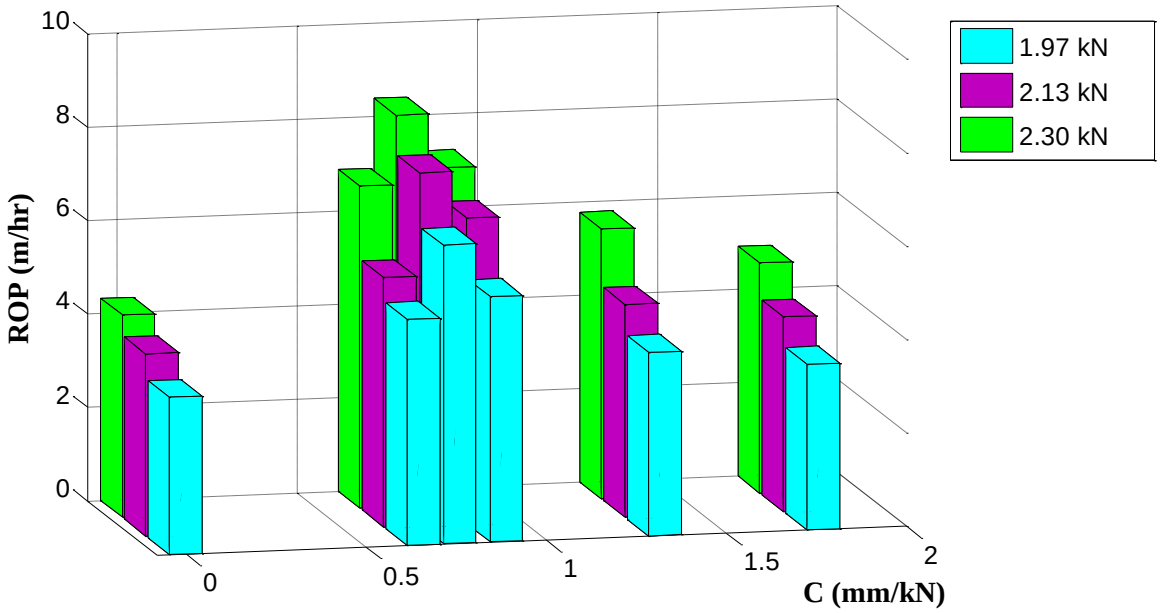

Figure 6-7: ROP vs. compliance at BHP=1378 kPa & 3 WOBs (1.97, 2.13, and 2.30 kN)

The high BHP MSE results are also shown in Figure 6-8. This figure displays the MSE versus compliance for selected levels of WOB. As can be seen, the MSE is changing inversely to the ROP with respect to the level of compliance. In short, the maximum points of the ROP graphs agree with the minimum points of the MSE graphs at all levels of WOB.

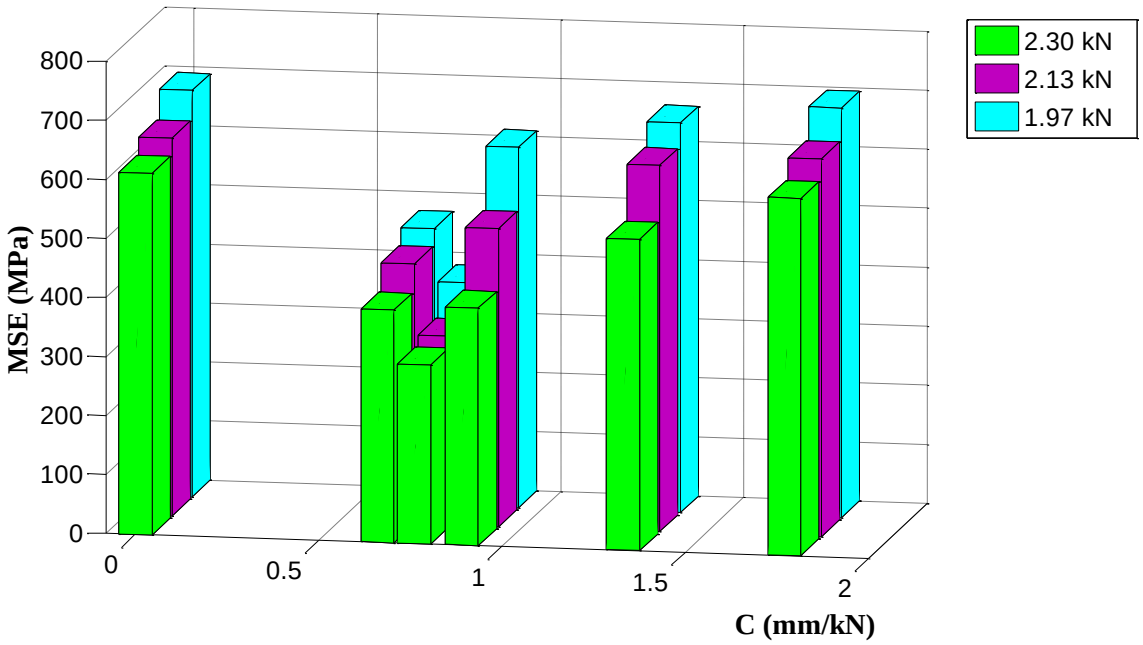

Figure 6-8: MSE vs. compliance at BHP=1378 kPa & 3 WOBs (1.97, 2.13, and 2.30 kN)

6-2. Effect of Compliance on Bit-Rock Displacement

From the experimental results in the preceding section, it is clear that the axial compliance plays a role in bit penetration. Compliance indicates the rigidity of an object and indicates the extent to which an object resists deformation in response to an applied force [17]. Therefore, at a constant applied force, the stiffer system (the system with lower compliance) shows less deformation and displacement. As an illustration, at a constant WOB, the rock displacement is higher when fewer mounts are used (having more compliance in the system). It should be noted that the WOB plays the role of

applied force in our system, and the configuration of compliance mounting system is used to change the compliance level.

The results of rock displacement versus compliance for different levels of WOB at low BHP are shown in Figure 6-9. The high BHP tests results are displayed in Figure 6-10. This depicted displacement is root mean square (RMS) of rock displacement. It can be concluded from these figures that increasing the compliance of the system or decreasing its stiffness at a constant WOB leads to higher displacement. Moreover, these figures reveal that when the compliance of system is constant, higher WOB (applied force) causes more displacement.

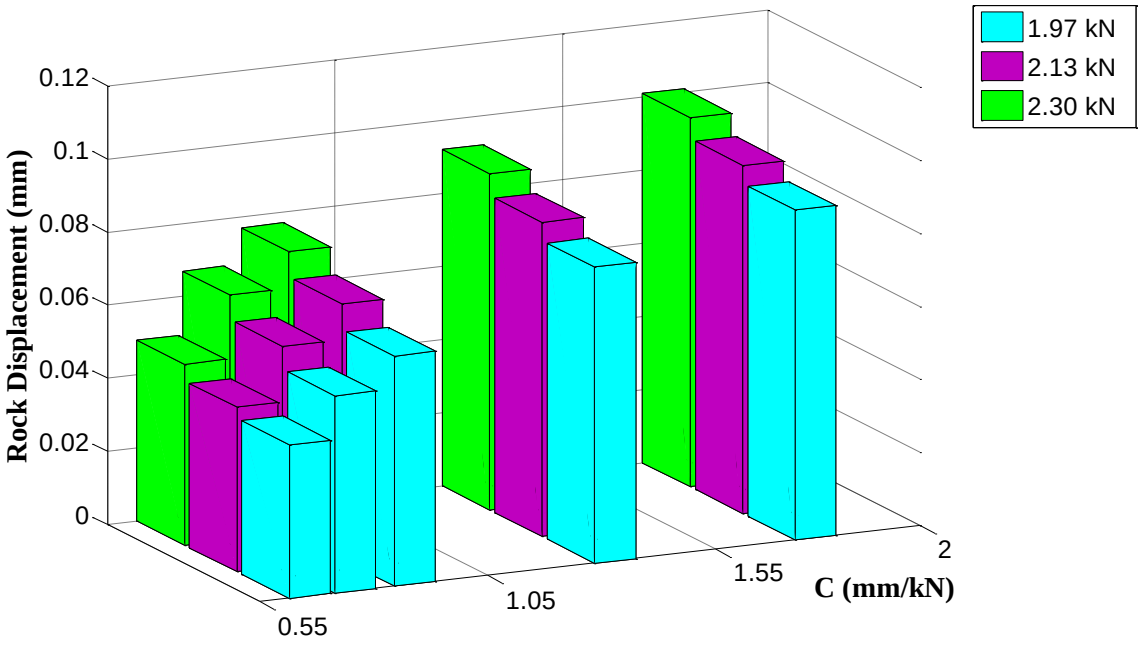

Figure 6-9: Rock displacement vs. compliance at BHP=138 kPa & 3 WOBs (1.97, 2.13, and 2.30 kN)

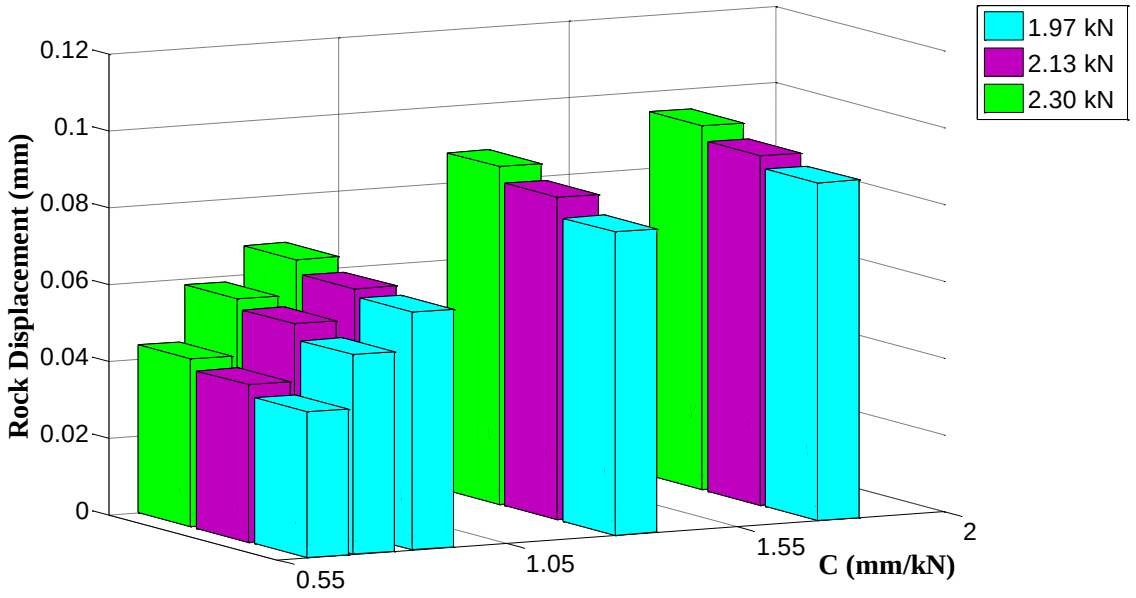

Figure 6-10: Rock displacement vs. compliance at BHP=1378 kPa & 3 WOBs (1.97, 2.13, and 2.30 kN)

In a related set of experiments, Elnahas also observed the same trend for displacement versus WOB at selected levels of compliance [22]. As presented in Figure 6-11, at a constant level of compliance (a fixed number of mounts), increasing the WOB in his tests led to higher displacement except for one offset point. He also observed that at constant WOB, a system with fewer mounts (higher compliance value) shows higher rock displacement.

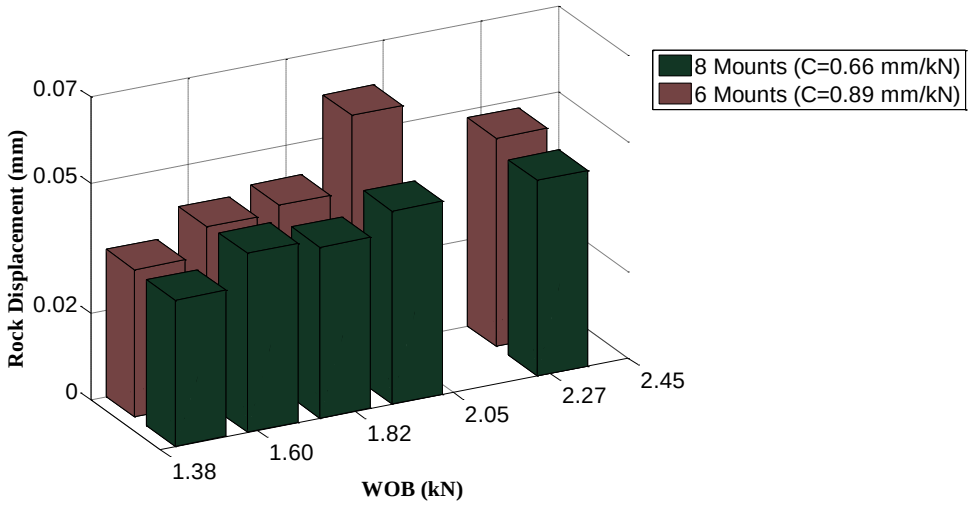

Figure 6-11: Rock displacement vs. WOB and compliance at BHP=172 kPa [22]

The bit-rock displacement during penetration plays a significant role in the interaction between rock and bit. In fact, variation of the displacement level between the rock and the bit causes both positive and negative changes in the ROP. Figures 6-12 and 6-13 show the ROP versus WOB and rock axial displacement at BHP=138 and 1378 kPa respectively. As previously stated, the induced axial displacement is result of changing the level of axial compliance in the system; in fact, it is determined by the characteristics of the test system, i.e. it is a dependent variable. As can be seen, in both high and low BHP, increasing the axial displacement up to an optimal level increases the ROP; however, further increase in the displacement causes a drop in the ROP. The reason behind this phenomenon is thoroughly explained in the next sections of this chapter.

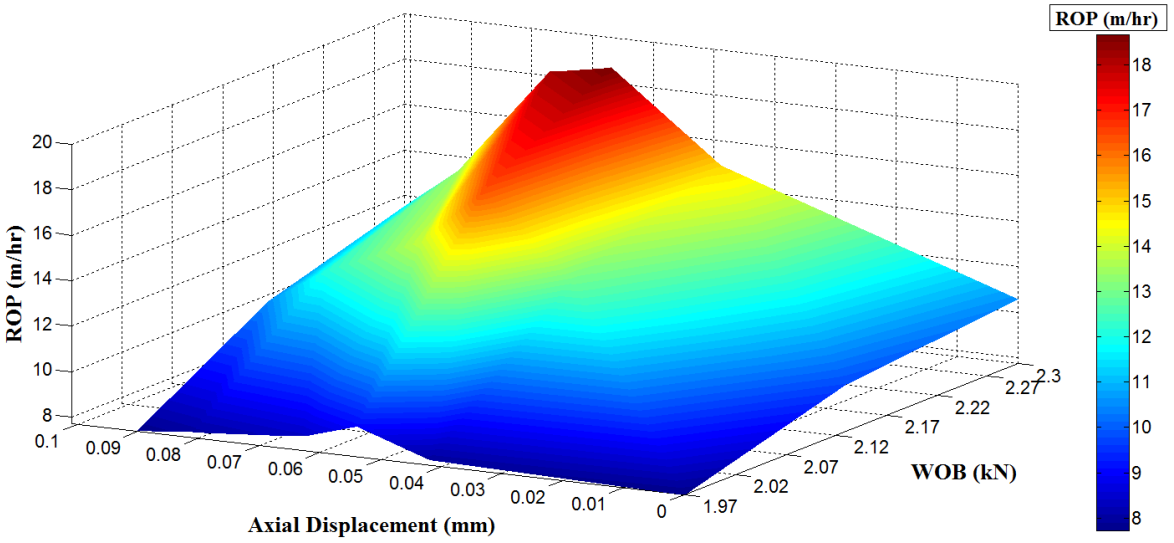

Figure 6-12: ROP vs. axial displacement and WOB at BHP= 138 kPa

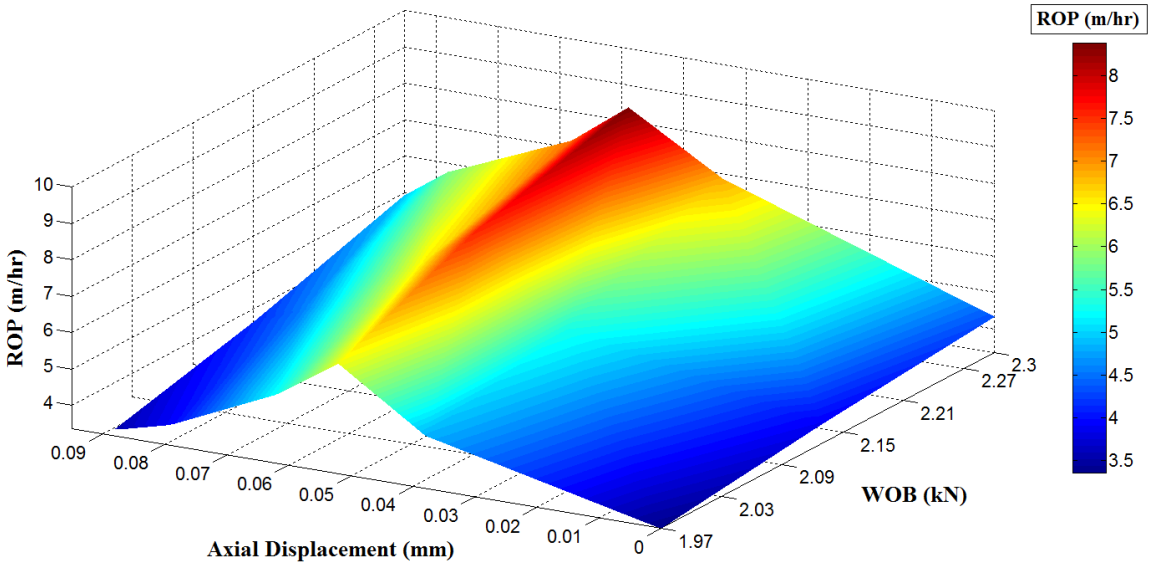

Figure 6-13: ROP vs. axial displacement and WOB at BHP= 1378 kPa

In the laboratory test rig with which the tests are conducted, (SDS), there are two movable segments: i) the drill bit, which is rigidly attached to the end of drill pipe and

drill head and ii) the rock, which is located above the compliance mounting plate. As explained in Chapter 3, the drill head itself is rigidly attached to the carriage. The carriage is also attached to the suspended weight wheel (Figure 3-1).

Thus, practically, we are faced with two movable parts during the penetration. The first part which represents the bit displacement is comprised of the drill bit, drill pipe, drill head and suspended weight. The second part, which represents the rock displacement, contains the rock and the drilling cell which is installed above the compliance mounting plate. The first part has by far higher mass and inertia in comparison with the second part. Furthermore, in mechanics, at a constant applied force a system with higher inertia and mass shows less displacement than one which has lower inertia and mass [17]. Consequently, it can be assumed that in the drill setup used, bit-rock displacement is mainly governed by rock displacement. Therefore, the measurement of rock displacement can be taken to represent the relative bit-rock displacement.

Moreover, it should be noted that due to the limitation of the LPT on the drill string, the recorded data from it cannot be used in combination with the LVDT on the rock mounting system to provide the relative motion of the bit and rock. Because the LPT has a tension string to measure the position and it has low accuracy which makes it inappropriate for measurement of bit-rock axial displacement. Furthermore, an accelerometer was mounted above the drill head cradle (Figures 3-18) to record the drill string vibration. However, due to its inappropriate position in the drill setup, there were too many noises in the recorded data from this sensor that makes it impossible to get any

accurate vibration results from it. So, the recorded data from the accelerometer on drill string was not used in this study.

6-3. Effect of Compliance on Bottom-hole Cleaning

As stated in Chapter 2, in recent years almost all PDC bits have had a chamfer. The main reason for introducing the chamfer is to avoid the diamond chipping during the cutting process of hard rocks [35]. In drilling with chamfered bits when the DOC is higher than the chamfer height, as happened in our tests, the crushed materials and fragments are trapped between the bit cutter face and the rock. Hence, additional friction forces are created at the bottom of the groove.

Previous experimental results showed that containment of the flow of crushed cuttings between the cutter and rock interface is one of the substantial factors in ROP reduction [7]. When such containment happens, the bit has to regrind the accumulated cuttings trapped in the crushed zone. Thus, the key to improvement of the bit's performance is improved cleaning of the accumulated cuttings at the bit-cutter interface. Based on Tutlougu's results [57] the accumulation of crushed materials in front of the cutter could even happen in atmospheric pressure drilling, but the presence of the confining pressure during drilling or increasing the depth of well exacerbates this effect [40]. During this study the pressure of drilling cell varies over two levels of 138, 1378 kPa, which are proportional to drilling operations at depths of 14 and 140 meters respectively. In both

cases the presence of BHP causes containment of the flow of generated chip in the crush zone.

The effect of crushed particles under the cutter was analysed by Ledgerwood [38]. His results showed that crushed particles under hydrostatic pressure have very high strength. In fact, he deduced that the strength of particles in such a condition is as high as the strength of virgin rock. In addition, a series of tests was conducted by Tutlouglu [57] to investigate the mechanics of rock cutting in a single cutter under atmospheric conditions. Based on the results, he stated that the major issue which limits the performance of a cutter is the accumulation of crushed materials in front of the cutter. Moreover, Mozaffari [40] in his rock-cutter simulation showed that in the presence of confining pressure during the cutting process, most of the energy is dissipated through the particle friction rather than breaking the rock and overcoming the bond forces. He also added that the crushed zone under the cutter plays a substantial role in the penetration process; indeed, when this part is perfectly clean an increase in the ROP and MRR is expected.

Therefore, novel methods should be tried to create a better BHC condition and it appears that using the compliance element is one of them. As discussed in the previous section of this chapter, introducing the compliance element in the system causes a displacement between the bit and the rock. It is also illustrated that increasing the compliance level (decreasing the number of mounts) leads to an amplification of this displacement (Figure 6-9).

Due to this induced displacement, the drill bit is lifted up a little bit from the rock surface. This upward movement in the drill bit creates space between the cutter tip and the rock surface, even though, part of the bit cutter is still involved in the penetration. It is theorized that the created space allows the drilling fluid to flush out the accumulated crushed materials and fragments which were trapped in the crushed zone between the bit and the rock. Moreover, part of the bit's compacting force on the crushed cuttings is released over the span of displacement which also facilitates a better cleaning in the penetration zone. However, this cleaning efficiency is a function of induced displcement between the rock and the bit, bit hydraulics, and bit geometry.

Figure 6-14 schematically shows the BHC at constant bit geometry and hydraulics. Since there is not any exact quantitative measurement for BHC, the vertical axis of this graph qualitatvely shows the BHC based on the proposed theory. As illustrated in this figure BHC can be divided into three modes based on the induced bit-rock displacement. In the first mode which is entitled "poor BHC", the displacement is too small to create enough space for the fluid flow to flush the accumulated cuttings. Thus, the crushed cuttings are still trapped in the penetration zone. In the second mode, due to an increase in the displacement, the fluid flow can flush out the crushed fragments and clean the crushed zone. In this mode which is called "medium to good BHC", increasing the displacement leads to better cleaning efficiency, and this trend continues towards maximizing the BHC. Finally, in the third mode, the bottom-hole is completely clean; therefore, further increase in the displacement does not have any effect on the BHC. This third mode is termed "perfect BHC". The same phenomenon was reported by Speer [56]. In his research to

find the optimum drilling technique, he stated that the positive effect of bit hydraulics in increasing the ROP is limited to the cleaning of all generated crushed materials and cuttings. Furthermore, Khorshidian et al. [15] declared that an appropriate BHC condition can improve the drill bit performance through cleaning the generated cutting materials. However, when the generated cuttings are cleaned efficiently, a further increase in hydraulic horsepower may constitute a negative impact on the bit performance by producing nozzle jet impact forces that counteract the WOB.

Accordingly, it can be asserted that creating bit-rock displacement by implementation of the compliance element in the system leads to a better BHC condition, and results in an increase in the ROP. In addition, it can be concluded that an increase in the compliance of the system improves the BHC due to the creation of more space for the drilling fluid to flush out the crushed cuttings. However, when the bottom-hole becomes completely clean, further increase in the compliance level cannot boost the BHC or positively affect the ROP. Figure 6-14 schematically shows this phenomenon. In this figure different patterns of compliance are shown with different coloured columns. As can be seen, after implementation of a specific number of mounts the bit-rock displacement is sufficient to clean all the crushed cuttings and maximize the BHC. Thus, further increase in the displacement is ineffective in BHC. It should be noted that the distance between different coloured columns in Figure 6-12 is scaled based on the displacement results of the tests at 2.13 kN WOB (Figure 6-9).

In contrast to the positive effect of compliance on the BHC, ROP and MSE, compliance can negatively affect the ROP by decreasing the involved cutting surface area. After implementation of different numbers and paterns of mount, the 7-mounts compliance pattern was optimal because despite being in the Medium-Good BHC range, it has a much more favorable penetration depth which offsets the suboptimal BHC patterns. This effect is thoroughly explained in the next section of this chapter.

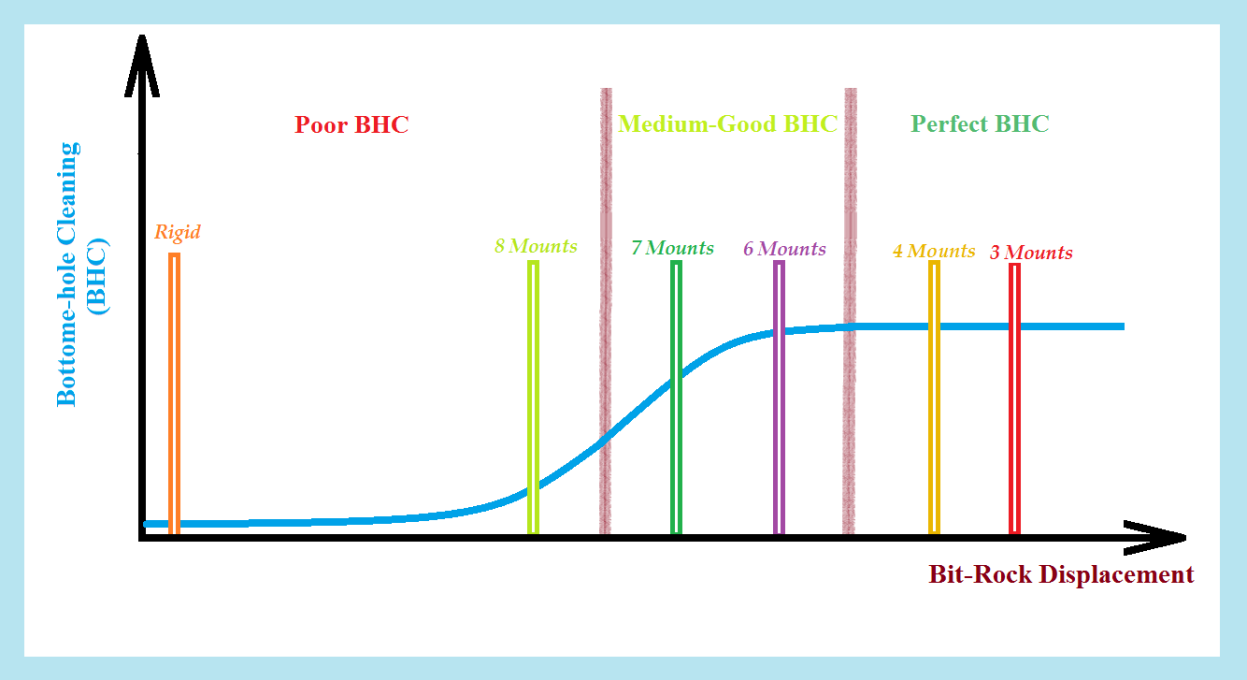

Figure 6-14: BHC vs. bit-rock displacement

6-4. Effect of Compliance on Cutting Surface Area

As discussed in the previous section, test results show that increase in the compliance of the system results in higher bit-rock displcament. The results also illuminate how this displacement can help BHC and lead to ROP enhancment. Despite the afromentioned positive effects of bit-rock displacement, increasing the distance between the rock and the bit can negatively affect the ROP and DOC. As explained in Section 6-1 there is direct relationship between the ROP and DOC; indeed, by having the ROP and dividing it by the RPM, the DOC can be calculated (Figure 6-3). In fact, increasing the rock-bit displacement changes the position of the cutter with respect to the rock surface, and cuases a reduction in the cutting surface area. The schematic position of the cutter tip with respect to the rock surface is shown in Figure 6-15. In our sysem the position of rock in not constant; in other words, by changing the rock position the relative position of the cutter tip changes as well. As can be seen, by decreasing the number of mounts (increasing the compliance value) higher rock displacment is achieved, and the position of the cutter tip shifts upward. It should be noted that the distance between different coloured lines is scaled based on the displacement results of the tests at 2.13 kN WOB.

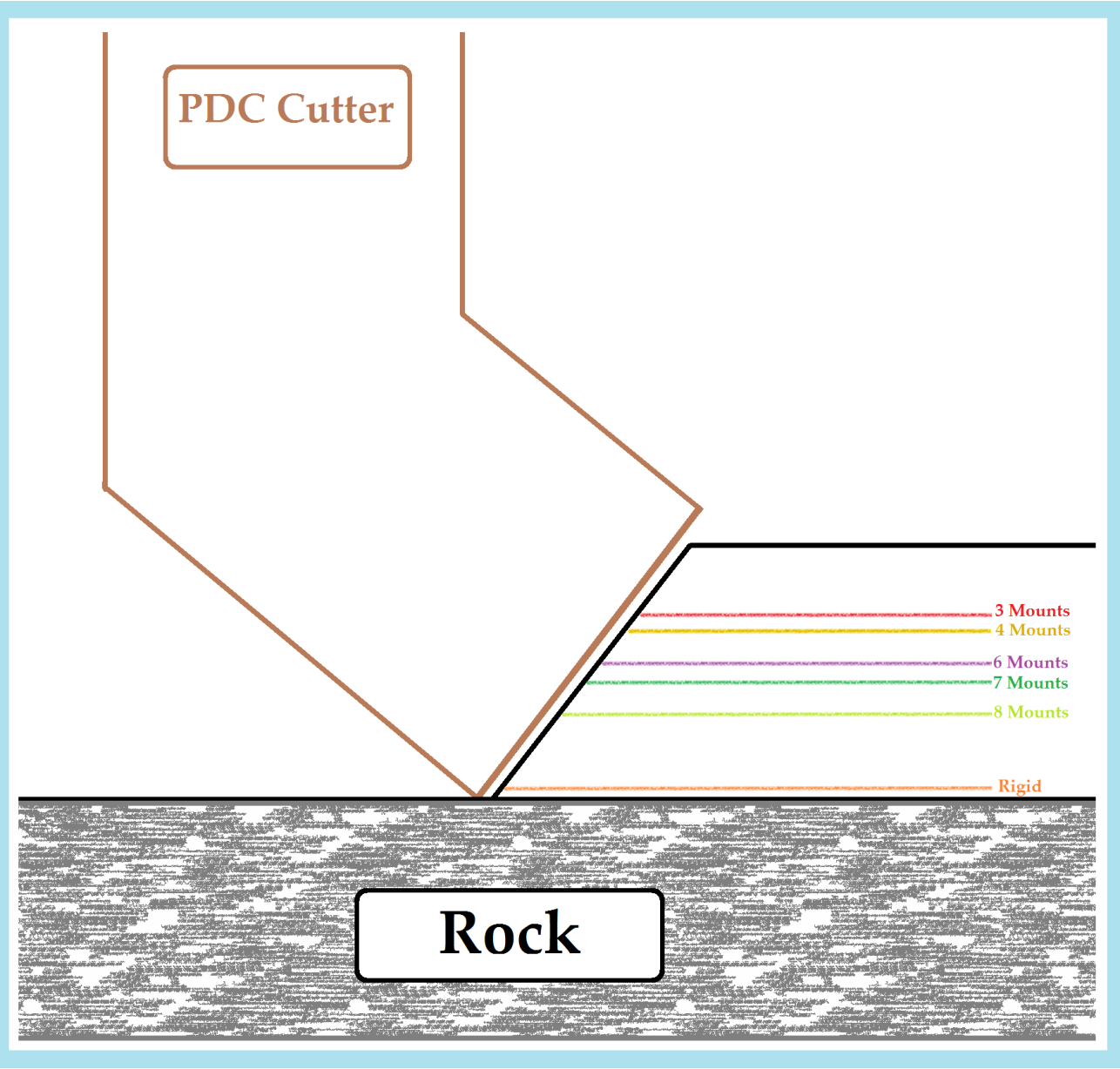

Figure 6-15: Cutter tip position vs. numbers of mounts

As explained in Gerbaud's penetration model [35], in the chamfered PDC bits the total force acting on the PDC cutter is comprised of three different forces. These forces are the cutting face force, chamfer force, and back cutter force. Among these three forces the cutting face force is considered a pure cutting force which is used for penetrating the rock

and creating the chips. The chamfer force and back cutter force are created due to the accumulation of crushed rock under the chamfer and on the back of the cutter respectively. These two forces do not play any role in penetrating the rock, and they are the results of additional friction surface on the bottom of the groove.

The cutting face force is transferred to the rock through the cutting surface and edge of crushed materials. In fact, the magnitude of this force is a function of the cutting cross section area and hydrostatic stress in the crushed materials which are trapped between the rock and the bit. Accordingly, decreasing the cutting surface area decreases the cutter's transmitted force to the rock, and results in generation of smaller chips and reduction in the ROP. As cited before, increasing the bit-rock displacement or increasing the partial bit-rock seperation can reduce the cutting surface area by decreasing the involved depth of cutter in the cutting action. For this reason cutting the number of mounts (increasing the compliance value) leads to diminishing the involved area of cutter with the rock, and decreasing the ROP.

Figure 6-16 schematically displays the involved area of cutter in the cutting action versus the bit-rock displacement. This bit-rock displcament can be interpreted as a partial bit-rock seperation even though part of the bit cutter is still involved in the penetration. It should be noted that the distance between different coloured columns in this figure is scaled based on the displacement results of the tests at 2.13 kN WOB (Figure 6-9).

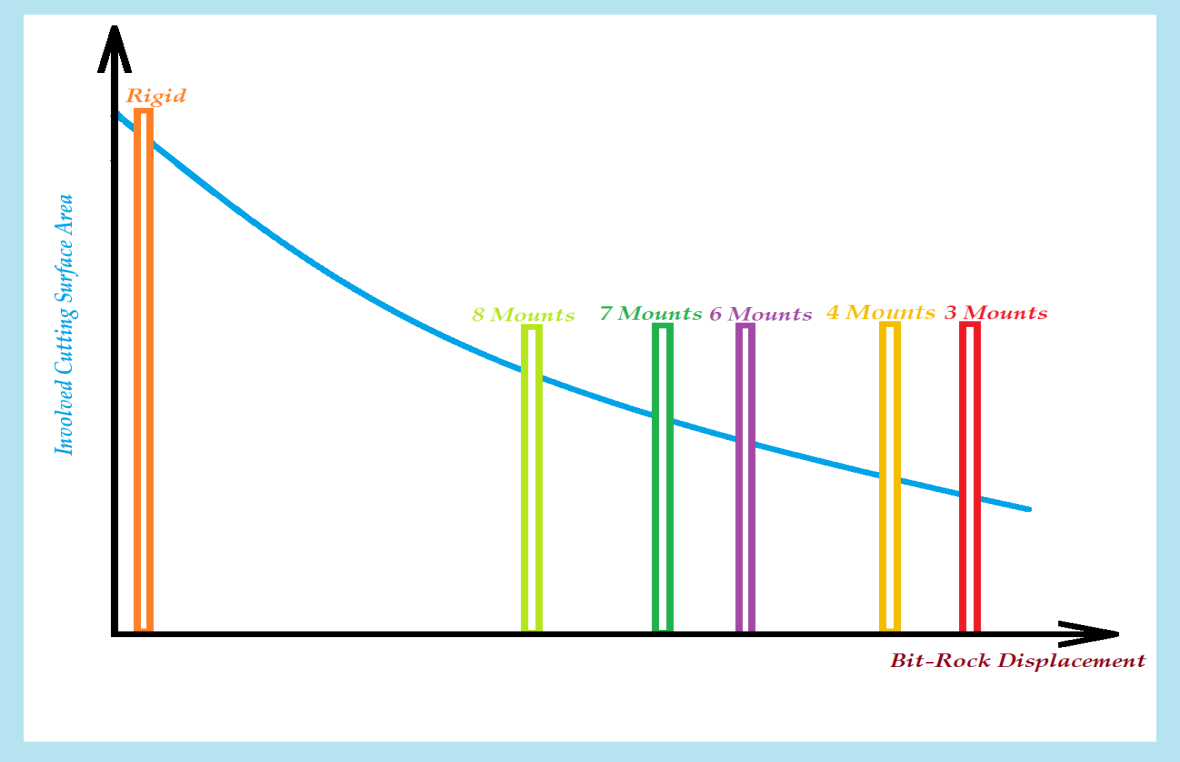

Figure 6-16: Cutting surface area vs. bit-rock displacement

The discussed reduction in the ROP is clearly depicted in Figures 6-4 and 6-7. As can be seen, by decreasing the number of mounts from 7 (C= 0.76 mm/kN) to 3 (C=1.78 mm/kN) a gradual decrease in the ROP is observed because of a decline in the cutting surface area. The MSE varies in an inverse trend to ROP; in fact, having less interface between the rock and the bit causes more energy to be consumed for penetration of a unit volume of rock. More energy consumption results in a higher MSE value for a system with a higher compliance level. The corresponding MSE graphs are also shown in Figures 6-5 and 6-8.

Based on what has been discussed in the last two sections of this chapter, it can be concluded that the presence of the compliance element in the drilling system is beneficial, because it creates bit-rock displacement, helps to clean the accumulated crushed materials in the penetration zone, and leads to ROP and MSE enhancement. However, increasing the compliance of the system more than its optimum value for the BHC not only does not help ROP and MSE enhancement, but also causes detraction in both of them. Figure 6-17 graphically shows both positive and negative effects of increasing compliance and corresponding bit-rock displacement. Indeed, its positive effect is creating a better BHC condition, and its negative effect is decreasing the cutting surface area. Therefore, there is an optimum level for compliance in which the bit- rock displacement is large enough for adequate flushing of the accumulated cuttings from the crushed zone, and at the same time the induced displacment does not severely decrease the cutting surface area. It should be noted that this optimum level of compliance is unique for each system in specific drilling conditions. This optimum level is shown by an intersection point of BHC and cutting surface area curves in the graph below. At this optimum point, the ROP and MSE reach their maximum and minimum values, respectively.

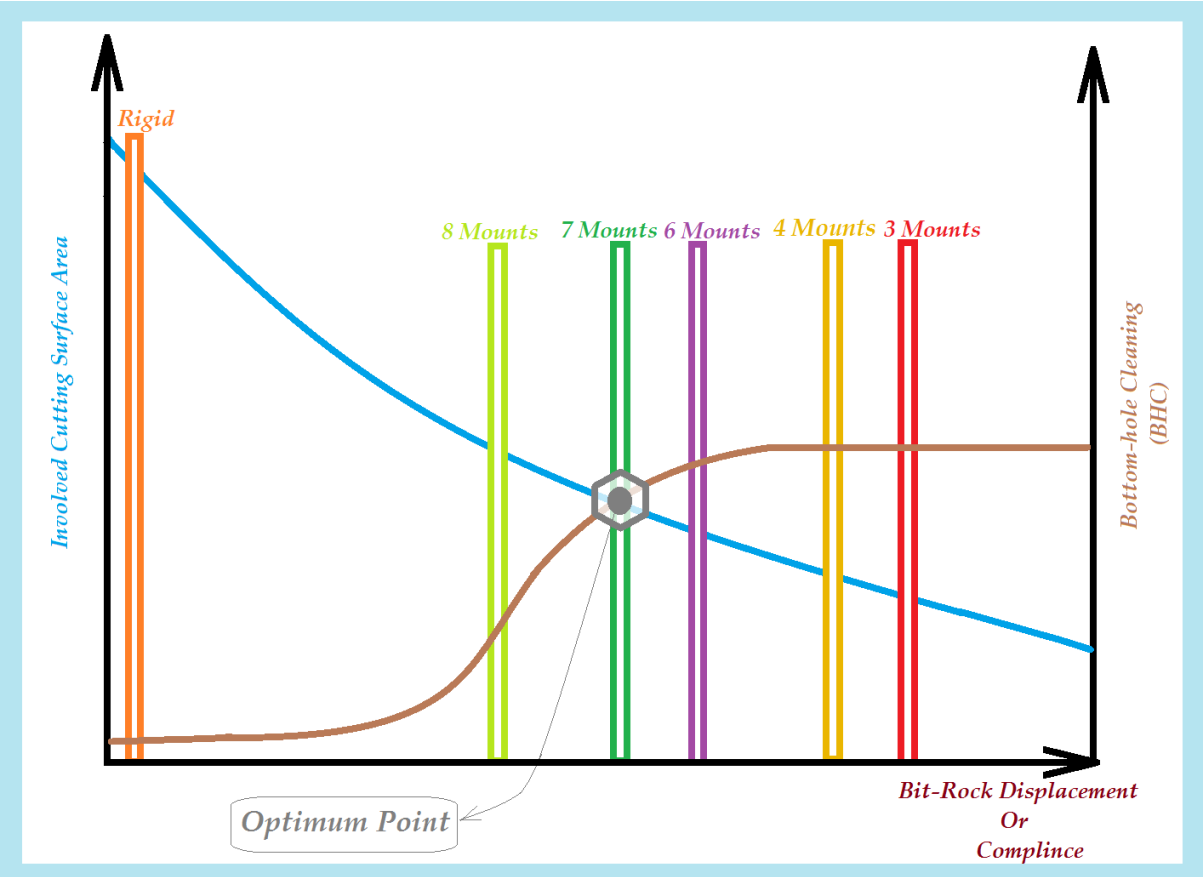

Figure 6-17: BHP and cutting surface area vs. bit-rock displacement

CHAPTER 7

7. Conclusion and Future Work

7-1. Conclusion

Finding a method to increase the ROP is still one of main objectives of drilling optimization in the drilling industry. Drilling field tests and numerical simulations show that there are relationships between BHA configuration (compliance and mass), BHA vibrations, and the ROP. In recent years, sophisticated down-hole tools (e.g. shock sub, Thruster, and Flex Stabilizer) have been designed and fabricated to mitigate unwanted BHA vibrations and increase the ROP. However, utilization of these tools in field tests shows both positive and negative effects on the drilling process. In order to conceptualize the mechanism behind these effects and further investigate the effect of a compliance element on the ROP, a laboratory test rig with a variable compliance feature was

developed. Different levels of compliance are achieved by changing the number and pattern of sandwich rubber mounts in the compliance mounting system. Experimental results verify that using the compliance element can enhance the ROP by creating bit-rock displacement and improving the BHC in the crushed zone, since one of the main reason for reduction in the ROP is the accumulation of crushed materials and fragments in the zone of penetration.

Tests results also show that at low WOB, the compliance element cannot cause a drastic change in the ROP, because the applied load on the mounting system is not sufficient for compliance mounts to show their effects. Moreover, at low WOBs the DOC is mostly under the chamfer depth, and practically, the main bit cutter face is not involved in the penetration process.

Additionally, at high WOB results show that decreasing the level of compliance down to an optimal level leads to a higher ROP due to the increase in the involved cutting surface area, and the creation of larger chips. However, further decrease in the compliance of the system causes an insufficient bit-rock displacement for cleaning the crushed materials in the penetration zone and ends in a drop in the ROP. Accordingly, this experimental study asserts that for each system there is an optimum value of compliance at which the rock-bit displacement is satisfactory for an adequate BHC. Additionally, at this optimum compliance level the cutting surface area is not severely affected by the induced bit-rock displacement.

7-2. Future Works

This study shows the effectiveness of the axial compliance element in ROP enhancement on a laboratory scale. Therefore, design and fabrication of a down-hole tool with the adjustable compliance feature and conducting drilling field tests with this tool can be worthy next steps for this research.

Designing a new down-hole measurement device to record the forces acting on the cutter and bit-rock position during penetration can be another development in this field. The collected data from this measurement device can be a good source for the compliance adjustment of the compliance tool in different drilling conditions.

The current work is performed with one PDC bit and showed great results. However, testing different types of bit with different geometries and numbers of cutter can be a good next step for investigating in this field, since bit geometry itself is one of the influential factors in bit-rock interaction. Other variables that could have affected the results probably included the masses of the rock and drill string, and friction in bushings. These aspects are worthwhile and they should be considered in the next steps of this research.

Finally, a comprehensive numerical simulation is still needed to model real bit-rock interaction for various field conditions. For example, ABAQUS software can be used to simulate the penetrations mechanism. The results of such simulations can greatly benefit the down-hole tool and bit designers.

References

1- Li, X., and Luo, Z. (2011). *China's Museums*. New York, Cambridge University Press.

2- Clark, M. S. (2012). The History of the Oil Industry. In *San Joaquin Valley Geology*. Retrieved February 2, 2014, from http://www.sjvgeology.org

3- History of Drilling. (n.d.). In *RIGS INTERNATIONAL*. Retrieved February 3, 2014, from http://www.rigsinternational.com

4- Schmalhorst, B. (1999). Dynamic Behaviour of a Bit-Motor-Thruster Assembly. *SPE/IADC Drilling Conference*. Amsterdam, The Netherlands: Society of Petroleum Engineers.

5- Zhu, T., Huang, X., and Vajjha, P. (2005). Downhole Harmonic Vibration Oil-Displacement System: A New IOR Tool. *SPE Western Regional Meeting*. Irvine, California, USA: Society of Petroleum Engineers.

6- Gharibiyamchi, Y. (2013). *Evaluation and Characterization of Hydraulic Pulsing Drilling Tools and Potential Impacts on Penetration Rate*, Final M.Eng. Thesis, Memorial University of Newfoundland, St. John's, NL, Canada.

7- Khorshidian, H. (2012). *Phenomena Affecting Penetration Mechanism of Polycrystalline Diamond Compact Bit*, Final M.Eng. Thesis, Memorial University of Newfoundland, St. John's, NL, Canada.

8- Khorshidian, H., Mozaffari, M., and Butt, S.D. (2012). The Role of Natural Vibrations In Penetration Mechanism of a Single PDC Cutter. *46th U.S. Rock Mechanics/Geomechanics Symposium*. Chicago, Illinois, USA: American Rock Mechanics Association.

9- Akbari, B., Butt, S.D., Munaswamy, K., and Arvani, F. (2011). Dynamic Single PDC Cutter Rock Drilling Modeling And Simulations Focusing On Rate of Penetration Using Distinct Element Method. *45th U.S. Rock Mechanics/Geomechanics Symposium*. San Francisco, California, USA: American Rock Mechanics Association.

10- Dunayevsky,V.A., Abbassian, F., and Judzis, A. (1993). Dynamic Stability of Drillstrings Under Fluctuating Weight on Bit. *SPE Drilling and Completion 8 (2)*, Volume 8, Issue 2, pp 84-92: Society of Petroleum Engineers.

11- Dubinsky, V.S.H., Henneuse, H.P., and Kirkman, M.A. (1992). Surface Monitoring of Downhole Vibrations: Russian, European, and American Approaches. *European Petroleum Conference*. Cannes, France: Society of Petroleum Engineers.

12- Richard, T., Detournay, E., Fear, M., Miller, B., Clayton, R., and Matthews, O. (2002). Influence of Bit-rock Interaction on Stick-slip Vibrations of PDC Bits. *SPE Annual Technical Conference and Exhibition*. San Antonio, Texas, USA: Copyright 2002, Society of Petroleum Engineers Inc.

13- Daracem 19A (n.d.). Grace Construction Products. In *Grace Construction* Retrieved February 7, 2014, from http://www.graceconstruction.com

14- Aggregate Source Evaluation Report. (May 30, 2011). In *AMEC Earth and Environmental*. St. John's, Newfoundland, Canada.

15- Khorshidian, H., Butt, S.D., Arvani, F. (2014). Influence of High Velocity Jet on Drilling Performance of PDC Bit under Pressurized Condition. *48th U.S. Rock Mechanics/Geomechanics Symposium*. Minneapolis, MN, USA: American Rock Mechanics Association.

16- Vibration-Damping Sandwich Mounts. (n.d.). In *McMASTER CARR*. Retrieved March 7, 2014, from http://www.mcmaster.com

17- Symon, K. R. (1971). *Mechanics*. London: Addison-Wesley Publishing Company.

18- Bailey, J. R., Elsborg, C.C., James, R.W., Pastusek, P.E., Prim, M.T., and Watson, W.W. (2013). Design Evolution of Drilling Tools to Mitigate Vibrations. *IADC/SPE Drilling Conference and Exhibition.* Amsterdam, The Netherlands: Society of Petroleum Engineers.

19- James, R.W., Pastusek, P.E., Kuhn, G.R., Andreev, A., Bailey, J.R., and Wang, L. (2012). Successful Optimization Strategies Combine to Deliver Significant Performance Boost at the Edge of the ERD Envelope, Sakhalin Island, Russia.

IADC/SPE Drilling Conference and Exhibition. San Diego, California, USA: Society of Petroleum Engineers.

20- Babapour, S. (2013). *Investigation of Enhancing Drill Cuttings Cleaning and Penetration Rate Using Cavitating Pressure Pulses*, Final M.Eng. Thesis, Memorial University of Newfoundland, St. John's, NL, Canada.

21- Warren, T.M., Oster, J.H., Sinor, L.A., and Chen, D.C.K. (1998). Shock Sub Performance Tests. *IADC/SPE Drilling Conference*. Dallas, Texas, USA: Society of Petroleum Engineers.

22- Elnahas, A. (2014). *Experimental Investigation of The Effect of Axial Vibration Generated by Pressure Pulses on Drilling Performance*, Final M.Eng. Thesis, Memorial University of Newfoundland, St. John's, NL, Canada.

23- Cunningham, R. A. (1968). Analysis of Downhole Measurements of Drill String Forces and Motions. *Journal of Manufacturing Science and Engineering*, Trans. ASME, Volume 90, Issue 2, pp 208-216.

24- Wolf, S.F., Zacksenhouse, M., and Arian, A. (1985). Field Measurements of Downhole Drillstring Vibrations. *Annual Technical Conference and Exhibition.* Las Vegas, Nevada, USA: Society of Petroleum Engineers.

25- Dareing, D. W. (1984). Guidelines for Controlling Drill String Vibrations. *Journal of Energy Resources Technology*, Volume 106, Issue 2, pp 272-277.

26- Garrett, W. R. (1962). The Effect of a Down Hole Shock Absorber on Drill Bit and Drill Stem Performance. *Petroleum Mechanical Engineering Conference.* Dallas, Texas, USA. ASME Paper.

27- Vance, J. M. (1972). Drill Pipe Vibration, What Conditions Favor the Use of a Shock Sub. *Transactions- Rotary Drilling Conference* (pp. 21-26): IADC.

28- Parfitt, S.L.H., and Abbasian, F. (1995). A Model for Shock Sub Performance Qualification. *SPE/IADC Drilling Conference.* Amsterdam, The Netherlands: Society of Petroleum Engineers.

29- ASTM Standard D7012-10, 2010, "Test Method for Compressive Strength and Elastic Moduli of Intact Rock Core Specimens under Varying States of Stress and Temperatures", ASTM International, West Conshohocken, PA, 2010, DOI: 10.1520/D7012-10, www.astm.org.

30- Allen, M.B. (1997). BHA Lateral Vibrations: Case Studies and Evaluation of Important Parameters. *SPE/IADC Drilling Conference*. New Orleans, Louisiana, USA: Society of Petroleum Engineers.

31- Zannoni, S.A., Cheatham, C.A., Chen, D.C.K., and Golla, C.A. (1993). Development and Field Testing of a New Downhole MWD Drillstring Dynamics Sensor. *SPE Annual Technical Conference and Exhibition*. Houston, Texas, USA, Society of Petroleum Engineers.

32- Reich, M., Hoving, P.G., and Makohl, F. (1995). Drilling Performance Improvements Using Downhole Thrusters. *SPE/IADC Drilling Conference.* Amsterdam, The Netherlands: Society of Petroleum Engineers.

33- Detournay, E., and Defourny, P. (1992). A phenomenological model for the drilling action of drag bits. *International Journal of Rock Mechanics and Mining Sciences & Geomechanics Abstracts*, Volume 29, Issue 1, pp 13-23.

34- Sellami, H., Fairhusrt, C., Deliac, E., and Delbast, B. (1989). The Role of In-situ Rock Stresses And Mud Pressure on the Penetration Rate of PDC Bits. *Rock at Great Depth, Maury & Fourmaintraus (eds)*, ISBN 9061919754, pp769-779.

35- Gerbaud, L., Menand, S., and Sellami, H. (2006). PDC Bits: All Comes From the Cutter/Rock Interaction. *IADC/SPE Drilling Conference*, Miami, Florida, USA: Society of Petroleum Engineers.

36- Detournay, E., Rochard, T., Shepherd, M. (2008). Drilling response of drag bits: Theory and experiment. *International Journal of Rock Mechanics and Mining Sciences,* Volume 45, Issue 8, pp 1347–1360.

37- Glowka, D.A. (1989). Use of Single-Cutter Data in the Analysis of PDC Bit Designs: Part 1- Development of a PDC Cutting Force Model. *Journal of Petroleum Technology*, Volume 41, Issue 8, pp 850 - 859.

38- Ledgerwood , L. W. (2007). PFC modeling of Rock Cutting under High Pressure Conditions. *1st Canada - U.S. Rock Mechanics Symposium.* Vancouver, Canada: American Rock Mechanics Association.

39- PDC Bit. (n.d.). Innovating While Drilling. In *Drilling Contractors*. Retrieved March 18, 2014, from http://www.drillingcontractor.org

40- Mozaffari, M. (2014). *Comprehensive Simulation of Single PDC Cutter Penetration using Distinct Element Modeling (DEM) Methods*, Final M.Eng. Thesis, Memorial University of Newfoundland, St. John's, NL, Canada.

41- Dupriest, F. E., and Koederitz, W. L. (2005). Maximizing Drill Rates with Real-Time Surveillance of Mechanical Specific Energy. *SPE/IADC Drilling Conference*. Amsterdam, The Netherlands: Society of Petroleum Engineers.

42- Payne, M.L., Abbasian, F., and Hatch, A.J. (1995). Drilling Dynamic Problems and Solutions for Extended-Reach Operations. *In Drilling Technology PD*-volume 65, ed. Vozniak, J.P., pp 191-203. New York: ASME

43- McCray, W. and Cole, F. W. (1959). *Oil Well Drilling Technology*. Oklahoma: University of Oklahoma Press, Norman, pp 351-356.

44- Kolle, J. (2004). HydroPulse Drilling, Final Report. Retrieved 18 Feb. 2014 from http://www.netl.doe.gov/technologies/oil-gas/publications/.../Final_34367.pdf

45- Pessier, R., and Damschen, M. (2011). Hybrid Bits Offer Distinct Advantages in Selected Roller-Cone and PDC-Bit Applications. *SPE Drilling & Completion*, Volume 26, Issue 1, pp 96-103.

46- Xia, M., Zhou, K., and Zhou, B. (2009). Experimental Study And PFC Modelling of Failure Process of Brittle Rock Under Uniaxial Compression. *43rd U.S. Rock Mechanics Symposium & 4th U.S. - Canada Rock Mechanics Symposium.* Asheville, North Carolina, USA: American Rock Mechanics Association.

47- Bourgoyne, A.T., Millhiem, K.K., Chenvert, M.E., and Young, F.S. (1986). *Applied Drilling Engineering*. Richardson, Texas, USA: Society of Petroleum Engineers.

48- Crouse, R., Chia, R. (1985). Optimization of PDC Bit Hydraulics by Fluid Simulation. *SPE Annual Technical Conference and Exhibition*. Las Vegas, Nevada, USA: Society of Petroleum Engineers.

49- Maurer, W. C. (1962). The Perfect - Cleaning Theory of Rotary Drilling. *Journal of Petroleum Technology,* Volume 14, Issue 11, pp 1270-1274: Society of Petroleum Engineers.

50- Garner, N.E. (1967). Cutting Action of a Single Diamond Under Simulated Borehole Conditions. *Journal of Petroleum Technology,* Volume 16, Issue 7, pp 937-942: Society of Petroleum Engineers.

51- Ledgerwood, W.C., Salisbury, D.P. (1991). Bit Balling and Wellbore Instability of Downhole Shales. *SPE Annual Technical Conference and Exhibition.* Dallas, Texas, USA: Society of Petroleum Engineers.

52- Wells, M., Marvel, T., and Beuershausen, C. (2008). Bit Balling Mitigation in PDC Bit Design. *IADC/SPE Asia Pacific Drilling Technology Conference and Exhibition.* Jakarta, Indonesia: Society of Petroleum Engineers.

53- Bit Balling. (n.d.). Drilling Operation. In *Oil and Gas Journal*. Retrieved March 20, 2014, from http:// www.ogj.com

54- Feenstra, R., and Van Leeuwen, J. J. M. (1964). Full-Scale Experiments on Jets in Impermeable Rock Drilling. *Journal of Petroleum Technology,* Volume 16, Issue 3, pp 329–336: Society of Petroleum Engineers.

55- Rabia, H. (1989). *Rig Hydraulic*. Newcastle, England: Entrac Software, pp 155-160.

56- Speer, J. W. (1959). A Method for Determining Optimum Drilling Techniques. *Gulf Coast Drilling and Production Meeting.* Lafayette, Louisiana, USA: Society of Petroleum Engineers.

57- Tutluoglu, L. (1984). *Mechanical rock cutting with and without high pressure water jets*. University Microfilms International, Ann Arbor, MI, PhD dissertation, Berkeley: University of California, Berkeley.

58- Zhang, Z. (2014). *Drillability Investigation on Three Concrete Designs as Synthetic Sedimentary Rocks*, Final M.Eng. Thesis, Memorial University of Newfoundland, St. John's, NL, Canada.

59- M. Benhaddadi, G. Olivier, R. Ibtiouen, J. Yelle, and J-F Tremblay (2011). Premium Efficiency Motors, Electric Machines and Drives, Dr. Miroslav Chomat (Ed.), ISBN:978-953-307-548-8, InTech, Available from: http://www.intechopen.com/books/electric-machines-and-drives/premium-efficiency-motors

60- Parts and Service. (n.d.). In *Milwaukee Tool Corporation*. Retrieved May 10, 2014, from http:// www.milwaukeetool.com

Appendix A: Grain Size Distribution of the Aggregates in Rock Specimen

Table A-1: Grain size distribution of aggregates in rock specimen [14]

Physical Requirements			
Laboratory Test and Designation	**Acceptance Requirements CSA A23.1-04 (max.)**	**Test Result**	**Meets Specification Y/N**
Fine Aggregate	Total % Passing		
10	100 - 100	100.0	
5	95 - 100	99.4	
2.5	80 - 100	82.0	
1.25	50 - 90	62.9	Y[1&2]
630 µm	25 - 60	44.7	
315 µm	10 - 35	26.4	
160 µm	2 - 10	10.3	
80 µm	0 - 5	2.6	
Amount Finer Than 80 µm CSA A23.2-5A	3% 5% if < 2µm fraction is less than 1%	2.3%	Y
Bulk Relative Density SSD Absorption CSA A23.2-6A	N/A	2.629 0.52%	n / a
Organic Color CSA A23.2-7A	Less than 3	1	Y
Clay Lumps CSA A23.2-3A	1%	0%	Y
Lightweight Particles CSA A23.2-4A	0.5%	< 0.5%	Y
Micro-Deval CSA A23.2-23A	20%	6.6%	Y
Magnesium Sulfate Soundness CSA A23.2-9A	16%	*In progress*	n / a
Alkali Reactivity (14 day) CSA A23.2-25A	0.15% 0.1% (with SCM)	0.074%	Y

(1) The Finnes Modulus of the sample was determine to be 2.7; CSA standard requires an FM between 2.3 and 3.1.

(2) The percent passing the 0.160mm sieve slightly exceeds specified gradation requirements.

Appendix B: Petrographic Analysis of the Aggregates in Rock Specimen

Table B-1: Petrographic analysis of aggregates in rock specimen [14]

Rock / Mineral Types	Total per sieve fraction (%)					
	5.00 – 2.50 mm	2.50 – 1.25 mm	1.25 – 0.630 mm	0.630 – 0.315 mm	0.315 – 0.160 mm	Weighted Content (%)
	17.4%	19.1%	18.2%	18.3%	16.1%	
Granite	80.0	72.5	27.4	6.3	-	38.1
Volcanic (undifferentiated)	17.3	8.4	7.9	1.2	0.6	7.0
Quartz	1.4	10.0	34.0	76.2	86.4	40.6
Feldspar	-	8.2	30.0	12.0	7.6	11.7
Biotite	-	-	-	2.8	3.8	1.3
Weathered Particles	1.3	0.9	0.7	1.5	1.6	1.2
Total	**100.0**	**100.0**	**100.0**	**100.0**	**100.0**	**99.9**